Characterization and Mitigation of Speckle Noise in Laser Doppler Vibrometer on Moving Platforms (LDVom)

Jin, J.

DOI
10.4233/uuid:a2e6b6ca-c4c1-4993-8254-991506ad6cd8

Publication date
2023

Document Version
Final published version

Citation (APA)
Jin, J. (2023). *Characterization and Mitigation of Speckle Noise in Laser Doppler Vibrometer on Moving Platforms (LDVom)*. [Dissertation (TU Delft), Delft University of Technology].
https://doi.org/10.4233/uuid:a2e6b6ca-c4c1-4993-8254-991506ad6cd8

Important note
To cite this publication, please use the final published version (if applicable).
Please check the document version above.

Characterization and Mitigation of Speckle Noise in Laser Doppler Vibrometer on Moving Platforms (LDVom)

Characterization and Mitigation of Speckle Noise in Laser Doppler Vibrometer on Moving Platforms (LDVom)

Proefschrift

ter verkrijging van de graad van doctor
aan de Technische Universiteit Delft,
op gezag van de Rector Magnificus prof. dr. ir. T.H.J.J. van der Hagen,
voorzitter van het College voor Promoties,
in het openbaar te verdedigen op
dinsdag 24 oktober 2023 om 10.00 uur

door

Yang JIN

Master of Engineering in Hydraulic Engineering,
Tsinghua University, China,
geboren te Jiangsu, China.

Dit proefschrift is goedgekeurd door de

promotoren: Prof. dr. Z. Li, Prof. dr. R.P.B.J. Dollevoet

Samenstelling promotiecommissie:

Rector Magnificus,	voorzitter
Prof. dr. Z. Li,	Technische Universiteit Delft
Prof. dr. ir. R.P.B.J. Dollevoet,	Technische Universiteit Delft
Onafhankelijke leden:	
Prof. dr. P.G. Steeneken,	Technische Universiteit Delft
Prof. dr. ir. M.A.N. Hendriks,	Technische Universiteit Delft
Prof. dr. ir. D.J. Rixen,	Technische Universität München, Duitsland
Prof. dr. Y. Ni,	De Hong Kong Polytechniek Universiteit, China
Dr. A.A. Nunez Vicencio,	Technische Universiteit Delft

Keywords: Laser Doppler vibrometer; speckle noise; signal processing

Printed by:

Cover:

ISBN …

An electronic version of this dissertation is available at
`http://repository.tudelft.nl/`.

To my family.

Yang Jin

Contents

Summary

Laser Doppler vibrometer (LDV) is a vibration-detecting instrument for noncontact and nondestrutive measurement. It is superior to classic contact transducers in terms of the wide frequency range and high measurement resolution. LDV on moving platforms (LDVom) is one of the LDV measurement technology to one-way scan the vibrating surface, so that it is applicable in large-scale measurement like railway tracks. Speckle noise is a significant signal issue for LDV technologies, especially for LDVom. It distorts the local vibration signal dramatically and reduces the overall signal-to-noise ratio to a quite low level. The one-way scanning nature of LDVom makes it impossible to simply average the signals for noise removal. In view of the speckle noise issue of LDVom, the goal of this dissertation is to acquire new understanding of the problem and proposed there upon-based de-speckling solutions. Three aspects are investigated to achieve the research goal: 1) numerical simulation of speckle noise and characterization of noise behaviors. It can provide insight into behaviour changes of speckle noise in response to some variables and possible tools for minimizing noise strength; 2) the theoretical Fourier spectrum of speckle noise series. The resulted frequency domain characteristics can help design the de-noise signal filter accordingly; 3) development of classic approach-based and newly designed de-speckling algorithms.

The first aspect focuses on the numerical simulation and characterization of LDVom speckle noise. Since the speckle noise originates from the variation of speckle patterns, the statistical distribution of speckle patterns is firstly investigated. The derived distribution of speckle pattern phasors is then used in the simulation of the measurement surface, and with the movement of focusing spot on the surface, speckle noise is numerically generated. The proposed numerical simulation approach for speckle noise is more realistic than those reported in the literature, by considering two important additional variables, the surface roughness and scanning speed. Surface roughness determines the reflection phases of laser and further affects the speckle pattern generated by the laser beam. The scanning speed influences the variation of the speckle pattern, and the phasor variation determines the speckle noise. Agreement has been achieved between numerical simulation and physical experiments in terms of time-series, fast Fourier spectra and amplitude distribution. Afterwards, both the numerically generated and experimentally acquired speckle noise are used for characterization. It shows that the speckle noise amplitude increases with the surface roughness to a critical value. With increasing scanning speed, the average speckle noise amplitude increases, while the signal drop-outs decreases in terms of the amplitude and density. The numerical simulation and the characterization of speckle noise provide great insights into possible strategies in reducing the noise effect.

The second aspect focuses on the Fourier spectrum of speckle noise and the there upon-based despeckling approaches. Fourier transform is theoretically conducted on the speckle noise series. By assuming an infinite LDV scanning surface, the trend of the oscillating frequency spectrum can be derived. The benefit of analyzing the Fourier spectrum is that

band-pass filters can be designed to mitigate the speckle noise. A periodic oscillation has been discovered in the Fourier spectra of the LDVom speckle noise, and the first frequency peak of this oscillation is proportional to the scanning speed. Based on this property, two depseckling strategies are proposed: 1) with large scanning speed, the vibration frequency is far lower that the first frequency peak of the noise, and therefore a low-pass filter can remove the most speckle noise; 2) by removing the trend of the oscillating frequency spectrum from the Fourier spectrum, the most speckle noise can be eliminated. These two strategies have been demonstrated effective through physical experiments.

The third aspect focuses on the algorithms to eliminate the speckle noise, based on either the classic signal-processing approach or a newly developed method. Firstly, a classic signal processing approach, named ensemble empirical mode decomposition (EEMD), is investigated to develop a two-step despeckling algorithm: 1) adaptively cutting off the signal drop-outs with moving root-mean square envelopes; and 2) removing the first few intrinsic mode functions (IMFs) related to the speckle noise. EEMD also provides the benefit of using Hilbert-Huang spectra for vibration analysis. The numerically simulated LDVom speckle noise is added to different non-linear signals with different signal-to-noise ratio, in order to investigate the effectiveness of the approaches. Signals from two experiments on a steel strip and a downscale V-Track test rig are also studied. The results indicate the effectiveness of EEMD-based approach in eliminating speckle noise. Secondly, an adaptive denoising and signal decomposition (ADSD) approach is proposed to eliminate the speckle noise and decompose the signal to different vibration modes. This approach can facilitate vibration analysis from LDVom signals. It consists of three steps. In the first step, the signal series is divided to n segments, on each we assume that the vibration is continuous along the scanning direction. In the second step, the Fourier spectrum is adaptively segmented, with each spectrum segment containing one vibration mode. In the third step, a mathematical optimization is conducted to extract each vibration mode. The results from numerical simulation and physical experiments indicate the despeckling effectiveness.

Overall, the major contribution of this dissertation includes a better understanding of the LDVom speckle noise and four proposed approaches: 1) an approach for realistically numerically simulate the LDVom speckle noise, which provides insight into the speckle noise behaviors; 2) a despeckling approach based on Fourier analysis of the speckle noise, which handling the speckle noise in the frequency domain; 3) an EEMD based approach and 4) an ADSD approach, which handle the speckle noise in the time domain and can facilitate vibration analysis from LDVom signals.

Samenvatting

Een Laser Doppler-vibrometer (LDV) is een instrument voor het detecteren van trillingen via contactloze en niet-destructieve metingen. Het is superieur aan klassieke contact-transducers wat betreft het brede frequentiebereik en de hoge meetresolutie. LDV op bewegende platforms (LDVom) is een van de LDV-meettechnologieën om het trillende oppervlak in één richting te scannen, zodat het toepasbaar is bij grootschalige metingen zoals spoorwegen. Speckle-ruis is een aanzienlijk signaalprobleem voor LDV-technologieën, vooral voor LDVom. Het vervormt het lokale trillingssignaal aanzienlijk en verlaagt de algehele signaal-ruisverhouding tot een vrij laag niveau. De eenrichtingsscantechniek van LDVom maakt het onmogelijk om de signalen eenvoudigweg te middelen om ruis te verwijderen. Het doel van dit proefschrift is om een nieuw begrip te verkrijgen op het probleem van speckle-ruis bij LDVom en daarop gebaseerde de-speckling oplossingen voor te stellen. Drie aspecten worden onderzocht om het onderzoeksdoel te bereiken: 1) numerieke simulatie van speckle-ruis en karakterisering van ruisgedrag. Dit kan inzicht bieden in gedragsveranderingen van speckle-ruis als reactie op variabelen en mogelijke tools om de sterkte van ruis te minimaliseren; 2) de theoretische Fourier-spectrum van speckle-ruisseries. De resulterende frequentiedomeinkarakteristieken kunnen helpen bij het ontwerpen van het ontruis signaalfilter; 3) ontwikkeling van op klassieke benaderingen gebaseerde en nieuw ontworpen de-speckling-algoritmes.

Het eerste aspect richt zich op de numerieke simulatie en karakterisering van speckle-ruis bij LDVom. Aangezien speckle-ruis voortkomt uit variaties in speckle-patronen, wordt allereerst de statistische verdeling van speckle-patronen onderzocht. De afgeleide verdeling van speckle-patroonfasoren wordt vervolgens gebruikt bij de simulatie van het meetoppervlak, en met de beweging van de focusvlek op het oppervlak wordt speckle-ruis numeriek gegenereerd. De voorgestelde numerieke simulatie aanpak voor speckle-ruis is realistischer dan die welke in de literatuur zijn voorgesteld, omdat hierbij twee extra variabelen worden beschouwd: de oppervlakteruwheid en de scansnelheid. De oppervlakteruwheid bepaalt de faseverschuivingen van de laserreflectie en heeft vervolgens invloed op het speckle-patroon dat wordt gegenereerd door de laserstraal. De scansnelheid beïnvloedt de variatie van het speckle-patroon en de variatie van de fasoren bepaalt de speckle-ruis. Overeenstemming is bereikt tussen de numerieke simulatie en fysieke experimenten wat betreft tijdsreeksen, snelle Fourier-spectra en amplitudedistributie. Vervolgens worden zowel de numeriek gegenereerde als experimenteel verkregen speckle-ruis gebruikt voor karakterisering. Hieruit blijkt dat de amplitude van de speckle-ruis toeneemt met de oppervlakteruwheid tot een kritische waarde. Bij toenemende scansnelheid neemt de gemiddelde amplitude van de speckle-ruis toe, terwijl het aantal signaaluitvallen afneemt in termen van amplitude en dichtheid. De numerieke simulatie en karakterisering van speckle-ruis bieden waardevolle inzichten in mogelijke strategieën om het effect van ruis te verminderen.

Het tweede aspect richt zich op het Fourier-spectrum van speckle-ruis en de daarop gebaseerde de-speckling-methodes. De Fourier-transformatie wordt theoretisch toegepast

op de speckle-ruisreeks. Door uit te gaan van een oneindig LDV-scanoppervlak kan de trend van het oscillerende frequentiespectrum worden afgeleid. Het voordeel van het analyseren van het Fourier-spectrum is dat er banddoorlaatfilters kunnen worden ontworpen om de speckle-ruis te verminderen. Er is een periodieke oscillatie ontdekt in de Fourier-spectra van het LDVom speckle-ruis, en de eerste frequentiepiek van deze oscillatie is evenredig met de scansnelheid. Op basis van deze eigenschap worden twee de-speckling-strategieën voorgesteld: 1) bij een hoge scansnelheid ligt de trillingsfrequentie veel lager dan de eerste frequentiepiek van het ruis, en daarom kan een laagdoorlaatfilter de meeste speckle-ruis verwijderen; 2) door de trend van het oscillerende frequentiespectrum uit het Fourier-spectrum te verwijderen, kan de meeste speckle-ruis geëlimineerd worden. Deze twee strategieën zijn succesvol gedemonstreerd in fysische experimenten.

Het derde aspect richt zich op de algoritmes om speckle-ruis te elimineren, gebaseerd op zowel de klassieke signaalverwerking als een nieuw ontwikkelde methode. Ten eerste wordt een klassieke signaalverwerkingsmethode, genaamd ensemble-empirische modusdecompositie (EEMD), onderzocht om een de-speckling algoritme te ontwikkelen bestaande uit twee stappen: 1) adaptief afsnijden van signaaluitval met behulp van bewegende rms-envelope; en 2) verwijderen van de eerste paar intrinsieke modusfuncties (IMF's) die verband houden met de speckle-ruis. EEMD biedt ook het voordeel van het gebruik van Hilbert-Huang-spectra voor trillingsanalyse. De numeriek gesimuleerde LDVom speckle-ruis wordt toegevoegd aan verschillende niet-lineaire signalen met verschillende signaal-ruisverhoudingen, om de effectiviteit van de methodes te onderzoeken. Signalen van twee experimenten op een stalen strip en het schaalmodel V-Track-testopstelling worden ook bestudeerd. De resultaten geven aan dat de op EEMD gebaseerde benadering effectief is in het elimineren van speckle-ruis. Ten tweede wordt een adaptieve ontruizing en signaaldecompositie (ADSD) benadering voorgesteld om speckle-ruis te elimineren en het signaal te decomponeren in verschillende trillingsmodi. Deze benadering vergemakkelijkt trillingsanalyse van LDVom-signalen. Het bestaat uit drie stappen. In de eerste stap wordt de signaalreeks verdeeld in n segmenten, waarbij wordt verondersteld dat de trilling continu is langs de scanrichting. In de tweede stap wordt het Fourier-spectrum adaptief gesegmenteerd, waarbij elk spectrumsegment één trillingsmodus bevat. In de derde stap wordt een wiskundige optimalisatie uitgevoerd om elke trillingsmodus te extraheren. De resultaten van numerieke simulatie en fysische experimenten geven de effectiviteit van de de-speckling aan.

De belangrijkste bijdrage van dit proefschrift omvat een beter begrip van speckle-ruis bij LDVom alsmede de vier voorgestelde methodes: 1) een benadering voor realistische numerieke simulatie van speckle-ruis bij LDVom, die inzicht biedt in het gedrag van speckle-ruis; 2) een de-speckling-benadering gebaseerd op Fourier-analyse van speckle-ruis, die de speckle-ruis behandelt in het frequentiedomein; 3) een op EEMD gebaseerde benadering; en 4) een ADSD-benadering, die de speckle-ruis behandelt in het tijdsdomein en trillingsanalyse van LDVom-signalen vergemakkelijkt.

Acknowledgments

Time has passed by so swiftly; in the blink of an eye, I have completed my doctoral studies. This lengthy yet fleeting academic journey has exposed me to numerous challenges and rewards, resembling a profound adventure of the mind and intellect, brimming with the pleasures of exploration and discovery. During this period, I have also gained a profound appreciation for the brevity of the student life. Each day of research and exploration has felt immensely precious, enriching my intellectual world, broadening my horizons, and shaping my future. Throughout this process, I've learned how to overcome setbacks, maintain resilience, and tirelessly pursue my dreams. Here, I would like to express my deepest gratitude.

First and foremost, I would like to express my heartfelt gratitude to my promoter, Professor Li. Throughout my entire doctoral research journey, Professor Li's presence has had a profound and lasting impact on my academic career. He has consistently guided me with selfless dedication and a rigorous academic attitude, providing invaluable advice and direction, whether in choosing research directions or designing experiments. Professor Li is not just a promoter but also a role model. His attentive teaching and unwavering support have enabled me to continuously progress and become a more comprehensive and in-depth researcher. He always encouraged me to push my limits and face academic challenges bravely, fostering a sense of determination and confidence in my research path. Furthermore, Professor Li has been incredibly supportive of all my research endeavors. He not only encouraged me to pursue innovation but also granted me the freedom and space to expand my academic thinking. This trust and support allowed me to fully unleash my creativity and explore new research areas, which has had a profound impact on my academic growth. Professor Li's guidance is a precious asset in my academic journey, one from which I will benefit for a lifetime.

At the same time, I would also like to thank my colleagues. I'm grateful to Alfredo for providing valuable writing guidance for my thesis. I appreciate Jan and Jurjen for their assistance with experiments. Without all of you, my doctoral research project would not have been possible.

I would also like to extend my heartfelt gratitude to my fellow graduate students, Pan Zhang, Yuancheng Zeng, Li Wang, Chunyan He, Wenli Jia and Yunlong Guo. In this academic journey, they have been indispensable companions. Not only have we supported and communicated with each other academically, but we have also lent each other a helping hand in the laboratory. However, their assistance goes beyond the academic realm. Life as an international student often comes with many challenges and moments of loneliness, but with their companionship, everything becomes easier to bear. We have not only studied together at school but have also shared many precious moments exploring this unfamiliar city, savoring the cuisine of different cultures, and participating in various recreational activities, infusing our academic life with vibrant colors and happiness. I deeply understand that without these wonderful fellow students, my doctoral journey would not have been

as exciting and memorable. Therefore, I want to sincerely thank them for their support and companionship, and I hope that our friendship will continue to thrive, creating more beautiful memories together.

I would also like to extend my deepest gratitude to my friends, Yuexiang Chen, Aihui Fu, Erqian Tang, Qing Yong, Zhengwei Wu, Xuan Chen, Runzhang Hong, Monica, Ze Chang, Lu Cheng, Jin Chang and Yun Wan. In my life, you have been like bright lighthouses, providing me with endless warmth and support. Whether it was the small everyday matters or major life events, you have always been there with me, and I feel incredibly fortunate. In a foreign land, your friendship has been the strength that has propelled me forward. Whenever I felt lost or lonely, you were always by my side, offering encouragement and solace. Your support has not only been evident in words but also in actions; we have taken care of each other, sharing the ups and downs of life. Exploring this unfamiliar city together, savoring various cuisines, and sharing moments of joy, these precious memories will forever be cherished in my heart. Our adventures and explorations have made life feel full of fun and excitement, and your companionship has made these moments even more unforgettable and meaningful.

Most importantly, I want to express my gratitude to my family. They have consistently been my rock, encouraging me to pursue my dreams no matter how great the difficulties and challenges I faced. Their love and support have been the wellspring of my motivation to move forward.

Finally, I would like to express special thanks to my beloved wife Li Bowen. She is also a PhD candidate at TU Delft. During this long journey of study, we supported each other, understood each other, and made progress together. Her support and understanding have been crucial to my success and I feel extremely lucky to have her as my life partner. Whenever I feel tired or confused, she gives me the strength and motivation to keep going. When my article was rejected and my scientific research was not going well, she always supported me unconditionally. During these PhD years, we not only overcame difficulties together, but also traveled all over Europe. I cherish our travels together, and this is also the life we enjoy together. In the years to come, I will continue to cherish our relationship and work hard for our shared future. My heartfelt thanks again to my wife; you are the most valuable asset in my life.

In conclusion, I want to express my gratitude to everyone who has supported me throughout my doctoral journey. Your help and encouragement have meant a great deal to me, and I will forever cherish it.

Yang
Delft, September 2023

1

Introduction

1

1.1 Laser Doppler Vibrometer on Moving Platforms (LDVom)

1.1.1 LDV development

A laser Doppler vibrometer (LDV) is a vibration detector based on the principle of Doppler frequency shift [1, 2, 3]. The instrument transmits a laser beam directly onto the vibration surface, and the frequency of the reflected laser beam is changed by the vibration. This frequency shift is proportional to the vibration velocity, and can be acquired from the interference between the reflected laser beam and the coherent reference beam. However, such configuration of the light path cannot identify the vibration direction, as only the absolute value of the frequency shift is obtained [2]. Therefore, an acousto-optic modulator named Bragg cell is implemented for the reference beam, which shifts the laser frequency much larger than the Doppler shift. The modulated frequency is then always positive, and the increase and decrease represents two different directions respectively. Figure 1.1 presents the simplified diagram of LDV [4].

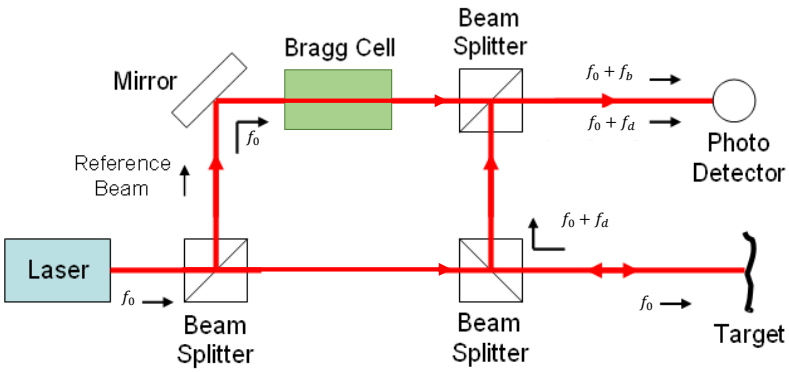

Figure 1.1: A simplified diagram of LDV light path

The advantages of LDV for structural monitoring is the noncontact sensing nature and the broad frequency range [5, 6]. It avoids mass-loading from traditional contact transducers, as the additional masses can change the vibration modes. Besides, for the surface unable to attach a transducer (e.g., high-temperature surface), an LDV is effective to monitor the vibration. For the frequency range, current technology has practically reach over 2 GHz [7], which is superior to contact transducers.

The LDV technologies for specific applications evolved during the last decades, including the single-point LDV, scanning LDV (SLDV), 3D-SLDV, and continuously scanning LDV (CSLDV). These technologies differ in their application scenarios [2]. A single-point LDV is the simplest one, which uses an LDV focusing on only one vibration point [8]. This

is suitable to monitor the crucial structural node. Since monitoring multiple structural nodes is required to analyze the vibration modes, the SLDV is developed by adding the 2-dimensional rotating mirrors [9, 10, 11, 12]. The structural surface is divided into elements, with nodes monitored by an LDV step by step. At each node, sufficient vibration is acquired, and during the monitoring process, the exciting source should not be changed. 3D-SLDV is applied when the vibration along three directions is required for analysis [13, 14]. However, the pointwise measurement is time-consuming for the large structures. An CSLDV can continuously scan the vibration surface along the preset scanning path [15, 16, 17, 18, 19]. It requires multiple reciprocating or cyclical scans for modal analysis, while specific algorithms can reconstruct the modal shape. However, the reciprocating or cyclical scanning is not applicable in large-scale structural monitoring.

1.1.2 LDVom

The concept of LDVom is first proposed by Li and Rixen [20]. An LDVom was designed to one-way scan the vibrating surface, so that it is applicable in large-scale measurement like railway tracks. Figure 1.2 presents an example LDVom installed on a down-scaled railway system. The advantages of this technology include that: 1) the reciprocating scanning is unnecessary for LDVom (saving measurement time); and 2) the exciting source is unnecessary to remained invariant (realistic vibration). These conditions are more realistic for monitoring real-world in-service structures. The development of LDVom may encounter multiple issues, including the signal quality and the response interpretation. Besides, since the LDV is mounted on moving platforms, the vibration spread from the platform would generate LDV vibrations. Among these, speckle noise is the essential signal issue handled in this dissertation.

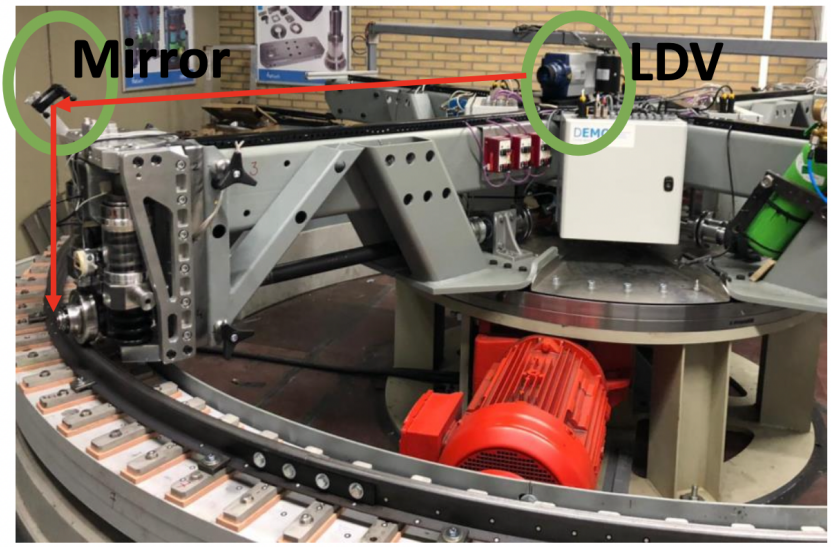

Figure 1.2: An LDVom installed on a down-scaled railway system.

1

1.2 LDV speckle noise

Speckle noise is a general issue of many wave-related technologies, for example, the synthetic aperture radar [21], medical ultrasound [22] and optical coherence tomography [23]. Different from environmental noise, speckle noise is internally produced by the wave reflection and interference. When the speckle affect the measurement precision adversely, it becomes noisy. However, there are some situations that the speckle is a useful measurement feature, e.g., measuring displacement from digital image correlation [24]. For LDV technologies, the speckle noise is troublesome as it buries signal features in the time domain and generate pseudo frequency peaks in the frequency domain [2]. Therefore, a systematic understanding of this noise is required for LDV development.

1.2.1 Mechanism of speckle noise

The source of speckle noise is called speckle patterns [2, 25, 26], which are produced by the diffuse reflections of waves on a rough surface. From a theoretically absolute smooth surface, the wavelets of the emitted beam will be reflected with the same phasors, so that the wavelets will not interfere with each other and the beam remains invariant during transmission. However, most target surfaces are significantly rough on the wavelength scale [27]. The wavelets of the emitted beam are reflected in different directions with different phases, and they will interfere with others. The destructive and constructive interference produces dark and bright illumination, called speckle patterns, observed from the detector. This phenomenon is extremely severe with the coherent wave, as the speckle pattern generated with single wavelength cannot be eliminated by averaging. For technologies used for image detection, the speckle patterns directly affect the imaging quality. The noise issue is more complicated for LDV as it applies Doppler effect for vibration detection. The effect of the speckle pattern is transformed to an additional phase for the inference beam in photodetector. This additional phase will not produce any error unless the speckle pattern changes. Therefore, the variation of the speckle pattern (or visibly, the motion of the laser focusing spot) is the source of LDV speckle noise.

According to the current LDV technologies, the translation of the focusing spot is most common to produce the speckle noise. There are two scenarios of the translation: 1) for single-point LDV and SLDV, the structure at the monitoring point has vibration momentum perpendicular to the incident laser; 2) for CSLDV and LDVom, the focusing spot continuously moves along the scanning path. Another motion type of the focusing spot is deformation, as the spot diameter can be enlarged or reduced. However, this scenario occurs rarely.

In the literature, there are two different types of speckle noise, signal drop-outs and normal speckle noise [2]. The signal drop-outs refer to the sudden dramatic increase and decrease of the signal amplitudes. Other speckle noise with normal amplitudes appears like pseudo vibration. Some researches owe the speckle noise to amplitude modulation and phase modulation from the inference laser beam, respectively. However, LDV only uses typical interferometry method to obtain the wavelength of the inference laser beam, which is phase-related. It seems that the dark speckle pattern dramatically drops the laser intensity compared with the bright speckle pattern, but it also dramatically changes the laser phase. Therefore, signal drop-outs are also phase-related speckle noise, not the light

amplitude-related.

1.2.2 Simulation of speckle noise

The simulation of the LDV speckle noise relies on two different factors, the properties of speckle patterns and the LDV measurement strategy. The real phasors of speckle patterns distributed on the target surface are difficult to acquire, especially for large-scale measurement. Therefore, a better understanding of the statistical properties is crucial for the simulation. Since 1960s, the statistical properties of speckle patterns have been investigated. The first systematical work to understand the speckle pattern properties was conducted by Goodman [27], who theoretically derived different orders of speckle pattern statistics. Based on the assumption that the surface roughness is considerable on the wavelength scale, Goodman [27] concluded for the first-order property that the light intensity of the speckle pattern obeys an exponential distribution and the light phase obeys an even distribution. This property has been the foundation of many speckle-related researches. In later researches, Fujii and Asakura [28] started considering different surface roughness, especially on the wavelength scale. They experimentally investigated the statistical distribution, with results showing that the speckle pattern varies much with the surface roughness. Ohtsubo and Asakura [29] also had the same observations through their theoretical derivation. And a similar investigation of the speckle pattern dependency on the surface roughness has also been conducted recently [30]. However, the light phase of the speckle pattern is rarely investigated in terms of the dependency on the surface roughness, as most technologies apply light intensity. According to the mechanism of speckle noise, the phase of the speckle pattern is the determine factor to generate speckle noise, which needs further investigation. This research gap will be the focus in this dissertation.

The second factor of simulation is about the LDV measurement strategy. In the Lagrangian coordinate system centered at one point of the target surface, the variation of the speckle pattern determines the speckle noise. Therefore, different features change during the variation of the speckle pattern, including the shape, size and location of the focusing spot. For example, while using a single-point LDV, the vibrating point moves towards and away from the LDV, and therefore the focusing spot size changes with the distance. Besides, due to bending deflection during vibration, the focusing spot moves around a vibrating point. For the CSLDV and LDVom, the focusing spot moves along the scanning path. These kinds of variation lead to the speckle noise.

There are different ways of simulating speckle noise in research investigations. For example, to simulate speckle noise in image signals, Bolter et al. [31] applied Gaussian white noise, which is too general and far different from the real speckle noise. Perreault & Auclair-Fortier [32] and Yamaguchi [33] simulated the laser intensities based on the statistical properties of speckle patterns. Similar simulations based on the statistical properties was conducted by Martino et al. [34], who applied the K-distribution and uniform distribution for the light intensity and phase, respectively. In the research of investigating the CSLDV speckle noise occurrence [25], the phase of the speckle pattern was assumed a sine function with multiple order harmonics centered at the scanning frequency, which simplified the noise much. In the previous investigation of simulating LDV speckle noise [35], the statistical properties investigated by Goodman are also the foundations. This approach divides the surface to unaligned elements and assigns the phasor randomly to each element.

The scanning strategy is to use a rectangular photodetector focusing on multiple elements and then moving at a constant speed. However, this approach is less realistic as the important factors of speckle patterns and the focusing spot are all not considered, which requires further investigation.

1.2.3 Consequences of LDV speckle noise

The consequences of LDV speckle noise depend on the measurement strategies, including the single-point LDV, SLDV, CSLDV and LDVom.

The single-point LDV acquires enough vibration signals from one target point. As aforementioned, the vibrating point moves towards and away from the LDV, and therefore the focusing spot size changes with the distance. Besides, due to bending deflection during vibration, the focusing spot moves around a vibrating point. However, these two mentioned variations of speckle patterns are small, and therefore the speckle noise is easy to handle. In addition, as the vibration of one point is mostly periodic, the frequency spectrum of the speckle noise will center at the vibration frequency and present multiple-order harmonics. As a result, the vibration mode is visible from the frequency spectrum.

The SLDV is an ensemble of the single-point LDV, as it acquires enough signals at one point and then moves to another. Therefore, the effect of speckle noise is similar to the single-point LDV [9]. The excitation is necessarily invariant during measurement for modal analysis. However, the speckle noise will not bury the vibration signal.

Severe speckle noise appears in the CSLDV. The CSLDV continuously scans along the vibrating surface, so that the speckle patterns vary rapidly, which would produce intense speckle noise. However, since the CSLDV requires multiple reciprocating or cyclical scans for modal analysis, the speckle noise is averaged on the scanning period. The averaged signal [36] can reduce most speckle noise and reveal the vibration modes.

Since continuously scanning produces intense speckle noise, the LDVom becomes the worst victim without multiple-scanning signals for averaging. According to experimental observations, the noise amplitude can exceed 30 times the true vibration, which entirely bury the real vibration. The signal-to-noise ratio of an LDVom can even fall below -15 db affected by the speckle noise. For this recently emerging technology LDVom, mitigating the speckle noise to improve signal quality is crucial [37].

1.2.4 Mitigation of speckle noise

Mitigation of LDV speckle noise has mainly concerned the CSLDV recently. The first basic strategy is to avoid the speckle noise. As the speckle pattern is generated from the rough surface, polishing the scanning surface can reduce surface roughness and therefore the speckle patterns become bright [38]. The speckle noise significantly drops with bright speckle patterns. However, this strategy becomes less applicable (time-consuming and laborious) in the large-scale measurements, especially for those long structures like railway tracks.

The second strategy is to avoid using the waveforms [39, 40]. As the speckle noise mainly buries the waveforms in the time series, it is applicable to avoid handling the speckle noise by calculating the vibration energy. This approach is suitable for some specific applications, e.g., identifying the defect location.

The third strategy is to average the vibration signals over the scanning period [36]. The exciting source is constant, so that the vibration modes remain invariant during the measurement. Therefore, the averaging strategy will not affect the modal analysis, but has a great effect on eliminating the speckle noise.

The fourth strategy is mainly focusing on the signal drop-outs [41, 42], which are the most troublesome speckle noise. Special algorithms were developed to either identify the signal drop-outs or mitigate the adverse effect.

A recent research handling the LDVom speckle noise is conducted by Zeng et al. [43], which developed a signal-processing framework to mitigate speckle noise. Comprehensive approaches were applied to detect and remove the signal drop-outs and then recover the time series. This approach has been validated on an LDVom mounted on a down-scale railway system.

1.3 Research questions

In view of the speckle noise issue of LDVom and the literature review, we attempt in this thesis to acquire new understanding of the problem and proposed there upon-based solutions. The main research question is:

What are the characteristics and mitigation approaches of LDVom speckle noise?

It is divided into the following sub-questions:

Q1. The speckle noise should be characterized based on numerical simulation and physical experiments. How to perform a realistic simulation of the LDVom speckle noise and acquire a deep understanding of its characteristics?

Q2. Based on the characteristics of the LDVom speckle noise shown in the Fourier spectrum, how to mitigate the speckle noise from the frequency domain?

Q3. How does the adaptive approach, ensemble empirical mode decomposition (EEMD), which processes signals from the time domain, perform on handling speckle noise?

Q4. How to develop a signal processing approach for mitigating speckle noise, as well as decomposing signals to frequency bands for vibration analysis?

To which answers are provided in Chapter 2-5.

1.4 Dissertation Outline

This dissertation answers the main research question step by step, from characterizing the LDVom speckle noise to mitigation approaches. A comprehensive understanding of speckle noise is crucial for solving the noise issue, and numerical simulation and physical experiments are effective tools to acquire such insights. In step 1 (Chapter 2), an approach to realistically numerically simulate the LDVom speckle noise is proposed, with the physical experiments for evaluation. Consequently, speckle noise is characterized in different aspects, including amplitude distribution and the relationships with other parameters. This numerical simulation method can also generate noise series for evaluating later the despeckling approaches. Since signal processing approaches are usually proposed in time and frequency domains, considering the LDVom speckle noise in these two domains for developing related solutions is crucial. In step 2 (Chapter 3), a further characterization of

speckle noise in the frequency domain is conducted using Fourier analysis, and the related despeckling methods are proposed based on the Fourier power spectrum. Meanwhile in step 3 (Chapter 4), an EEMD-based signal processing approach, which processes signals from the time domain, is investigated to eliminate speckle noise. In order to facilitate vibration analysis from LDVom signals, a signal processing approach for despeckling and at the same time decomposing signals to frequency bands is required, which is proposed in step 4 (Chapter 5). In more details:

Chapter 2 answers the research sub-question **Q1**. The numerical simulation considers two variables that affect speckle patterns: surface roughness and the scanning speed. This simulation is evaluated by comparing with experimentally acquired noise. The amplitude distribution and frequency distribution of the speckle noise, as well as the relationship between speckle noise and the aforementioned two variables, are investigated using numerically generated and experimentally acquired speckle noise.

Chapter 3 answers the research sub-question **Q2**. The speckle noise characteristic in the frequency domain is further investigated using Fourier analysis. Based on the finding that constant intervals appear between frequency peaks in power spectrum, two strategies have been proposed to eliminate speckle noise from frequency domain.

Chapter 4 answers the research sub-question **Q3**. A despeckling algorithm is developed using the adaptive signal processing approach, EEMD, which processes signals from the time domain. It is then compared with several other classic signal processing approaches. This research provides an insight into the performance of previous approaches to eliminate speckle noise and gives a despeckling solution through redesigning the classic approaches

Chapter 5 answers the research sub-question **Q4**. As clean signals are usually decomposed to certain frequency bands for vibration analysis, a signal processing approach for despeckling and at the same time decomposing signals is proposed. This approach is based on the assumption of a continuous structure along the scanning path. The signal features from both time and frequency domains are considered. This proposed method is evaluated with physical experiments and compared with other classic signal processing approaches.

In Chapter 6, the major conclusions of this dissertation work and the recommendations for future work are presented.

Chapter 7 and 8 in the Appendices are additional researches that investigate the theories and fast implementation of the classic signal approach empirical mode decomposition (EMD). These two researches attempt to bridge the theory gap of EMD and its time-consuming issue.

References

[1] AB Stanbridge and DJ Ewins. “Modal testing using a scanning laser Doppler vibrometer”. In: *Mechanical systems and signal processing* 13.2 (1999), pp. 255–270.

[2] SJ Rothberg, MS Allen, P Castellini, D Di Maio, JJJ Dirckx, DJ Ewins, Ben J Halkon, P Muyshondt, N Paone, T Ryan, et al. “An international review of laser Doppler vibrometry: Making light work of vibration measurement”. In: *Optics and Lasers in Engineering* 99 (2017), pp. 11–22.

[3] EP Tomasini and P Castellini. *Laser Doppler Vibrometry*. Springer, 2020.

[4] *Laser Doppler Vibrometer, howpublished = https://www.polytec.com/eu/vibrometry/technology/laser-doppler-vibrometry, note = Accessed: 2023-05-18.*

[5] P Castellini, M Martarelli, and EP Tomasini. "Laser Doppler Vibrometry: Development of advanced solutions answering to technology's needs". In: *Mechanical systems and signal processing* 20.6 (2006), pp. 1265–1285. DOI: 10.1016/j.ymssp.2005.11.015. URL: https://www.sciencedirect.com/science/article/pii/S0888327005002220.

[6] L Chen, D Zhang, Y Zhou, C Liu, and S Che. "Design of a high-precision and non-contact dynamic angular displacement measurement with dual-Laser Doppler Vibrometers". In: *Scientific reports* 8.1 (2018), pp. 1–11. DOI: 10.1038/s41598-018-27410-4. URL: https://www.nature.com/articles/s41598-018-27410-4.

[7] https://www.polytec.com/int/vibrometry/technology/laser-doppler-vibrometry. Accessed: 2023-02-08.

[8] O Nishizawa, T Satoh, X Lei, and Y Kuwahara. "Laboratory studies of seismic wave propagation in inhomogeneous media using a laser Doppler vibrometer". In: *Bulletin of the Seismological Society of America* 87.4 (1997), pp. 809–823.

[9] P Sriram, JI Craig, and S Hanagud. "A scanning laser Doppler vibrometer for modal testing". In: *International Journal of Analytical and Experimental Modal Analysis* 5 (1990), pp. 155–167.

[10] AB Stanbridge and DJ Ewins. "Measurement of translational and angular vibration using a scanning laser Doppler vibrometer". In: *Shock and Vibration* 3.2 (1996), pp. 141–152.

[11] R Akamatsu, T Sugimoto, N Utagawa, and K Katakura. "Proposal of non contact inspection method for concrete structures using high-power directional sound source and scanning laser doppler vibrometer". In: *Japanese Journal of Applied Physics* 52.7S (2013), 07HC12.

[12] C Liu, C Zang, and B Zhou. "A novel algorithm for determining the pose of a scanning laser Doppler vibrometer". In: *Measurement Science and Technology* 31.2 (2019), p. 025202.

[13] M Maguire and I Sever. "Full-field strain measurements on turbomachinery components using 3D SLDV technology". In: *AIP Conference Proceedings*. Vol. 1740. 1. AIP Publishing LLC. 2016, p. 080001.

[14] B Witt, D Rohe, and T Schoenherr. "Full-field strain shape estimation from 3D SLDV". In: *Rotating Machinery, Optical Methods & Scanning LDV Methods, Volume 6: Proceedings of the 37th IMAC, A Conference and Exposition on Structural Dynamics 2019*. Springer. 2019, pp. 31–45.

[15] MS Allen and MW Sracic. "A new method for processing impact excited continuous-scan laser Doppler vibrometer measurements". In: *Mechanical Systems and Signal Processing* 24.3 (2010), pp. 721–735.

[16] YF Xu, DM Chen, and WD Zhu. "Damage identification of beam structures using free response shapes obtained by use of a continuously scanning laser Doppler vibrometer system". In: *Mechanical Systems and Signal Processing* 92 (2017), pp. 226–247.

[17] DM Chen, YF Xu, and WD Zhu. "Identification of damage in plates using full-field measurement with a continuously scanning laser Doppler vibrometer system". In: *Journal of Sound and Vibration* 422 (2018), pp. 542–567.

[18] Z Huang and C Zang. "Fast modal rotation measurement using a dual sinusoidal-scan continuously scanning laser Doppler vibrometer". In: *Measurement Science and Technology* 31.8 (2020), p. 085201.

[19] D Di Maio, P Castellini, M Martarelli, S Rothberg, MS Allen, WD Zhu, and DJ Ewins. "Continuous Scanning Laser Vibrometry: A raison d'être and applications to vibration measurements". In: *Mechanical Systems and Signal Processing* 156 (2021), p. 107573.

[20] Li Z. and Rixen D. *Method for detection of a flaw or flaws in a railway track, and a rail vehicle to be used in such a method.* NL 2007315. 2011.

[21] JS Lee, L Jurkevich, P Dewaele, P Wambacq, and A Oosterlinck. "Speckle filtering of synthetic aperture radar images: A review". In: *Remote sensing reviews* 8.4 (1994), pp. 313–340.

[22] PS Hiremath, PT Akkasaligar, S Badiger, and G Gunarathne. "Speckle noise reduction in medical ultrasound images". In: *Advancements and breakthroughs in ultrasound imaging* 1.8 (2013), pp. 1–8.

[23] M Szkulmowski, I Gorczynska, D Szlag, M Sylwestrzak, A Kowalczyk, and M Wojtkowski. "Efficient reduction of speckle noise in Optical Coherence Tomography". In: *Optics express* 20.2 (2012), pp. 1337–1359.

[24] D Lecompte, ASHJD Smits, S Bossuyt, H Sol, J Vantomme, Da Van Hemelrijck, and AM Habraken. "Quality assessment of speckle patterns for digital image correlation". In: *Optics and lasers in Engineering* 44.11 (2006), pp. 1132–1145.

[25] M Martarelli and DJ Ewins. "Continuous scanning laser Doppler vibrometry and speckle noise occurrence". In: *Mechanical Systems and Signal Processing* 20.8 (2006), pp. 2277–2289.

[26] P Martin and S Rothberg. "Introducing speckle noise maps for laser vibrometry". In: *Optics and Lasers in Engineering* 47.3-4 (2009), pp. 431–442.

[27] JW Goodman. *Statistical properties of laser sparkle patterns.* Tech. rep. STANFORD UNIV CA STANFORD ELECTRONICS LABS, 1963.

[28] H Fujii and T Asakura. "Effect of surface roughness on the statistical distribution of image speckle intensity". In: *Optics communications* 11.1 (1974), pp. 35–38.

[29] J Ohtsubo and T Asakura. "Statistical properties of speckle patterns produced by coherent light at the image and defocus planes". In: *Optik* 45.1 (1976), pp. 65–72.

[30] NA Mansour, AM Abd-Rabou, AE Elmahdy, RM El-Agmy, and MM El-Nicklawy. "Dependence of speckle contrast on the light spectral broadening and the roughness root mean square". In: *Optik* 133 (2017), pp. 140–149.

[31] R Bolter, M Gelautz, and F Leberl. "SAR speckle simulation". In: *International archives of photogrammetry and remote sensing* 31 (1996), pp. 20–25.

[32] C Perreault and MF Auclair-Fortier. "Speckle simulation based on B-mode echographic image acquisition model". In: *Fourth Canadian Conference on Computer and Robot Vision (CRV'07)*. IEEE. 2007, pp. 379–386.

[33] I Yamaguchi. "Digital simulation of speckle patterns". In: *Speckle 2018: VII International Conference on Speckle Metrology*. Vol. 10834. International Society for Optics and Photonics. 2018, p. 1083409.

[34] G Di Martino, A Iodice, D Riccio, and G Ruello. "A physical approach for SAR speckle simulation: First results". In: *European Journal of Remote Sensing* 46.1 (2013), pp. 823–836.

[35] S Rothberg. "Numerical simulation of speckle noise in laser vibrometry". In: *Applied Optics* 45.19 (2006), pp. 4523–4533.

[36] J Zhu, Y Li, and R Baets. "Mitigation of speckle noise in laser Doppler vibrometry by using a scanning average method". In: *Optics letters* 44.7 (2019), pp. 1860–1863.

[37] S Rahimi, Z Li, and R Dollevoet. "Measuring with laser Doppler vibrometer on moving frame (LDVMF)". In: *AIP Conference Proceedings*. Vol. 1600. American Institute of Physics. 2014, pp. 274–286.

[38] YF Xu, DM Chen, and WD Zhu. "Modal parameter estimation using free response measured by a continuously scanning laser Doppler vibrometer system with application to structural damage identification". In: *Journal of Sound and Vibration* 485 (2020), p. 115536.

[39] P Chiariotti, M Martarelli, and GM Revel. "Delamination detection by multi-level wavelet processing of continuous scanning laser Doppler vibrometry data". In: *Optics and Lasers in Engineering* 99 (2017), pp. 66–79.

[40] Ł Pieczonka, Ł Ambroziński, WJ Staszewski, D Barnoncel, and P Pérès. "Damage detection in composite panels based on mode-converted Lamb waves sensed using 3D laser scanning vibrometer". In: *Optics and lasers in engineering* 99 (2017), pp. 80–87.

[41] J Vass, R Šmıd, RB Randall, P Sovka, C Cristalli, and B Torcianti. "Avoidance of speckle noise in laser vibrometry by the use of kurtosis ratio: Application to mechanical fault diagnostics". In: *Mechanical Systems and Signal Processing* 22.3 (2008), pp. 647–671.

[42] P Hosek. "Algorithm for signal drop-out recognition in IC engine valve kinematics signal measured by laser Doppler vibrometer". In: *Optics & Laser Technology* 44.4 (2012), pp. 1101–1112.

[43] Y Zeng, A Nunez, and Z Li. "Speckle noise reduction for structural vibration measurement with laser Doppler vibrometer on moving platform". In: *Mechanical Systems and Signal Processing* 178 (2022), p. 109196.

2

Numerical simulation and characterization of speckle noise for laser Doppler vibrometer on moving platforms (LDVom)

Laser Doppler Vibrometer (LDV) is extensively applied in remote and precise vibration measurements for structural monitoring. Speckle noise is a severe signal issue restricting LDV applications, mainly when an LDV scans from moving platforms. Realistic simulations and thorough characterizations of speckle noise can support the despeckle procedure. A novel approach to numerically simulate speckle noise is proposed based on the statistical properties of speckle patterns. Surface roughness and other affecting factors are thoroughly studied. The simulated distributions agree well with the literature when investigating speckle properties. Single-point and continuously scanning speckle noise are both numerically generated and experimentally acquired. Their corresponding time-series and fast Fourier spectra present good agreement. In addition, similar amplitude distributions, approximating a Gaussian distribution, are achieved. Speckle noise is different from Gaussian white noise because of the varying frequency distribution. The speckle noise grows with increasing surface roughness to a critical value. When simulating and acquiring the scanning speckle noise, the noise energy increases with the scanning speed, but the signal drop-outs decrease in intensity and density. These promising results demonstrate the simulation accuracy and can further support despeckle procedures.

This chapter is based on the paper: Jin, Y., Dollevoet, R., & Li, Z. (2022). Numerical simulation and characterization of speckle noise for laser Doppler vibrometer on moving platforms (LDVom). Optics and Lasers in Engineering, 158, 107135.

2.1 Introduction

Laser Doppler Vibrometer (LDV) is a noncontact and nondestructive instrument for precise vibration measurement [1]. It has been extensively used in structural health monitoring (e.g., [2, 3]) as an alternative to traditional contacting transducers. Its physical mechanism is the Doppler effect, as the target movement can cause the frequency shift of lasers. LDV is technically superior to attached sensors, acquiring vibrations remotely and continuously (e.g., measuring very long structures such as railway tracks at high speeds) and avoiding mass loading that possibly changes vibration modes [4]. In addition, the instrument has a measuring frequency over 1 GHz and a vibration velocity resolution of 1 mm/s, suitable for scenarios requiring high-frequency and high-spatial-resolution analysis. In recent decades, the LDV measurement technique has evolved from single-point measurement to pointwise measurement (scanning LDV (SLDV)) and then to the continuous scanning technique (continuous SLDV (CSLDV)) [1]. The pointwise measurement is a set of single-point measurements, and the SLDV acquires sufficient signals at each point. This technique is time-consuming. The CSLDV avoids this issue, but it requires multiple reciprocating scans (e.g., [4, 5, 6]) for modal testing and noise removal. The signal integrated by those from numerous reciprocating cycles derives the structural mode shapes. Thus, the excitation source and the structural conditions should be constant during one CSLDV measurement. An LDV on moving platforms (LDVom) [7] is proposed for one-way continuously scanning vibrating surfaces, especially for long or large structures where multiple reciprocating scans are inapplicable. The instantaneous mode shape is acquired, and either the excitation source or the structural conditions could be time-variant. However, a significant signal issue, speckle noise [1, 8], becomes extremely troublesome for the LDVom since the noise effect cannot be averaged without multiple scanning.

Speckle noise is a significant issue that distorts the acquired vibration, adversely affecting signal interpretation. The noise is attributed to an optical phenomenon, namely speckle patterns, as coherent laser scattering from an optically rough surface alters the phases [9]. The laser wavelets interfere constructively or destructively and thus produce a speckle pattern with bright and dark spots. The signal outputs are phasor summations of the reflected wavelets, and thereby speckle variation, including translation and deformation of the focusing spot, results in signal fluctuations, namely speckle noise. According to the aforementioned scanning techniques, translation of the focusing spot occurs in two cases: (1) the structure at the focusing spot vibrates or (2) the laser continuously scans over the structure. In physical experiments, the noise amplitude reaches over 30 times the true vibration, and the signal-to-noise ratio falls below -15 db [10]. Several approaches have been developed in recent studies to reduce adverse effects, but these approaches are either poorly effective or applicability-limited. For example, Vass et al. [11] and Hosek [12] developed algorithms to eliminate signal drop-outs, but dominant speckle noise with normal amplitudes remained; Chiariotti et al. [13] and Pieczonka et al. [14] overlooked time-frequency information and only calculated the energy distribution for defect identification. These studies lack a comprehensive analysis of speckle noise, while knowing the noise characteristics can support the despeckle procedure. Others mitigated speckle noise according to the noise features, e.g., averaging signals over the cyclical measurement [15] and attaching retroreflective tapes to enhance the reflections [16]. Still, these approaches are not applicable in field measurements including railway inspection. Therefore, the real-

istic simulation and thorough characterization of speckle noise for better a understanding of the issue should be studied.

Noise simulation and characterization require accurate phasor calculation over the speckle patterns and proper simulation of the LDVom scanning procedure. The surface roughness dominantly affects the speckle pattern [17, 18], while the scanning procedure is influenced by the focusing spot, the scanning speed and the sampling frequency. Some studies have investigated the properties of speckle patterns but lack a thorough consideration of surface roughness. Goodman [19] systematically derived the statistical properties of laser speckle patterns, but he assumed large surface roughness beyond the laser wavelength; Ohtsubo and Asakura [20] derived the intensity distribution but not the phase distribution that is significant for LDV signals; Fujii and Asakura [21] experimentally investigated the statistical distribution of the speckle intensity but not of the phase. Recently, the simulation of speckle patterns in image signals was considered. Bolter [22] adopted Gaussian white noise, which is significantly different from speckle noise. Perreault et al. [23] and Yamaguchi [24] simulated the laser intensities but ignored the phases. Martino et al. [25] adopted the K-distribution for the light intensity and uniform distribution for the light phase, but their assumption simplified the contribution of surface roughness. To the best of our knowledge, the sole study for simulating the speckle noise in LDV signals was conducted by Rothberg [26]. The speckle noise simulated in [26], where a surface passes through a stationary laser beam with a constant speed, is similar to that in LDVom. However, the noise should be affected by surface roughness and the aforementioned factors in the LDVom scanning procedure, which have not been considered. In other research, Martin and Rothberg [9] experimentally investigated the relationship between the speckle noise and the focusing spot, while other scanning factors were not included. Therefore, the speckle-noise simulation and characterization that thoroughly consider the related factors remain to be investigated, and such a study is significant for speckle mitigation and avoidance.

In this paper, we propose a novel approach to numerically simulate the speckle noise in LDVom signals, and then characterize the noise for a better understanding of the issue. Speckle noise from the single-point vibration is also characterized since sometimes important structural nodes need constant monitoring. When analyzing the statistical properties, we consider the surface roughness thoroughly and derive the complex distribution of laser phases. Then, the speckle noise is simulated in different situations by varying the scanning speed and the surface roughness. Pure speckle noise is experimentally acquired to evaluate the simulation accuracy. The remainder of this paper is organized as follows: Section 2.2 derives the statistical properties and describes the simulation approach; Section **??** evaluates the simulation accuracy by comparing with the experimental results and then characterizes the speckle noise in different situations; Section **??** discusses the possible effect of the commercial demodulation system on our experimental results; and Section **??** concludes this paper.

2.2 Methodology

2.2.1 Statistical properties of speckle patterns

Since there are numerous cases of microscopic structure of the scanning surface, a better understanding of the statistical properties is necessary. The monochromatic wave equation [27] to present the field incident at (x, y, z) is

$$u(x, y, z; t) = A(x, y, z)e^{i2\pi\nu t} = \mid A(x, y, z) \mid e^{i\theta(x,y,z)}e^{i2\pi\nu t} \tag{2.1}$$

where, t is the transmission time, ν is the optical frequency, and $A(x, y, z)$ represents a complex phasor with the phase $\theta(x, y, z)$. Then the light intensity of the field (x, y, z) can be calculated as

$$I(x, y, z) = \lim_{T\to\infty} \frac{1}{T} \int_{-T/2}^{T/2} \mid u(x, y, z; t) \mid^2 dt = \mid A(x, y, z) \mid^2 \tag{2.2}$$

Considering that the complex amplitude $A(x, y, z)$ results from the summation of the laser wavelets illuminating a speckle pattern [27], the phasor amplitude can be represented by

$$A(x, y, z) = \sum_{k=1}^{n} \mid a_k \mid e^{i\phi_k} \tag{2.3}$$

where, $\mid a_k \mid$ and ϕ_k represent the amplitude and phase of the kth wavelet respectively, and n is the wavelet number in the speckle pattern ([20] and [28] provide the estimator of n). According to Equations (2.2) & (2.3), the wavelet amplitude $\mid a_k \mid$ equals $\frac{\sqrt{I_0}}{n}$ (I_0 is the incident light intensity). Without loss of generality, we can set the incident light intensity $I_0 = 1$. The phase ϕ_k of the reflected wavelet is proportional to the height of the irregularities of the rough surface [29, 30, 31]

$$\phi_k = \frac{4\pi}{\lambda} h_k \tag{2.4}$$

where h_k is the departure of the surface height from its mean value and λ is the optical wavelength. According to Equation (2.4), we can derive the statistical relationships between the speckle pattern and the surface roughness

$$\begin{aligned} \mu_\phi &= \frac{4\pi}{\lambda} R_a \\ \sigma_\phi &= \frac{4\pi}{\lambda} R_q \end{aligned} \tag{2.5}$$

where, μ_ϕ and σ_ϕ represent the mean and standard deviation of the phases respectively, and R_a and R_q represent the mean roughness and root-mean-square roughness of the surface respectively. The phase ϕ_k becomes a random variable that is determined by the random variable h_k. According to Equation (2.3), we can obtain that

$$A(x, y, z) = \frac{1}{n} \sum_{k=1}^{n} e^{i\phi_k} = \frac{1}{n} \sum_{k=1}^{n} cos\phi_k + i\frac{1}{n} \sum_{k=1}^{n} sin\phi_k = A_1 + iA_2 \tag{2.6}$$

where $A_1 = \frac{1}{n}\sum_{k=1}^{n} cos\phi_k$ is the real component of the phasor and $A_2 = \frac{1}{n}\sum_{k=1}^{n} sin\phi_k$ is the imaginary component. When n is a large positive integer, according to the central limit theorem (Lindeberg-Levy Theorem), we can obtain that

$$\epsilon_1 = \frac{A_1 - \mu_1}{\sigma_1/\sqrt{n}} \sim N(0,1)\ ;\ \epsilon_2 = \frac{A_2 - \mu_2}{\sigma_2/\sqrt{n}} \sim N(0,1) \tag{2.7}$$

where, μ_1 and σ_1 are the mean and standard deviation of $cos\phi_k$, μ_2 and σ_2 are the mean and standard deviation of $sin\phi_k$, and $N(0,1)$ represents the standard normal distribution. On this basis, the joint probability density function of A_1 and A_2 is yielded as follows

$$f_A(A_1, A_2) = \frac{n}{2\pi\sigma_1\sigma_2} e^{-\frac{\frac{(A_1-\mu_1)^2}{\sigma_1^2} + \frac{(A_2-\mu_2)^2}{\sigma_2^2}}{2/n}} \tag{2.8}$$

According to Equations (2.2) and (2.6), the intensity I and phase φ of a speckle pattern can be expressed as

$$\begin{aligned} I = I(x,y,z) = \mid A(x,y,z) \mid^2 = A_1^2 + A_2^2 \\ tan\varphi = \frac{A_2}{A_1} \end{aligned} \tag{2.9}$$

Considering Equation (2.8), we can obtain the joint probability density function of I and φ

$$f_{I,\varphi}(I,\varphi) = \mid J \mid f_A(A_1, A_2) = \frac{n}{4\pi\sigma_1\sigma_2} e^{-\frac{\frac{(\sqrt{I}cos\varphi-\mu_1)^2}{\sigma_1^2} + \frac{(\sqrt{I}sin\varphi-\mu_2)^2}{\sigma_2^2}}{2/n}} \tag{2.10}$$

where J is the Jacobi conversion matrix. Therefore, the independent distributions of I and φ can be acquired by integrating Equation (2.10) separately.

However, the integration to calculate the phase φ distribution is very troublesome. According to Equation (2.9), $tan\varphi$ is a variable generated by the ratio of two independent normal variables, thus obeying the distribution derived from a known probability density function in [32].

$$\begin{aligned} f_\varphi(tan\varphi) &= \frac{nbd}{\sqrt{2\pi}a^3\sigma_1\sigma_2}\left[\Phi(\frac{b}{a}) - \Phi(-\frac{b}{a})\right] + \frac{1}{\pi a^3\sigma_1\sigma_2} e^{-c/2} \\ a &= \sqrt{(tan\varphi)^2/\sigma_2^2 + 1/\sigma_1^2} \\ b &= \mu_2 tan\varphi/\sigma_2^2 + \mu_1/\sigma_1^2 \\ c &= \mu_2^2/\sigma_2^2 + \mu_1^2/\sigma_1^2 \\ d &= e^{\frac{b^2 - ca^2}{2a^2}} \end{aligned} \tag{2.11}$$

where the function Φ is the cumulative density function of the standard Gaussian distribution. Since μ_1, μ_2, σ_1, and σ_2 are determined by μ_ϕ and σ_ϕ, the relationship between the variables I and φ and the surface roughness is established. This expression is suitable for applications with wide-range surface roughness.

In addition, the expressions of Equations (2.10) and (2.11) also cover those in the literature. For example, when $\sigma_1/\sqrt{n} = \sigma_2/\sqrt{n} = \sigma$ and $\mu_1 = \mu_2 = 0$, we can obtain the same expression as in [19, 26] that the variable I follows an exponential distribution and φ follows an even distribution.

2

2.2.2 LDV speckle noise

LDV utilizes the Doppler frequency shift produced by the relative motions to detect the vibrations. The signal received by the photodetector is the summation vector of the target and reference laser beams, and the intensity scalar can be expressed as [33]:

$$I_d = I_R + I_T + 2\sqrt{I_R I_T}cos[2\pi f_R t - \frac{4\pi}{\lambda}\int v dt + (\varphi_R - \varphi_T)] \tag{2.12}$$

where, I_d is the detected intensity, I_R and φ_R are the intensity and phase of the reference beam, I_T and φ_T are the intensity and phase of the target beam respectively, f_R is the frequency of the reference beam, λ is the incident wavelength, and v is the vibration velocity of the target. Therefore, the frequency shift of the target beam is

$$f_{beat} - f_R = -\frac{2}{\lambda}v + \frac{1}{2\pi}\frac{d(\varphi_R - \varphi_T)}{dt} \tag{2.13}$$

Considering that the target beam illuminates P speckle patterns (each with phase φ_{Tp} and intensity I_{Tp}) and the reference beam illuminates Q speckle patterns (each with phase φ_{Rq} and intensity I_{Rq}), the resultant intensity I_{res} and phase φ_{res} are related to the summations incident on the photodetector [26]

$$\begin{aligned} I_{res} = 2\sqrt{I_R I_T} = \frac{1}{A}\{&[\sum_{q=1}^{Q}\sum_{p=1}^{P} A_{pq}\sqrt{I_{Rq}I_{Tp}}sin(\varphi_{Rq} - \varphi_{Tp})]^2 \\ &+ [\sum_{q=1}^{Q}\sum_{p=1}^{P} A_{pq}\sqrt{I_{Rq}I_{Tp}}cos(\varphi_{Rq} - \varphi_{Tp})]^2\}^{1/2} \end{aligned} \tag{2.14}$$

$$\begin{aligned} tan\varphi_{res} &= tan(\varphi_R - \varphi_T) \\ &= \frac{\sum_{q=1}^{Q}\sum_{p=1}^{P} A_{pq}\sqrt{I_{Rq}I_{Tp}}sin(\varphi_{Rq} - \varphi_{Tp})}{\sum_{q=1}^{Q}\sum_{p=1}^{P} A_{pq}\sqrt{I_{Rq}I_{Tp}}cos(\varphi_{Rq} - \varphi_{Tp})} \end{aligned} \tag{2.15}$$

where, A_{pq} is the overlapping area of the pth target and qth reference speckle patterns. Phase variation dominantly contributes to the speckle noise even when the laser intensity is adequate. According to Equation (2.13), the measured vibration V_m is the true vibration v polluted by a noisy component.

$$V_m = \frac{\lambda}{2}(f_R - f_{beat}) = v - \frac{\lambda}{4\pi}\frac{d(\varphi_{res})}{dt} = v - \frac{\lambda}{4\pi}\cdot\frac{1}{1 + tan^2(\varphi_{res})}\frac{d(tan(\varphi_{res}))}{dt} \tag{2.16}$$

where $-\frac{\lambda}{4\pi}\frac{d(\varphi_{res})}{dt}$ is the so-called speckle noise or 'pseudo vibration', and the expression is rewritten with the deviation of $tan(\varphi_{res})$. Sharp variations of the phase φ_{res} generate LDV speckle noise, adding unwanted fluctuations in the vibration signal. Therefore, the

intensity and phase distributions of speckle patterns on the scanning surface affect the LDV signals. The statistical properties in subsection 2.2.1 can be utilized for the speckle-noise simulation.

Assuming the speckle patterns are rectangular and densely distributed as in [26], the scanning surface is divided into $e \times f$ speckle elements, as shown in Fig. 2.1. The size of each speckle element should ensure that sufficient laser wavelets will transmit onto a speckle and the sharp variation of the surface roughness can be characterized. Hereafter, since the true surface outliers h_k in Equation (2.4) are difficult to acquire, we use the roughness parameters R_a & R_q to assign intensities and phases to the speckle elements according to Equations (2.10) & (2.11).

The target beam illuminates a particular area with α speckles × β speckles (the red rectangle in Fig. 2.1) on the scanning surface. The intensities and phases of speckles inside the focusing spot (the red rectangle) constitute the contribution of the target beam. The edges of the focusing spot would cut the speckle elements, and thus the overlapping area A_{pq} that each speckle has inside the focusing spot should also be calculated. Since the reference beam is relatively stationary during scanning, its contribution can be simulated as the expectation values of variables I_{Tp} and φ_{Tp} [26]. Therefore, the resultant phase of the target and reference beams can be determined by Equation (2.15).

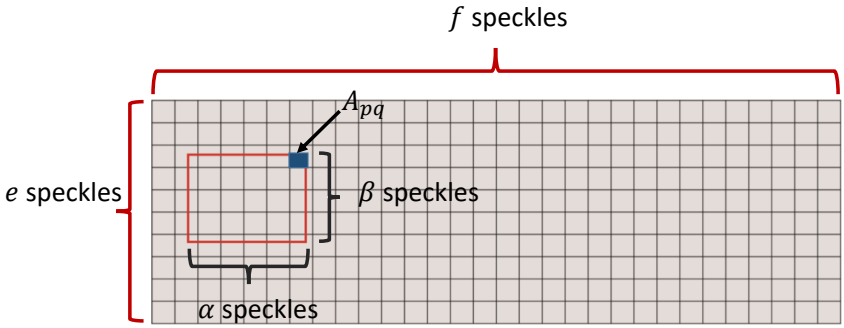

Figure 2.1: Example of the divided scanning surface and the focusing spot (red rectangle)

2.2.3 Single-point noise

First, we concern about speckle noise with a single-point measurement. The vibration at a single-point can cause bending, stretching and twisting deformations of the vibrating structure. These cause relative motion between the laser and the target surface even if the laser is stationary. If the vibration is periodical, the focusing spot will move with the vibration period (the yellow arrows in Fig. 2.2 show an example). For the time-neighboring samples in a signal, the displacement $\Delta\vec{x}$ of the focusing spot in a time increment is equal to the vibration velocity $\vec{v}$ divided by the sampling frequency f_s.

$$\Delta\vec{x} = \frac{\vec{v}}{f_s} \tag{2.17}$$

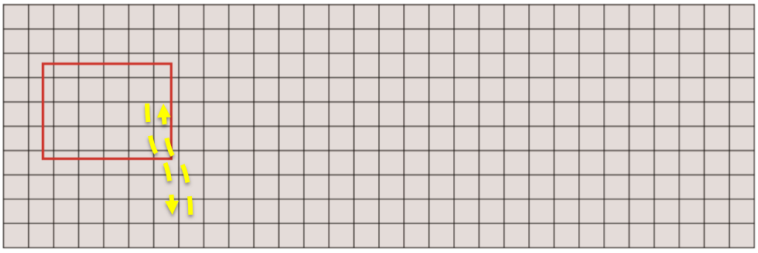

Figure 2.2: Example schematic of generating single-point noise. The focusing spot (red rectangle) moves with the vibration period.

Then the algorithm for simulating the single-point speckle noise is proposed as follows:

Algorithm 1 Simulation of the single-point speckle noise

Input: the surface roughness parameters, the surface size, the vibration of the focusing node, and the sampling frequency;
1. Divide the surface into $e \times f$ speckle elements, and locate the initial focusing spot;
2. Assign the intensities and phases to the speckle elements according to Equations (2.10) & (2.11);
3. Calculate the resultant phase according to Equation (2.15), and move the focusing spot according to Equation (2.17) to acquire the time series of $tan(\varphi_{res})$;
4. Calculate the speckle noise according to Equation (2.16);
Output: the time series of speckle noise.

2.2.4 Continuously scanning speckle noise

Second, we are concerned about the measurement strategy of capturing the instantaneous vibrations by continuous scanning. When an LDVom continuously scans the target surface, the focusing spot moves along the scanning direction, and the variation inside the photodetector produces the scanning speckle noise. The scanning speed (SS) v_s and the sampling frequency (SF) f_s are two significant factors for simulating speckle noise, as they determine the moving rates of the focusing spot. If the SS-to-SF ratio (SFR) is large, the time-neighboring sampled positions will depart from each other with no overlapping speckle patterns, which results in sharp speckle noise. Otherwise, the noise amplitudes become relatively small.

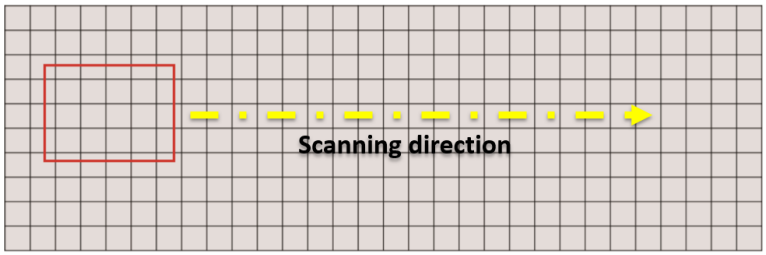

Figure 2.3: Example scheme of scanning the vibration surface. The focusing spot (red rectangle) moves along the scanning direction.

During the scanning period, the displacement of the focusing spot between two time-neighboring sampled positions can be expressed as

$$\Delta\vec{x} = SFR = \frac{\vec{v}_s}{f_s} \tag{2.18}$$

Since the target laser focuses the area α speckles $\times$ β speckles at a time instant, the number of overlapped speckle patterns between time-neighboring sampled positions is calculated as follows:

$$N_{overlap} = \begin{cases} \beta(\alpha - \dfrac{\Delta x}{d}) = \beta(\alpha - \dfrac{v_s}{df_s}), & \alpha > \dfrac{v_s}{df_s} \\ 0, & \alpha \leq \dfrac{v_s}{df_s} \end{cases} \tag{2.19}$$

where d is the length of a speckle pattern. With the increase in $N_{overlap}$, the difference between neighboring positions decreases, and thus the speckle noise attenuates. The algorithm for simulating the scanning speckle noise is proposed as follows:

Algorithm 2 Simulation of continuously scanning speckle noise

Input: the surface roughness parameters, the surface size, the scanning speed, and the sampling frequency;
1. Divide the surface into $e \times f$ speckle elements, and locate the initial focusing spot;
2. Assign the intensities and phases to the speckle elements according to Equations (2.10) & (2.11);
3. Calculate the resultant phase according to Equation (2.15), and move the focusing spot along the scanning direction according to Equation (2.18) to acquire the time series of $tan(\varphi_{res})$;
4. Calculate the speckle noise according to Equation (2.16);
Output: the time series of speckle noise.

2.3 Simulation results

In this section, we demonstrate the validity of the simulation approach by comparing with physical experiments. In order to evaluate our derivation of statistical properties, the

phasor distributions of speckle patterns are compared with the experimental work in [20]. Then, to evaluate the simulation of speckle noise, the time series, fast Fourier transform (FFT) spectra, and noise amplitude distribution are compared with the experimental results. Generally, the time series and FFT spectra can roughly compare the similarities between simulation and experiments. Due to the periodical property, the FFT spectra of single-point speckle noise can quantify the noise [34]. The twice-FFT curve of scanning speckle noise can show some similarities although it has no known physical meaning. The probability density function of all magnitudes in the noise series is an effective tool to evaluate the simulation results. After evaluating our simulation approach, several properties of speckle noise are investigated.

2.3.1 Evaluating the statistical properties

The statistical properties of the speckle patterns constitute the foundation of numerical simulations, thereby requiring appropriate evaluations of the derived distributions. The experimental work in [20] revealed the distribution of the intensity I for rough surfaces (with R_q = 0.14, 0.07, 0.047, 0.04 μm) illuminated by the He-Ne laser (with wavelength 0.6328 μm). These parameters are utilized in our simulation to acquire comparison results. Since the microscopic structure of the rough surface is unprovided, a Gaussian distribution is adopted to generate h_k randomly. The probability density function of $I/\langle I\rangle$ ($\langle I\rangle$ is the mean of I) is illustrated in Fig. 2.4. Our simulated results demonstrate good agreement with the experimental results in [20]. With the decrease in the surface roughness, the probability curves vary from a negative exponential distribution (which agrees with Goodman's results [19]) to a Gaussian distribution centered at $I/\langle I\rangle = 1$. These results indicate the accuracy of simulating the statistical properties.

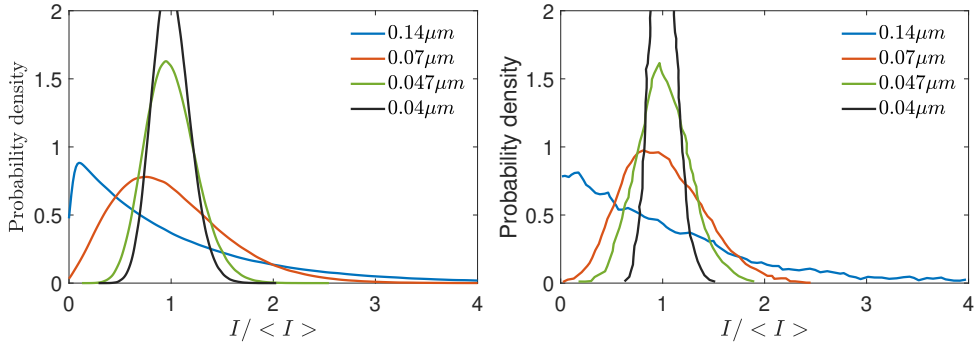

Figure 2.4: (**a**) The simulated probability density function of $I/\langle I\rangle$; (**b**) The experimental results reproduced from [20]. The laser wavelength is 0.6328 μm.

To investigate the relationship between phase φ and the surface roughness, the probability density function of φ is presented in Figure 2.5a. The phase curves are symmetric by 0. When the surface is sufficiently smooth, the speckle phases mostly appear at 0, which

indicates that the specular laser wavelets vary little from the incident light. With increasing surface roughness, the phase φ becomes uniformly distributed, agreeing with Goodman's results [19]. Considering the effect of laser wavelength, the relationship between the speckle contrast $\sigma_I/\langle I\rangle$ and surface roughness R_q is shown in Fig. 2.5b. With a smooth surface, the speckle pattern is almost bright and thus the contrast $\sigma_I/\langle I\rangle$ is nearly 0. With the increasing surface roughness, the speckle pattern becomes dark and bright, and thus its contrast increases. This increasing trend ends at a critical value R_{qc} of the surface roughness. These curves agree with the results in [18] & [21]. The critical value R_{qc} is positively correlated to the incident wavelength since the wavelength determines the laser resolution to the surface roughness.

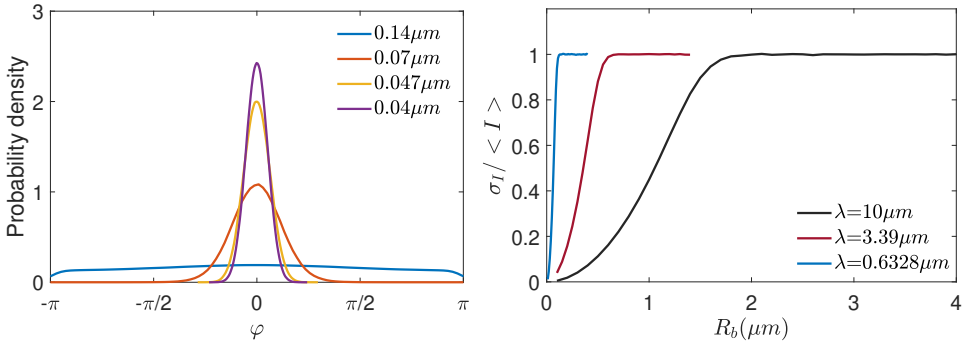

(a) (b)

Figure 2.5: (**a**) The simulated probability density function of φ (with laser wavelength of 0.6328 μm); (**b**) The relationship between the speckle contrast and surface roughness.

2.3.2 Experimental setup

Physical experiments are conducted in the laboratory to evaluate the simulation results. Fig. 2.6 presents the experimental setup that measures a cantilever strip of length 540 mm. The LDV transmits a laser beam deflected by a rotating mirror to the target surface. (1) When acquiring the single-point speckle noise, the focused node of the strip slightly vibrates at 500 Hz excited by a shaker. Then the LDV acquires the 500 Hz vibration and the speckle noise. (2) When the mirror rotates, the laser continuously scans the steel strip at a constant speed along the scanning direction (Fig. 2.6a). The laser beam only scans the sample once, not repeatedly or periodically, which satisfies the basic concept of an LDVom. The scanning speed is adjustable. There are no vibrations of the target, and thus the LDVom acquires pure speckle noise. The sampling frequency is 102400 Hz.

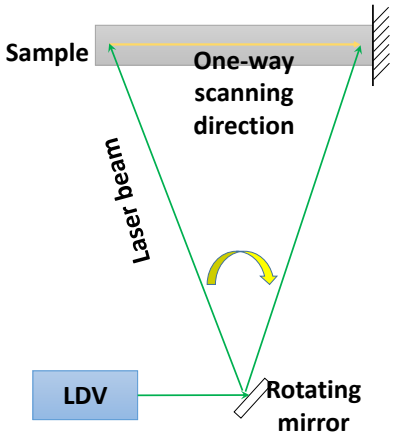

(a)

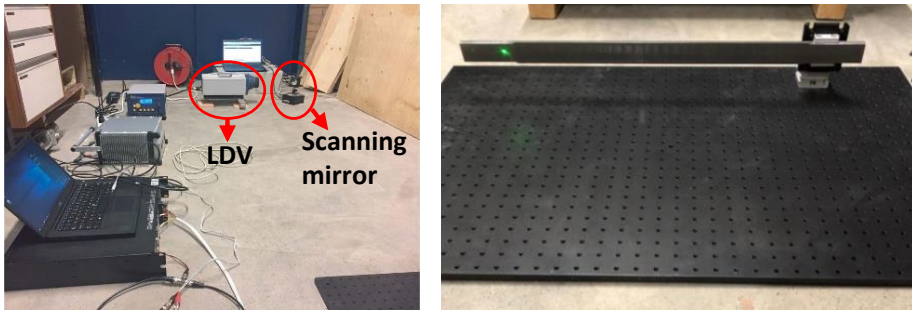

(b)

Figure 2.6: (**a**) Scheme of the physical experiments; (**b**) experimental set-up for acquiring speckle noise.

2.3.3 Single-point simulation

First, the single-point speckle noise is simulated according to the algorithm in subsection 2.2.3, since sometimes important structural nodes need constant monitoring. The frequency of the single-point vibration is simulated as 512 Hz. The simulated frequency of 512 Hz has a small difference from the experimental frequency of 500 Hz, to identify whether the speckle noise is vibration-related. In [34], the peak intervals in the FFT spectra of speckle noise are equaling to motion frequency. We also want to evaluate if the peak intervals change with the vibration frequency. The simulated focusing spot is set 700×700 μm^2 and the laser wavelength is 1.55 μm. These parameters are the same as the LDV. The size of the speckle element is 5×5 μm^2, and the sampling frequency is 102400 Hz.

Figure 2.7 presents the time series of the numerically simulated (with R_a = 0 and R_q =0.47μm) and experimentally acquired speckle noise (the single-point vibrations have been removed by subtracting from the LDV signals the vibration input), as well as the FFT spectra. The simulated series of speckle noise presents cyclical fluctuations arising from the 512 Hz vibration, and thus the noise period is 1/512 s. The experimental noise also presents a period of 0.002 s due to the 500 Hz vibration. A good agreement is visible in the FFT spectra.

The intervals between frequency spikes in the simulated spectrum are constant (512 Hz), and those in the experimental spectrum are also constant (500 Hz). Actually, these intervals equal the frequency of the spot motion [34] and thus equal the vibration frequency in this scenario. These well-agreed results demonstrate that the proposed approach is effective in simulating single-point speckle noise. However, the true vibration mixed with the speckle noise at the vibration frequency (512 Hz in the simulation and 500 Hz in the experiment). Although a bandpass filter is effective to remove other harmonics, the vibration energy would be enlarged or underestimated.

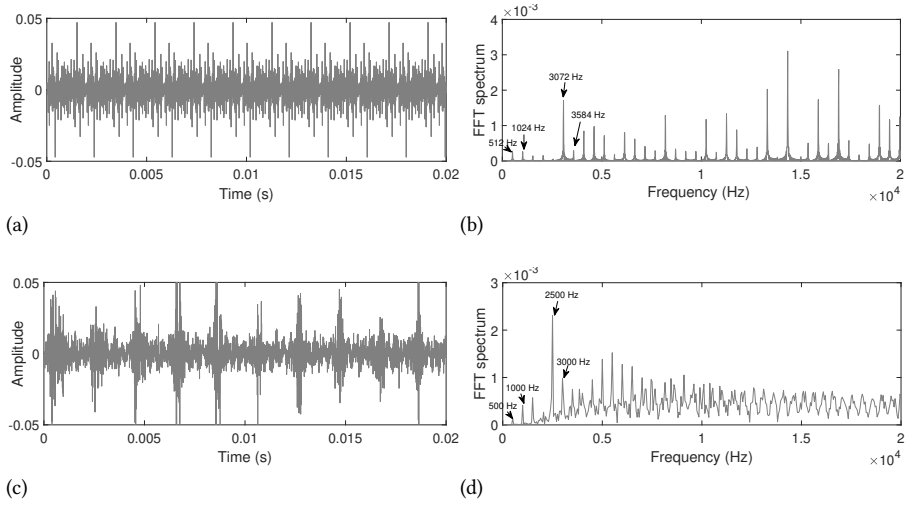

Figure 2.7: (**a**) The simulated speckle noise with R_a = 0 and R_q =0.47μm; (**b**) The FFT spectrum of **a**; (**c**) The experimental speckle noise; (**d**) The FFT spectrum of **c**.

Fig. 2.8 illustrates the probability density function (PDF) of the noise amplitude, as well as a Gaussian distribution. The simulated noise presents a similar distribution to the experimental noise, which indicates the accuracy of our simulation. The speckle noise amplitude approximately obeys a Gaussian distribution. However, the speckle noise is different from Gaussian white noise since the power spectrum is not uniformly distributed (Fig. 2.7).

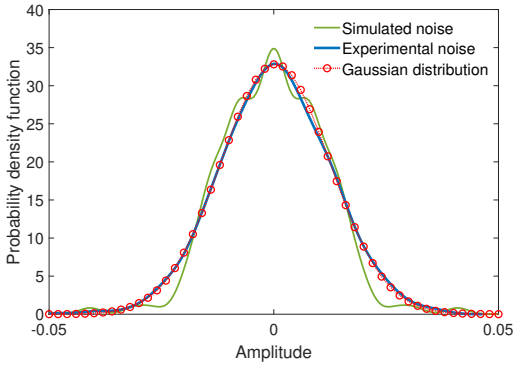

Figure 2.8: The probability density function of simulated and experimental noise, as well as a Gaussian distribution.

Fig. 2.9 presents the relationship between the surface roughness R_q and the root-mean-square (RMS) of the noise amplitude. The noise energy increases with the surface roughness when $R_q \leq R'_{qc}$, and fluctuates around a constant when $R_q > R'_{qc}$ (the critical value R'_{bc} is related to the laser wavelength). The increasing noise energy is related to the increasing variance of phase (e.g., Fig. 2.5a). Therefore, reducing the surface roughness (e.g., by polishing the surface) in small-scale measurement will significantly mitigate speckle noise.

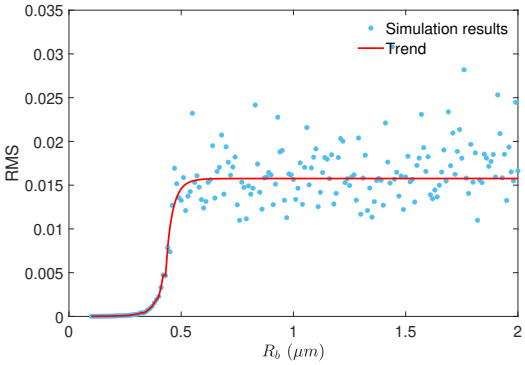

Figure 2.9: The relationship between the surface roughness R_q and RMS of the noise amplitude.

2.3.4 Continuously scanning simulation

Second, we simulate the LDVom speckle noise in continuous scanning, utilizing the algorithm in subsection 2.2.4. The simulation parameters are the same as those in subsection 2.3.3. The scanning surface is 40×540 mm^2 divided into 8000×108000 rectangle elements. The sampling frequency is 102400 Hz.

Fig. 2.10 shows the time series as well as the FFT spectra of both numerically simulated (with R_a = 0 and R_q =0.47μm) and experimentally acquired speckle noise. The scanning speed is v_s =0.1 m/s. The speckle noise appears in two forms [1], the signal drop-outs with extremely large magnitudes and the normal dominant noise with small magnitudes. For

both time series, the dominant noise energy is within magnitudes ≤ 0.005, and the signal drop-outs with large magnitudes occasionally appear. Good agreement is achieved between the FFT spectra, as the noise energy increases in the frequency domain and both spectrum curves present similar fluctuations. Different from the FFT spectra of the single-point noise, the intervals between the spikes are nonconstant since the scanning is not cyclical.

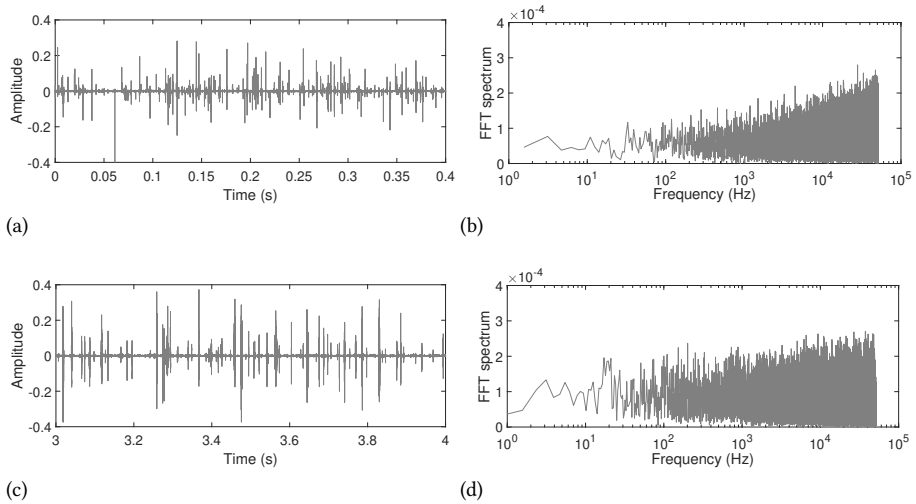

Figure 2.10: (**a**) Simulated scanning speckle noise with R_a = 0 and R_q =0.47μm; (**b**) FFT spectrum of **a**; **c**) Experimental speckle noise (zoom-in between 3 s and 4 s); (**d**) FFT spectrum of **c**. The scanning speed is v_s =0.1 m/s.

To further visualize the simulation accuracy, we conduct FFT on the frequency spectrum in Fig. 2.10, with the results presented in Fig. 2.11. The curves decrease exponentially with the increasing τ. The intervals between curve peaks are constant, 6.81×10^{-3} s and 6.78×10^{-3} s for the simulated and experimental results, respectively. These results present good agreement and thus demonstrate the accuracy of our simulation.

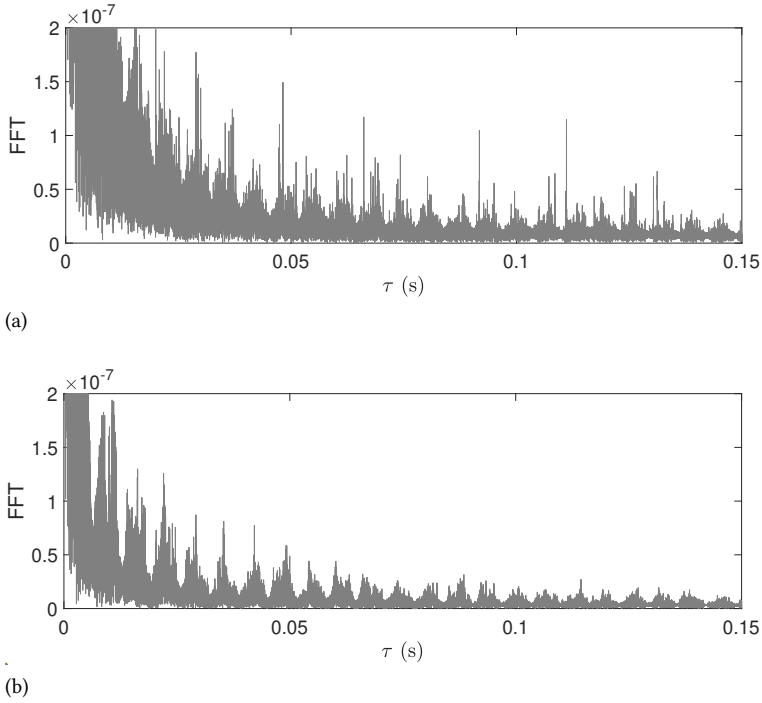

Figure 2.11: FFT on the (**a**) simulated frequency spectrum; (**b**) experimental frequency spectrum.

The PDF of the noise amplitude and a Gaussian distribution are illustrated in Fig. 2.12. The PDF curves of the simulated and experimental noise are almost identical. The scanning noise approximately obeys a Gaussian distribution, similar to the single-point noise. However, the speckle noise is different from Gaussian white noise since the power spectrum is not uniformly distributed.

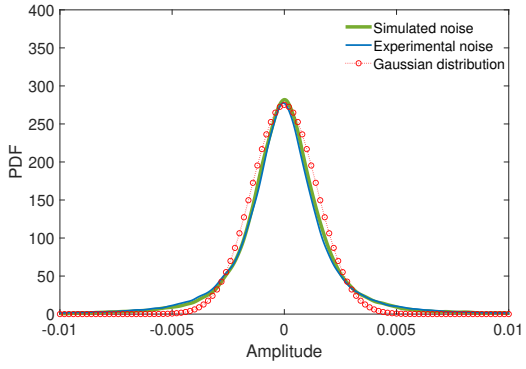

Figure 2.12: The probability density function of simulated and experimental scanning noise, as well as Gaussian distribution.

To investigate the effect of the scanning speed, we assign the parameters v_s = 1, 3, 10 m/s (f_s = 102400 Hz, R_a = 0 and R_q =0.47μm) in both numerical simulations and experiments, with the speckle noise shown in Fig. 2.13. The simulated noise presents good agreement with the experimental results. The dominant noise magnitudes increase with increasing scanning speed, but the signal drop-outs decrease in intensity and density. The magnitudes of the signal drop-outs become smaller and the signal drop-outs appear less frequently. This result is also visible in the RMS curve illustrated in Fig. 2.14, as the simulated noise energy presents an increasing trend despite fluctuations. Therefore, reducing the scanning speed can effectively mitigate the speckle-noise energy.

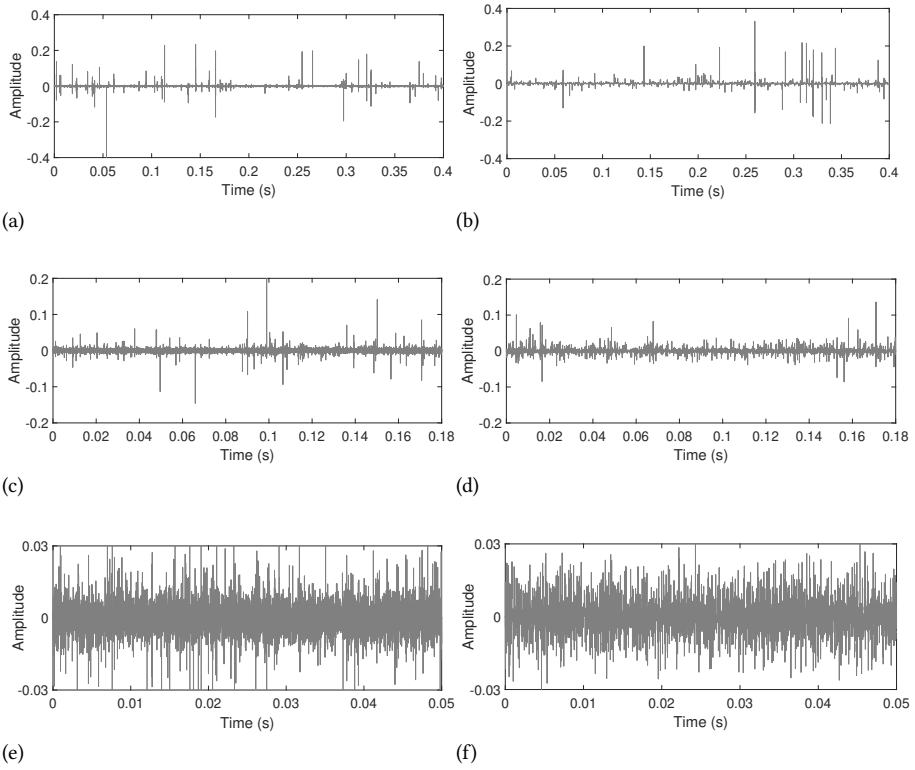

Figure 2.13: (**a**) Simulated scanning speckle noise with v_s =1 m/s; (**b**) Experimental scanning speckle noise with v_s =1 m/s; (**c**) Simulated scanning speckle noise with v_s =3 m/s; (**d**) Experimental scanning speckle noise with v_s =3 m/s; (**e**) Simulated scanning speckle noise with v_s =10 m/s; (**f**) Experimental scanning speckle noise with v_s =10 m/s.

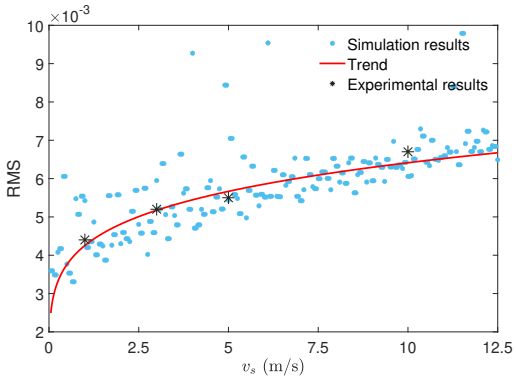

Figure 2.14: The relationship between the scanning speed v_s and RMS of the noise amplitude.

Further simulations are intended to investigate the relationship between the noise amplitude RMS and the surface roughness, as shown in Fig. 2.15. Similar to the single-point noise, the scanning noise energy increases with the surface roughness when $R_q \leq R'_{qc}$, and fluctuates around a constant when $R_q > R'_{qc}$. Therefore when additional operations on the scanning surface are convenient, reducing the surface roughness, such as polishing the surface, is an effective strategy to mitigate speckle noise.

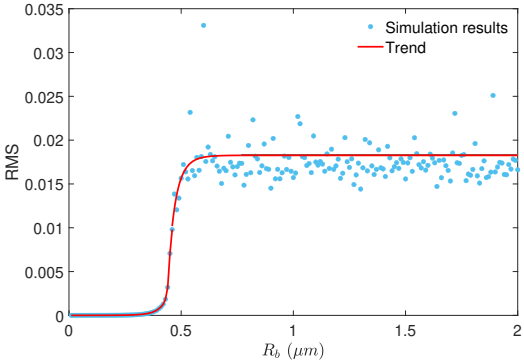

Figure 2.15: The relationship between the surface roughness R_q and RMS of the scanning noise amplitude.

2.4 Discussion

In this paper, we use a commercial LDV from Polytec (model No. RSV-150) to conduct the experiments. It could be a significant issue of our noise analysis if the demodulation system of RSV-150 alters the original signal. Therefore, we discuss some evidences regarding the outputs of the RSV-150 LDV.

Firstly, the LDV header acquires the modulation frequency according to equation (2.12). The polytec system uses an acousto-optic modulator to shift the laser frequency by a carrier frequency of 40 MHz (add 40 MHz to the modulation frequency), in order to distinguish

between movements away from and towards the detector [35, 36]. The demodulator is a PM or FM demodulator which is necessary for any LDV to acquire the Doppler frequency shift [37]. The carrier frequency and the demodulator are required for any general LDV, not only the polytec system, and these two components cannot alter the output of the Doppler frequency shift [38]. Therefore, the speckle noise output from RSV-150 is original according to equation (2.13).

Secondly, the promising consistence between our theoretical and experimental results indicate that the speckle noise output from RSV-150 is original. In both single-point and continuously scanning results, the numerically simulated and experimentally acquired speckle noise presents similar amplitude distributions, FFT spectra and energy trends. The agreement indicates that RSV-150 does not alter the original signal.

2.5 Conclusion

In this paper, we propose a novel approach for numerically simulating the speckle noise in LDVom signals, and then characterize this noise for a better understanding of the signal issue. Single-point speckle noise is also characterized since sometimes important structural nodes need constant monitoring. When investigating the statistical properties, we thoroughly consider the related factors, including the surface roughness. The complex distribution of the speckle phases is then derived. The distributions of the speckle intensity and phase agree well with the experimental results in the literature. These promising statistical properties constitute the foundation of simulating speckle noise.

The single-point and continuously scanning speckle noise are both numerically simulated and experimentally acquired, and their corresponding time-series and FFT spectra present good agreement. For the single-point speckle noise, the intervals of frequency peaks in the FFT spectra are constant and equal to the vibration frequency. The cyclical motion of the laser spot arises from the vibration, and thus the speckle noise presents the same period as the vibration. The simulated noise amplitude presents a similar distribution to the experimental result, approximating a Gaussian distribution. The noise energy increases with the surface roughness when $R_q \leq R_{qc}$, and fluctuates around a constant when $R_q > R_{qc}$. These amplitude and energy properties are also visible for continuously scanning speckle noise. In addition, the energy of the continuously scanning speckle noise increases with the scanning speed, but the signal drop-outs decrease in intensity and density. These results demonstrate the simulation accuracy, and the characteristics of the speckle noise can contribute to future research concerning despeckling procedures or noise avoidance.

Some strategies for mitigating speckle noise are supported by noise characteristics and should be investigated in future research:

i. For single-point speckle noise, the frequency spectra present harmonics that are multiples of the vibration frequency. Therefore, the true vibration is mixed with the speckle noise at the vibration frequency. Although a bandpass filter is effective in removing other harmonics, the vibration energy would be enlarged or underestimated;

ii. During continuously scanning, the noise energy increases with the scanning speed. Therefore, reducing the scanning speed can effectively mitigate speckle noise;

iii. The speckle noise energy increases with surface roughness; thus, reducing the surface roughness, such as polishing the surface, is an effective strategy to mitigate speckle noise. However, it is effective in experimental investigation but not in field measurement.

References

[1] SJ Rothberg, MS Allen, P Castellini, D Di Maio, JJJ Dirckx, DJ Ewins, Ben J Halkon, P Muyshondt, N Paone, T Ryan, et al. "An international review of laser Doppler vibrometry: Making light work of vibration measurement". In: *Optics and Lasers in Engineering* 99 (2017), pp. 11–22.

[2] HH Nassif, M Gindy, and J Davis. "Comparison of laser Doppler vibrometer with contact sensors for monitoring bridge deflection and vibration". In: *Ndt & E International* 38.3 (2005), pp. 213–218.

[3] S Sels, B Ribbens, B Bogaerts, J Peeters, and S Vanlanduit. "3D model assisted fully automated scanning laser Doppler vibrometer measurements". In: *Optics and Lasers in Engineering* 99 (2017), pp. 23–30.

[4] YF Xu, DM Chen, and WD Zhu. "Damage identification of beam structures using free response shapes obtained by use of a continuously scanning laser Doppler vibrometer system". In: *Mechanical Systems and Signal Processing* 92 (2017), pp. 226–247.

[5] MS Allen and MW Sracic. "A new method for processing impact excited continuous-scan laser Doppler vibrometer measurements". In: *Mechanical Systems and Signal Processing* 24.3 (2010), pp. 721–735.

[6] DM Chen, YF Xu, and WD Zhu. "Identification of damage in plates using full-field measurement with a continuously scanning laser Doppler vibrometer system". In: *Journal of Sound and Vibration* 422 (2018), pp. 542–567.

[7] S Rahimi, Z Li, and R Dollevoet. "Measuring with laser Doppler vibrometer on moving frame (LDVMF)". In: *AIP Conference Proceedings*. Vol. 1600. American Institute of Physics. 2014, pp. 274–286.

[8] SJ Rothberg, JR Baker, and NA Halliwell. "Laser vibrometry: pseudo-vibrations". In: *Journal of Sound and Vibration* 135.3 (1989), pp. 516–522.

[9] P Martin and S Rothberg. "Introducing speckle noise maps for laser vibrometry". In: *Optics and Lasers in Engineering* 47.3-4 (2009), pp. 431–442.

[10] Y Jin and Z Li. "Eliminating Speckle Noises for Laser Doppler Vibrometer Based on Empirical Wavelet Transform". In: *2021 13th International Conference on Measurement*. IEEE. 2021, pp. 72–75.

[11] J Vass, R Šmıd, RB Randall, P Sovka, C Cristalli, and B Torcianti. "Avoidance of speckle noise in laser vibrometry by the use of kurtosis ratio: Application to mechanical fault diagnostics". In: *Mechanical Systems and Signal Processing* 22.3 (2008), pp. 647–671.

[12] P Hosek. "Algorithm for signal drop-out recognition in IC engine valve kinematics signal measured by laser Doppler vibrometer". In: *Optics & Laser Technology* 44.4 (2012), pp. 1101–1112.

[13] P Chiariotti, M Martarelli, and GM Revel. "Delamination detection by multi-level wavelet processing of continuous scanning laser Doppler vibrometry data". In: *Optics and Lasers in Engineering* 99 (2017), pp. 66–79.

[14] Ł Pieczonka, Ł Ambroziński, WJ Staszewski, D Barnoncel, and P Pérès. "Damage detection in composite panels based on mode-converted Lamb waves sensed using 3D laser scanning vibrometer". In: *Optics and lasers in engineering* 99 (2017), pp. 80–87.

[15] J Zhu, Y Li, and R Baets. "Mitigation of speckle noise in laser Doppler vibrometry by using a scanning average method". In: *Optics letters* 44.7 (2019), pp. 1860–1863.

[16] YF Xu, DM Chen, and WD Zhu. "Modal parameter estimation using free response measured by a continuously scanning laser Doppler vibrometer system with application to structural damage identification". In: *Journal of Sound and Vibration* 485 (2020), p. 115536.

[17] JW Goodman. "Dependence of image speckle contrast on surface roughness". In: *Optics Communications* 14.3 (1975), pp. 324–327.

[18] NA Mansour, AM Abd-Rabou, AE Elmahdy, RM El-Agmy, and MM El-Nicklawy. "Dependence of speckle contrast on the light spectral broadening and the roughness root mean square". In: *Optik* 133 (2017), pp. 140–149.

[19] JW Goodman. *Statistical properties of laser sparkle patterns*. Tech. rep. STANFORD UNIV CA STANFORD ELECTRONICS LABS, 1963.

[20] J Ohtsubo and T Asakura. "Statistical properties of speckle patterns produced by coherent light at the image and defocus planes". In: *Optik* 45.1 (1976), pp. 65–72.

[21] H Fujii and T Asakura. "Effect of surface roughness on the statistical distribution of image speckle intensity". In: *Optics communications* 11.1 (1974), pp. 35–38.

[22] R Bolter, M Gelautz, and F Leberl. "SAR speckle simulation". In: *International archives of photogrammetry and remote sensing* 31 (1996), pp. 20–25.

[23] C Perreault and MF Auclair-Fortier. "Speckle simulation based on B-mode echographic image acquisition model". In: *Fourth Canadian Conference on Computer and Robot Vision (CRV'07)*. IEEE. 2007, pp. 379–386.

[24] I Yamaguchi. "Digital simulation of speckle patterns". In: *Speckle 2018: VII International Conference on Speckle Metrology*. Vol. 10834. International Society for Optics and Photonics. 2018, p. 1083409.

[25] G Di Martino, A Iodice, D Riccio, and G Ruello. "A physical approach for SAR speckle simulation: First results". In: *European Journal of Remote Sensing* 46.1 (2013), pp. 823–836.

[26] S Rothberg. "Numerical simulation of speckle noise in laser vibrometry". In: *Applied Optics* 45.19 (2006), pp. 4523–4533.

[27] JW Goodman. *Speckle phenomena in optics: theory and applications*. Roberts and Company Publishers, 2007.

[28] JC Dainty. *Laser speckle and related phenomena*. Vol. 9. Springer science & business Media, 2013.

[29] HM Pedersen. "Object-roughness dependence of partially developed speckle patterns in coherent light". In: *Optics Communications* 16.1 (1976), pp. 63–67.

[30] U Persson. "Real time measurement of surface roughness on ground surfaces using speckle-contrast technique". In: *Optics and Lasers in Engineering* 17.2 (1992), pp. 61–67.

[31] R Erf. *Speckle metrology*. Elsevier, 2012.

[32] A Cedilnik, K Kosmelj, and A Blejec. "The distribution of the ratio of jointly normal variables". In: *Metodoloski zvezki* 1.1 (2004), p. 99.

[33] NA Halliwell. "Laser vibrometry". In: *Optical Methods in Engineering Metrology*. Springer, 1993, pp. 179–211.

[34] M Martarelli and DJ Ewins. "Continuous scanning laser Doppler vibrometry and speckle noise occurrence". In: *Mechanical Systems and Signal Processing* 20.8 (2006), pp. 2277–2289.

[35] *Laser Doppler vibrometry technology from Polytec*. https://www.polytec.com/int/vibrometry/technology/laser-doppler-vibrometry. Accessed: 2022-04-04.

[36] *Polytec RSV-150*. https://www.polytec.com/int/vibrometry/products/special-application-vibrometers/rsv-150-remote-sensing-vibrometer. Accessed: 2022-04-04.

[37] A Dräbenstedt, J Sauer, and C Rembe. "Remote-sensing vibrometry at 1550 nm wavelength". In: *AIP Conference Proceedings*. Vol. 1457. American Institute of Physics. 2012, pp. 113–121.

[38] RF Strean, LD Mitchell, and AJ Barker. "Global noise characteristics of a laser Doppler vibrometer—I. Theory". In: *Optics and lasers in engineering* 30.2 (1998), pp. 127–139.

3

Mitigating speckle noise in laser Doppler vibrometer using Fourier analysis

We propose two strategies for eliminating the speckle noise in the laser Doppler vibrometer according to Fourier analysis. Fourier transform is theoretically conducted on the speckle pattern phases, whose variation dominantly contributes to the speckle noise. The calculated and experimental frequency spectrum of speckle noise both present oscillations of the frequency series (frequency peaks have constant intervals). (1) A low-pass filter can remove the noise if the vibration frequency is far lower than the first frequency peak of the noise. (2) The vibration energy can be revealed by removing the oscillating frequency trend. The physical experiments demonstrate the effectiveness of both despeckling strategies.

3.1 Introduction

A laser Doppler Vibrometer (LDV) is an optical instrument extensively applied for non-contact vibration measurement [1, 2, 3]. Superior to attaching transducers, the LDV offers remote vibrometry (e.g., from a high-temperature surface) and avoids mass-loading undesired for light structures [4]. Precise measurements in time and frequency domains are available [5], as an LDV achieves the measuring frequency of 1 GHz and spatial resolution of 1 mm/s. In addition, the LDV on moving platforms (LDVom) [6] can one-way continuously scan the vibrating surface and monitoring the structures, especially those large or long like railway tracks.

A significantly concerned issue, speckle noise [7, 8], that continuously buries the vibration signals becomes extremely troublesome in LDVom signals. The signal dropouts can exceed 40 times the vibration amplitude, and the dominant noise reduces the signal-to-noise ratio (SNR) to -15 db [9]. With periodic scanning, the speckle noise becomes

This chapter is based on the paper: Jin, Y., & Li, Z. (2022). Mitigating speckle noise in a laser Doppler vibrometer using Fourier analysis. Optics Letters, 47(18), 4742-4745.

pseudo-random, as its components centralize at the scanning frequency and distribute in the relevant harmonics [10]. This situation is convenient to handle by avoiding the coincidence of the scanning and vibration frequencies [11]. The difficulty in noise removal increases by one-way scanning, as the noise randomly distributes in time and frequency domains. Thus classic signal processing approaches, such as band-pass filters and wavelet transform, lose their denoising effects without additional strategies. Numerous methods for eliminating the speckle noise have been developed in recent researches; however, they are inappropriate to handle LDVom signals. For example, calculating the vibration energy can average the noise effect and identify defect locations [12, 13], but disregards the waveforms crucial to the modal analysis. The moving average approach developed in [14] requires a scanning frequency much larger than the vibration frequency. Enhancing the surface reflection can mitigate the speckle noise [15] but is inapplicable in large-scale measurements. Physical characteristics of the speckle noise can instruct despeckling procedures and thus should arouse research concerns.

An optical phenomenon, laser speckle patterns produced by the coherent laser beams scattering from an optically rough surface, is the origin of the LDV speckle noise [10]. The surface deviations at the laser-wavelength scale induce the variant phases of incident wavelets. The reflected wavelets interfere constructively or destructively, producing bright or dark spots that constitute a speckle pattern. It generates intense noise when the photodetector translates or deforms. Statistical analysis and Fourier analysis have been utilized to characterize the speckle patterns [16, 17, 18, 19]; but to our best knowledge, most former researches concentrate on the light intensity, contrast and relationships with surface roughness. The variation of the resultant phase in the photodetector dominantly contributes to the speckle noise, but the relevant theoretical analysis stagnates in the simplified statistical properties. Fourier analysis can characterize the noise spectrum and promote corresponding de-speckle approaches, which should be subjected to researches.

In this letter, we propose two novel strategies for eliminating the speckle noise in the LDVom signals according to Fourier properties. Fourier analysis is theoretically conducted on the variation of the speckle phases. The despeckling approaches are developed according to the derived frequency spectrum and then evaluated with physical experiments.

3.2 Method

An LDV acquires the surface vibration according to the Doppler frequency shift. The principal optical element of an LDV is an electronic interferometer, where the reference laser beam is coherent with that diffusely reflected from the rough surface. The difference between the detected and reference laser frequencies (f_d & f_r) derives the measured vibration velocity v_m [20].

$$v_m = \frac{\lambda}{2}(f_r - f_d) = \frac{\lambda}{4\pi}(2\pi f_r - \frac{d\varphi_d}{dt}) = v - \frac{\lambda}{4\pi}\frac{d\varphi_{res}}{dt} \tag{3.1}$$

where $\varphi_d = 2\pi(f_r t - 2vt/\lambda + \varphi_{res}/2\pi)$ is the detected laser phase and λ is the laser wavelength. The acquired vibration v_m deforms from the true vibration v by the phase variation $-\lambda d\varphi_{res}/(4\pi dt)$, namely the LDV speckle noise. The resultant phase φ_{res} arises from the laser speckle patterns illuminated inside the photodetector. Therefore, the variation of speckle patterns relevant to photodetector translation produces unwanted speckle noise.

A speckle pattern $\mathcal{P}$ is the phasor summation of the coherent wavelets reflected from a rough surface [20]

$$\mathcal{P} = \sum_{n=1}^{N} a_n e^{j\phi_n} = \mathcal{R} + j\mathcal{I} \tag{3.2}$$

where N is the number of scattered wavelets, a_n is the wavelet amplitude, ϕ_n is the wavelet phase, j represents the imaginary unit, and $\mathcal{R}$ and $\mathcal{I}$ represent the real and imaginary parts respectively. The phase $\varphi = tan^{-1}\mathcal{I}/\mathcal{R}$ and intensity $I = \mathcal{R}^2 + \mathcal{I}^2$ of the speckle pattern approximately obey the uniform and exponential distributions, respectively [20]. Considering that the transmission laser illuminates κ speckle patterns (each with the phase $\varphi_s(\alpha,\beta)$ and intensity $I_s(\alpha,\beta)$, (α,β) is the coordinate) and the reference beam retains the original phasor, the resultant phase φ_{res} can be expressed as [20]

$$tan\varphi_{res} = \frac{\sum_\alpha \sum_\beta \sqrt{I_s(\alpha,\beta)} sin(\varphi_s(\alpha,\beta) - \varphi_r)}{\sum_\alpha \sum_\beta \sqrt{I_s(\alpha,\beta)} cos(\varphi_s(\alpha,\beta) - \varphi_r)} \tag{3.3}$$

where φ_r is the phase of the reference beam. Fourier analysis provides the frequency spectrum for characterizing the signals and mitigating the noise. The Fourier transform on the speckle noise can be conducted as

$$\begin{aligned} F(\omega) &= \mathcal{F}(-\frac{\lambda}{4\pi}\frac{d\varphi_{res}}{dt}) = -j\frac{\lambda\omega}{4\pi}\mathcal{F}(\varphi_{res}) = -j\frac{\lambda\omega}{4\pi}\mathcal{F}(sin^{-1}(x)) \\ &= -j\frac{\lambda\omega}{4\pi}\mathcal{F}(\sum_0^\infty \frac{(2n-1)!!}{(2n)!!}\frac{x^{2n+1}}{2n+1}) \end{aligned} \tag{3.4}$$

where $F(\omega)$ is the frequency function, $x = sin\varphi_{res}$ is derived from Eq. (3.3), $\mathcal{F}$ represents Fourier transform, $\omega = 2\pi f/f_s$ is the angular frequency, f is the ordinary frequency, and f_s is the sampling frequency. The last expression in Eq. (3.4) uses the Maclaurin series. The module $|F(\omega)|$ represents the frequency spectrum with its calculation related to the autocorrelation function. During LDV scanning, the neighbouring-sampled spots share numerous overlapped speckle patterns, which enhance the autocorrelation property. Assuming an infinite scanning series with random speckle patterns, the autocorrelation function of $sin^{-1}(x)$ is written as

$$
\begin{aligned}
R_{\varphi,\varphi}(t) =& R_{\varphi,\varphi}[\sum_{0}^{\infty}\frac{(2n-1)!!}{(2n)!!}\frac{x^{2n+1}}{2n+1}] \\
=& \sum_{p,q} C_{p,q}\frac{1}{\bar{I}_s^{\,p+q}}E((\sum sin(\varphi_s(\alpha,\beta)-\varphi_r))^p \\
& \times(\sum sin(\varphi_s(\alpha+v_st,\beta)-\varphi_r))^q) \\
=& \sum_{p,q} C_{p,q}\frac{1}{\bar{I}_s^{\,p+q}}(E(\sum_{k} sin^{p+q}(\varphi_{s_k}-\varphi_r)) \\
& + E(\sum_{e}\prod_{b=1}^{p+q} sin(\varphi_{s_{e,b}}-\varphi_r))) \\
=& \sum_{p,q} C_{p,q}\frac{1}{(2\bar{I}_s)^{p+q}}\binom{p+q}{(p+q)/2}\frac{\kappa}{\pi L^2} \\
& \times(2L^2 cos^{-1}(\frac{v_st}{L}) - 2\sqrt{v_s^2t^2(L^2-v_s^2t^2)})
\end{aligned}
\tag{3.5}
$$

where $\bar{I}_s$ is the I_s average, v_s is the scanning speed (the speed of the focusing spot moving on the target surface; assumed along the direction of α), $E(\cdot)$ calculates the statistical expected value, $\sum_k \cdot$ represents the summation on overlapped speckles between the positions of (α,β) and $(\alpha+v_st,\beta)$, $\sum_e \cdot$ represents the other summations, L is the diameter of the focusing spot, $C_{p,q} = ((p-2)!!(q-2)!!)/(pq(p-1)!!(q-1)!!)$, and p,q are odd. The component $E(\sum_e\prod_b \cdot)$ equals to 0 for an infinite time-series according to the uniform distribution of φ_s, while the component $E(\sum_k \cdot)$ is proportional to the overlapped spot area between time 0 and t. The last expression of equation (3.5) is based on $t \le L/v_s$, and $R_{\varphi,\varphi}(t)$ equals to 0 with $t > L/v_s$ because of none overlapped speckle patterns. Therefore, the frequency spectrum can be written as

$$
\begin{aligned}
|F(\omega)| &= \frac{\lambda\omega}{4\pi}\sqrt{|\mathcal{F}(R_{\varphi,\varphi}(t))|} \\
&= \frac{\lambda\kappa\omega}{4\pi^2L^2}\sqrt{\xi|\mathcal{F}(2L^2cos^{-1}(\frac{v_st}{L}) - 2L^2\sqrt{(\frac{v_st}{L})^2(1-(\frac{v_st}{L})^2)})|} \\
\xi &= \sum_{p,q} C_{p,q}\frac{1}{(2\bar{I}_s)^{p+q}}\binom{p+q}{(p+q)/2}, \quad p,q \text{ are odd}
\end{aligned}
\tag{3.6}
$$

Equation (3.6) provides the significant curve trend of the speckle-noise spectrum, and the actual spectrum should contain fluctuations owing to the finite scanning series. Fig. 3.1 illustrates both the theoretical and the experimental trends of the frequency spectrum. The frequency curve calculated by equation (3.6) oscillates with constant intervals (1024 Hz) between frequency peaks. With the physical experiments, the trend of the frequency curve also presents constant intervals (820 Hz) between the frequency peaks. The experimental spectrum does not present an increasing trend because of the residual low-frequency vibration of the structure. The interval between frequency peaks is theoretically v_s/L in (3.6), but the physical meaning of this value still needs investigation. According to this property, two strategies can be developed to mitigate the speckle noise: (1) a low-pass

filter (LPF) is enough if the vibration frequency is far lower than the first frequency peak $v_s/2L$, and (2) adaptively removing the oscillation trend from the frequency spectrum can reveal the actual vibration energy. The trend of the frequency curve in a short window $f \in [f_\tau - f_0, f_\tau + f_0]$ approximates a sinusoid; thus, Eq. (3.7) provides an optimization method to pointwisely fit the trend of the frequency curve with the oscillation period v_s/L.

$$\begin{aligned} &\min_{a_0,b_0,\varphi} \quad (y_t(f) - y(f))^2 \\ &s.t. \quad y_t(f) = a_0 e^{b_0 f} sin(\frac{v_s}{L} f + \varphi) \\ &a_0,\ b_0 \in [-\infty, \infty],\ \varphi \in [0, 2\pi],\ f \in [f_\tau - f_0, f_\tau + f_0] \\ &\text{Output: } y_t(f_\tau) \end{aligned} \tag{3.7}$$

where, $y_t(f)$ is the optimized curve trend in the moving window $f \in [f_\tau - f_0, f_\tau + f_0]$, $2f_0$ is the window length, and the frequency curve trend at each point f_τ is acquired by this optimization.

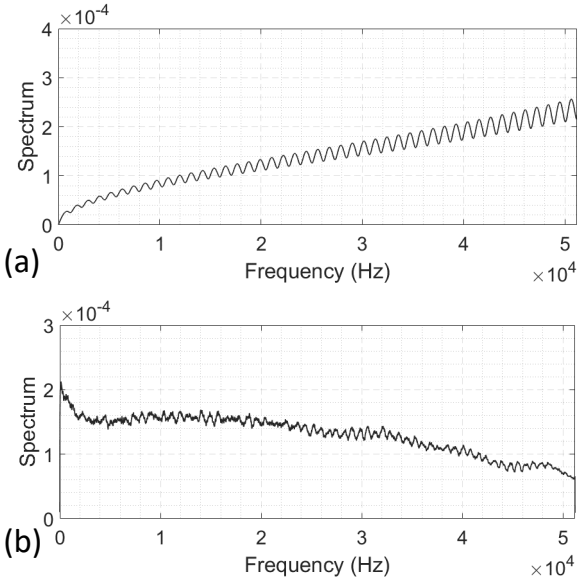

Figure 3.1: (a) The frequency spectrum trend of the speckle noise calculated by equation (3.6). (b) The frequency spectrum trend of the experimental speckle noise.

3.3 Results

Two experiments are conducted to evaluate the two de-speckle strategies, respectively. Fig. 3.2 presents the experimental scheme. An LDV transmits laser beams deflected by the rotating mirror onto the surface of a steel strip. By controlling the mirror, the focusing spot moves along the scanning direction, and we keep the basic concept of LDVom, one-way continuously scanning for one time. The steel strip is mounted as a cantilever beam with the

end excited by a shaker. The artificial excitation is predefined as a 500 Hz sinusoidal wave for conveniently evaluating the despeckling result. The first experiment is intended to test the LPF when the vibration frequency is lower than $v_s/2L$. Three scanning speeds of 20 m/s, 10m/s and 0.1 m/s are compared, with $v_s/2L$ = 15 kHz, 7.5 kHz and 75 Hz respectively. The sampling frequency is 102,400 Hz.

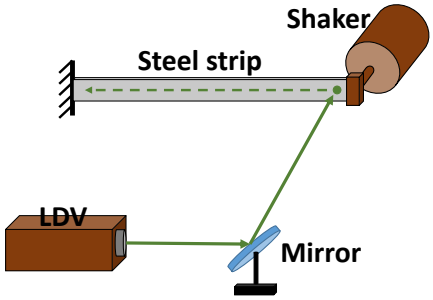

Figure 3.2: The scheme of experiments.

Figure 3.3 illustrates the original vibration signals and the despeckling results. The noise intensely fluctuates to distort the vibrations, and numerous signal drop-outs appear. As aforementioned, we feed the signals into a LPF with the cutoff frequency of 700 Hz. With v_s = 20 m/s and 10 m/s, the despeckling result has revealed the vibration around 500 Hz with time-variant amplitudes. The vibration curve visibly agrees well with the original signal trend, and the SNR increases 21.25 db and 16.75 db respectively. These indicate the de-speckle effectiveness. However, with v_s = 0.1 m/s, the LPF result preserves numerous distortions (marked with blue circles) arising from the speckle noise, and the SNR only increases 10.81 db. Therefore, the LPF is effective to eliminate the speckle noise if we control the scanning speed $v_s > 2Lf_v$ in the experiments, where f_v is the vibration frequency.

The second experiment is designed to evaluate the other despeckling strategy, first extracting the oscillation trend (Eq. (3.7)) of the frequency curve and then removing this trend to acquire the actual vibration energy. The scanning speed is 0.1 m/s, and the sampling frequency is 102400 Hz. The calculated frequency-peak interval of the Fourier spectrum is v_s/L = 150 Hz. Two signal segments with weak and extremely weak vibrations are analyzed by the proposed approach.

Figure 3.4 illustrates the signals with vibration amplitudes around 0.05 and the corresponding Fourier spectrum. The vibration mode is visible in the Fourier spectrum. The original signal between 5.25 s and 5.3 s contains intense noise which nearly buries the vibrations. The LPF has poor performance in this situation as the intense noise results in large amplitude distortions (Fig. 3.3 (c)). First we calculate the spectrum trend according to Eq. (3.7). Despite the intensive fluctuations, the spectrum fits well with the approximated trend (Fig. 3.4 (a)). Then, we cut off the spectrum with the trend and calculate the 500 Hz amplitude equalling 0.0481. If the spectrum is not cut off, the 500 Hz amplitude is 0.0514 with a 7% error, which would affect precise measurements. The signal time series is

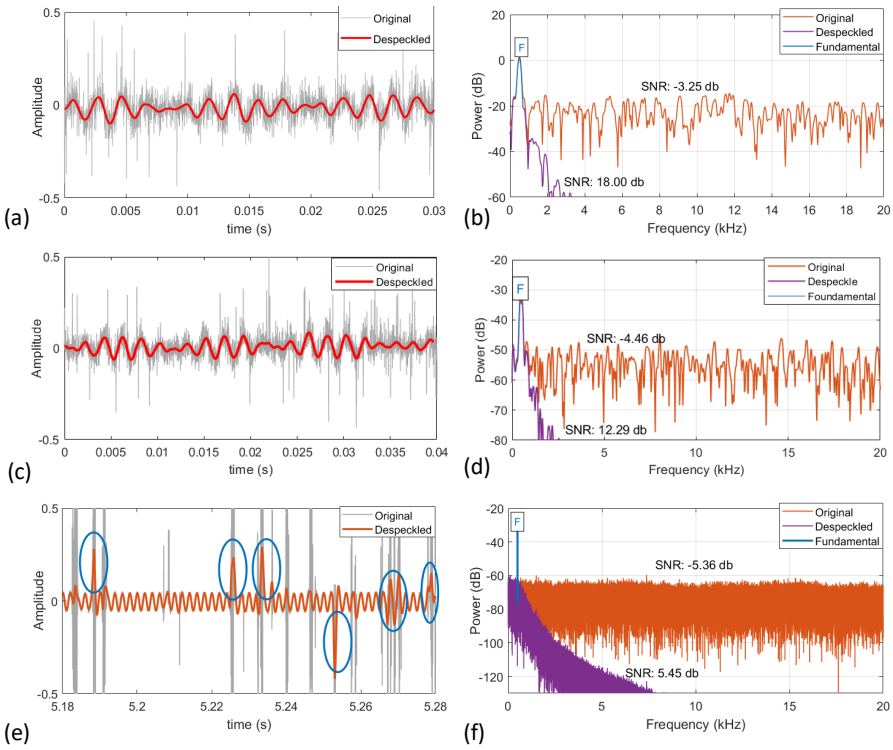

Figure 3.3: (a) The original and despeckled signals with v_s = 20 m/s. (b) The corresponding power spectrum of (a). (c) The original and despeckled signals with v_s = 10 m/s. (d) The corresponding power spectrum of (c). (e) The original and despeckled signals with v_s = 0.1 m/s. (f) The corresponding power spectrum of (e).

then reconstructed with the initial phase and the revealed amplitude. It has revealed the vibration around 500 Hz, indicating the effectiveness in eliminating the speckle noise.

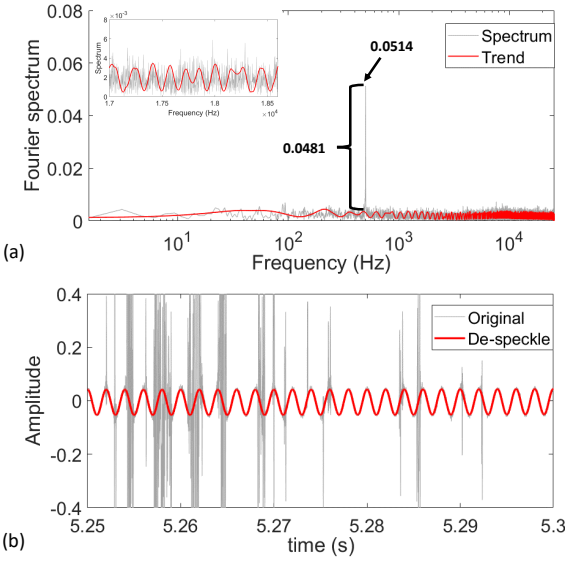

Figure 3.4: (a) Fourier spectrum and the trend. (b) The original signal and the despeckling result between 5.25 s and 5.3 s.

Figure 3.5 illustrates the signals with extremely weak vibrations (amplitudes around 0.004) and the corresponding Fourier spectrum. The original signal between 4 s and 4.05 s contains intense noise. Similar to the aforementioned, the frequency curve presents the trend with frequency-peak intervals of 150 Hz. The 500 Hz amplitude after cutting off the spectrum trend remains 0.00397. If the spectrum is not cut off, the 500 Hz amplitude is 0.00498 with a 25% error, which is unacceptable. The reconstructed time series reveals the 500 Hz vibration, which fits well with the acquired signals. Therefore, the second despeckling strategy is effective regardless of the vibration intensity.

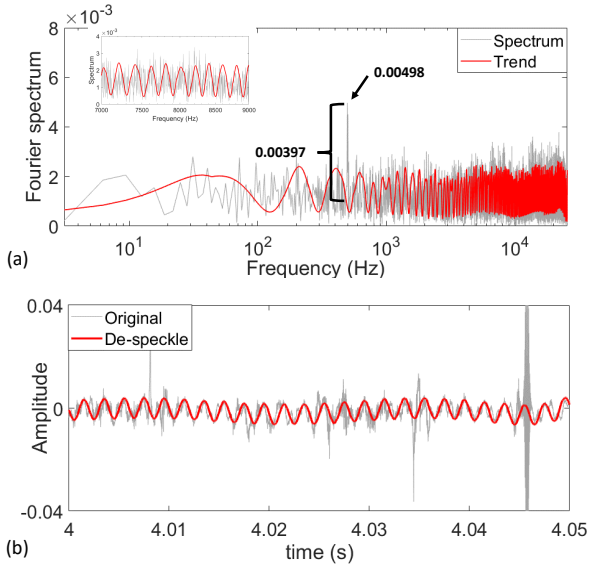

Figure 3.5: (a) Fourier spectrum and the trend. (b) The original signal and the despeckling result between 4 s and 4.05 s.

3.4 Conclusion

In summary, two novel despeckling strategies have been proposed in this letter according to Fourier properties. By theoretically conducting Fourier transform on the variation of the speckle phases, the frequency spectrum of the speckle noise presents oscillations with constant frequency-peak intervals. This agrees well with the experimental spectrum trend. Therefore, (1) a LPF can remove the noise if the vibration frequency is far lower than the first frequency peak of the speckle noise, and (2) the vibration energy can be revealed by removing the oscillating frequency trend. The corresponding experiments have indicated that the two strategies based on Fourier analysis are effective in eliminating the speckle noise.

For the first strategy, the scanning speed should be the largest possible one according to Fig. 3.1, so that the noise level at f_v is lowest. However, the scanning speed is also limited by the equipment ability, the scanning resolution required (e.g., if the resolution is 0.1 mm and the sampling frequency is 0.1 MHz, then the maximum scanning speed is 10 m/s) and so on. Therefore, the scanning speed is carefully chosen in real applications. Future development of digital equipment can improve the scanning ability.

We also want to mention that an infinite scanning series with random speckle patterns is assumed in theoretical analysis. This assumption would not affect the first strategy since the noise level is quite low with the frequency less than $v_s/2L$. However, in the real situation with small-scale measurement, more fluctua- tions will appear in addition to the oscillating Fourier spectrum of speckle noise (Fig. 3.1). Thus the second strategy, which only remove the oscillating spectrum, will be affected.

In the future applications, a LPF unit can be installed between the LDV and the signal

acquisition instrument with fast scanning $v_s > 2Lf_v$. If the scanning speed limited by the equipment is improved, this strategy is more effective due to the simple LPF unit and possible realization of real-time despeckling. With $v_s \leq 2Lf_v$, the second strategy can complement the despeckling procedure in post-processing. However, this strategy is less effec- tive with short time series or too many vibration modes. A more applicable strategy for short time series and many vibration modes should be investigated in future work.

References

[1] S Sels, S Vanlanduit, B Bogaerts, and R Penne. "Three-dimensional full-field vibration measurements using a handheld single-point laser Doppler vibrometer". In: *Mechanical Systems and Signal Processing* 126 (2019), pp. 427–438. DOI: 10.1016/j.ymssp.2019.02.024. URL: https://www.sciencedirecta.com/science/article/abs/pii/S0888327019301074.

[2] Y Fu, M Guo, and PB Phua. "Spatially encoded multibeam laser Doppler vibrometry using a single photodetector". In: *Optics letters* 35.9 (2010), pp. 1356–1358. DOI: 10.1364/OL.35.001356. URL: https://www.osapublishing.org/ol/abstract.cfm?uri=ol-35-9-1356.

[3] T Miles, M Lucas, and S Rothberg. "Bending vibration measurement on rotors by laser vibrometry". In: *Optics letters* 21.4 (1996), pp. 296–298. DOI: 10.1364/OL.21.000296. URL: https://www.osapublishing.org/ol/abstract.cfm?uri=ol-21-4-296.

[4] P Castellini, M Martarelli, and EP Tomasini. "Laser Doppler Vibrometry: Development of advanced solutions answering to technology's needs". In: *Mechanical systems and signal processing* 20.6 (2006), pp. 1265–1285. DOI: 10.1016/j.ymssp.2005.11.015. URL: https://www.sciencedirect.com/science/article/pii/S0888327005002220.

[5] L Chen, D Zhang, Y Zhou, C Liu, and S Che. "Design of a high-precision and noncontact dynamic angular displacement measurement with dual-Laser Doppler Vibrometers". In: *Scientific reports* 8.1 (2018), pp. 1–11. DOI: 10.1038/s41598-018-27410-4. URL: https://www.nature.com/articles/s41598-018-27410-4.

[6] S Rahimi, Z Li, and R Dollevoet. "Measuring with laser Doppler vibrometer on moving frame (LDVMF)". In: *AIP Conference Proceedings*. Vol. 1600. American Institute of Physics. 2014, pp. 274–286.

[7] SJ Rothberg, JR Baker, and NA Halliwell. "Laser vibrometry: pseudo-vibrations". In: *Journal of Sound and Vibration* 135.3 (1989), pp. 516–522.

[8] SJ Rothberg, MS Allen, P Castellini, D Di Maio, JJJ Dirckx, DJ Ewins, Ben J Halkon, P Muyshondt, N Paone, T Ryan, et al. "An international review of laser Doppler vibrometry: Making light work of vibration measurement". In: *Optics and Lasers in Engineering* 99 (2017), pp. 11–22.

[9] Y Jin and Z Li. "Eliminating Speckle Noises for Laser Doppler Vibrometer Based on Empirical Wavelet Transform". In: *2021 13th International Conference on Measurement*. IEEE. 2021, pp. 72–75.

[10] P Martin and S Rothberg. "Introducing speckle noise maps for laser vibrometry". In: *Optics and Lasers in Engineering* 47.3-4 (2009), pp. 431–442.

[11] M Martarelli and DJ Ewins. "Continuous scanning laser Doppler vibrometry and speckle noise occurrence". In: *Mechanical Systems and Signal Processing* 20.8 (2006), pp. 2277–2289.

[12] Ł Pieczonka, Ł Ambroziński, WJ Staszewski, D Barnoncel, and P Pérès. "Damage detection in composite panels based on mode-converted Lamb waves sensed using 3D laser scanning vibrometer". In: *Optics and lasers in engineering* 99 (2017), pp. 80–87.

[13] P Chiariotti, M Martarelli, and GM Revel. "Delamination detection by multi-level wavelet processing of continuous scanning laser Doppler vibrometry data". In: *Optics and Lasers in Engineering* 99 (2017), pp. 66–79.

[14] J Zhu, Y Li, and R Baets. "Mitigation of speckle noise in laser Doppler vibrometry by using a scanning average method". In: *Optics letters* 44.7 (2019), pp. 1860–1863.

[15] YF Xu, DM Chen, and WD Zhu. "Modal parameter estimation using free response measured by a continuously scanning laser Doppler vibrometer system with application to structural damage identification". In: *Journal of Sound and Vibration* 485 (2020), p. 115536.

[16] JW Goodman. *Statistical properties of laser sparkle patterns*. Tech. rep. STANFORD UNIV CA STANFORD ELECTRONICS LABS, 1963.

[17] JW Goodman. "Dependence of image speckle contrast on surface roughness". In: *Optics Communications* 14.3 (1975), pp. 324–327.

[18] SJ Kirkpatrick, DD Duncan, and EM Wells-Gray. "Detrimental effects of speckle-pixel size matching in laser speckle contrast imaging". In: *Optics letters* 33.24 (2008), pp. 2886–2888. DOI: 10.1364/OL.33.002886. URL: https://www.osapublishing.org/ol/abstract.cfm?uri=ol-33-24-2886.

[19] JC Dainty. *Laser speckle and related phenomena*. Vol. 9. Springer science & business Media, 2013.

[20] JW Goodman. *Speckle phenomena in optics: theory and applications*. Roberts and Company Publishers, 2007.

4

Removing speckle noise from the signals of a laser Doppler vibrometer on moving platforms (LDVom) by ensemble empirical mode decomposition

With increasing requirements for structural stability and durability, effective monitoring strategies for existing and potential damage are necessary. A laser Doppler vibrometer on moving platforms (LDVom) can remotely capture large-scale structural vibrations, but speckle noise, a significant signal issue mainly when one-way continuously scanning from moving platforms, restricts its applications. A novel approach based on ensemble empirical mode decomposition (EEMD) is proposed to eliminate speckle noise. Moving root-mean-square (MRMS) thresholds are used to cut off signal drop-outs. With both numerically simulated and experimentally acquired signals, the proposed EEMD-based approach reveals the true vibrations despite the low initial signal-to-noise ratio (SNR). Other methods fail to eliminate the speckle noise. In physical experiments, the despeckled signal energy is concentrated at defect locations in the Hilbert-Huang spectrum. The identified damage locations agree well with the actual damage locations. Therefore, the developed approach demonstrates advantages and robustness of eliminating speckle noise in LDVom signals for damage inspection.

This chapter is based on the paper: Jin, Y., Dollevoet, R., & Li, Z. (2022). Removing speckle noise from the signals of a laser Doppler vibrometer on moving platforms (LDVom) by ensemble empirical mode decomposition. Measurement Science and Technology, 33(12), 125205.

4.1 Introduction

Structures deteriorate owing to mechanical loading and the consequent damage [1]. Although the evolution of materials [2] and construction technologies [3] has improved durability, long-term fatigue inevitably results in material defects threatening safe operation [4]. Therefore, an effective monitoring strategy is necessary for discovering damage, especially in the early stages. Modal analysis of structures under excitation is extensively applied to characterize the damage [5] [6], promoting the development of the needed instruments. Mainstream contact-measurement techniques, including contact sensors and ultrasound detectors, have been successful in scientific research and industrial applications [7] [8], but the drawbacks of adding unnecessary masses and thus possibly changing modes have aroused numerous concerns. In addition, the contact sensors are inconvenient for measuring locations that are difficult to reach and scanning very long structures such as railway tracks at high speed. Therefore, noncontact technologies for acquiring vibration signals have been the subject of recent research.

A laser Doppler vibrometer (LDV) is a noncontact and nondestructive instrument for capturing the vibration velocity of object surfaces [9]. This instrument is based on Doppler effect, as the target vibration results in a frequency shift between the emitted and reflected laser beams [10]. It is worth noting that an LDV is appropriate for high-frequency and high-precision analysis, as its measuring frequency can be over 1 GHz and the geometric resolution of the vibration velocity can reach 1 mm/s. Recently, the LDV measurement systems have been demonstrated to be effective in laboratory experiments for vibration analysis (e.g., [11] [12]). However, the researches hardly applied LDV systems in monitoring large-scale structures, e.g., railway tracks, owing to the limitations of measurement techniques and signal quality [10] [13].

Major LDV measurement techniques includes a single-point LDV, a scanning LDV (SLDV), and a continuous SLDV (CSLDV), which are summarized in [10], but these techniques are not suitable for large-scale measurement. A single-point LDV [14] only acquires vibrations at one point, and the setup should move when measuring another point. The SLDV measurement [15, 16, 17, 18] is an ensemble of single-point measurements with the setup simplified by rotating mirrors. However, it requires long-time acquisition at each point, which is time-consuming. A CSLDV continuously scans the vibrating surface, but it requires multiple reciprocating or cyclical scans for modal analysis [19, 20, 21, 22, 23]. In addition, SLDV and CSLDV need cyclical excitation, and thus the mode would not change during measurement. However, reciprocating or cyclical scans and cyclical artificial excitation cannot be realized in large-scale measurements. In contrast, an LDV on moving platforms (LDVom) [24] can one-way continuously scan the sample surface, especially those long structures like railway tracks. This technique is totally different from the previous ones (compared in Table 4.1) and provides the possibility for large-scale measurements. However, improving signal quality becomes a primary task for the LDVom [24].

Speckle noise is a significant issue polluting the signals, which should be a priority in signal processing [10] [13] [25]. This noise is physically generated by the variation of laser speckle patterns, as introduced in subsection 4.2.1. Therefore, the variation rate affected by measurement techniques and the laser speckle patterns affected by laser wavelength and surface roughness [26] are the all influencing factors of speckle noise. This is not a noise

generated by the instrumental units but by the laser beams [27]. For the single-point LDV or SLDV, speckle noise is extremely weak [9] since the variation rate of laser speckle patterns is nearly 0. In CSLDV measurements, the noise level increases, but the noise becomes pseudo-random since the signal spectrum consists of harmonic sidebands centering at the vibration frequency and spacing by the scanning frequency [10, 25]. Some strategies, such as the energy-based approaches [28], a scanning-average method [29], and polishing the vibrating surface [30],are effective in mitigating CSLDV speckle noise.

However, the aforementioned strategies are unsuitable to handle LDVom speckle noise: (1) with one-way measurement, the time series becomes crucial in addition to the energy spectrum. This is because only one measuring sample containing the vibration amplitude and phase at each point is acquired; (2) the scanning-average method can only be used to handle cyclical measurements like the CSLDV. LDVom signals cannot be averaged since the signals only contain the instantaneous vibration at each measuring point; (3) polishing the vibrating surface is unsuitable in large-scale measurement (e.g., the railway tracks over 1,000 km). Besides, in physical experiments, the noise amplitudes can exceed 30 times that of the true vibration, and the signal-to-noise ratio (SNR) can drop below -15 dB [31]. To handle the severe noise and improve the signal quality, an effective approach for removing LDVom speckle noise remains to be found.

Empirical mode decomposition (EMD) is a self-adaptive approach proposed by Huang et al. [32] for nonlinear and nonstationary signal analysis. It decomposes signals into multiple intrinsic mode functions (IMFs) containing instantaneous frequency information, and thus, the corresponding Hilbert transform has physical meaning. Differing from the wavelet transform and bandpass filters (BPFs) with certain bandwidths, the bandwidth of EMD is naturally determined by the signal itself. Since IMFs correspond to local modal responses, the decomposition results and Hilbert-Huang spectrum can highlight the abnormal local modes for defect inspection [33] [34]. In addition, EMD has the potential to eliminate distortions by noise and to preserve the actual oscillations, since each IMF presents continuity of the instantaneous frequencies. Numerous studies have developed EMD-based approaches for eliminating the environmental and instrumental noise of, e.g., lidar signals [35], electrocardiography signals [36] and seismic signals [37]. Nonetheless, speckle noise is much more complicated, as frequent signal drop-outs exceed multiple times normal amplitudes and dominant noise components continuously distort actual oscillations. To the best of our knowledge, no research has utilized EMD for LDV speckle noise removal. Mode mixing is a significant issue affecting IMF components when applying EMD, and thus Wu & Huang [38] developed ensemble empirical mode decomposition (EEMD) assisted by white noise to address this problem.

In this paper, we propose an EEMD-based approach for speckle noise removal in LDVom signals. The despeckling effect is evaluated in both numerically synthesized and experimentally acquired signals. The remainder of this paper is organized as follows: section 4.2 introduces the LDV system and the despeckling algorithm; section 4.3 investigates the applicability of the developed approach in simulated signal analysis; section 4.4 analyzes the experimentally acquired signals for defect inspection; and section 4.5 discusses and concludes this paper.

Table 4.1: Comparson between different LDV measurement techniques

LDV technique	Measurement strategy	Excitation source	Noise level	De-noise approach
Single-point	single-point	No requirement	weak	No need
SLDV	pointwise	cyclical	weak	No need
CSLDV	cyclical continuous scan	cyclical	medium	Energy-based, averaging, polishing surface
LDVom	one-way continuous scan	No requirement	intense	Not applicable

4.2 Methodology

4.2.1 Speckle noise and its simulation

Speckle noise, or 'pseudo vibration' [39], is LDV measurement noise produced by an optical phenomenon called speckle patterns. When an optically rough surface is illuminated by a coherent laser beam, the incident wavelets are reflected in diverse directions; thus, their phases vary according to the surface deviations. The wavelets of the scattered laser interfere destructively or constructively, generating disorderly distributed dark-bright spots, namely, speckle patterns. Since the LDV photodetector focuses on the spot portion of the object surface, the signal output is generally the phasor summation of the interfered laser wavelets. When scanning from moving frames, the translation and deformation of the focusing spot result in significant speckle noise, as the light intensities and phases are dramatically altered over the variant speckle patterns. Specifically, signal drop-outs are extreme speckle noise produced by sharply varying speckle patterns.

The detected intensity, I, acquired by the photodetector is the combination of transmission and reference laser beams, and it can be expressed as [40]

$$I = I_R + I_T + 2\sqrt{I_R I_T}\cos[2\pi f_R t - \frac{4\pi}{\lambda}\int v\,dt + (\varphi_R - \varphi_T)] \tag{4.1}$$

where, I_T & I_R are intensities of the transmission and reference beams respectively, f_R is the frequency shift of the reference beam, λ is the laser wavelength, v is the vibration velocity of the targeted surface, and φ_T & φ_R are the phases of the transmission and reference beams respectively. According to equation 4.1, the beat frequency that the LDV system acquires is

$$f_{beat} = f_R - \frac{2}{\lambda}v + \frac{1}{2\pi}\frac{d(\varphi_R - \varphi_T)}{dt} \tag{4.2}$$

Considering the focusing spot A illuminated by the transmission beam with P wavelets (each with the phase ϕ_{Tp} and intensity I_{Tp}) and the reference beam with Q wavelets (each with the phase ϕ_{Rq} and intensity I_{Rq}), the resultant intensities and phases of speckles can be calculated by the following equations [27]:

$$I_{res} = 2\sqrt{I_R I_T} = \frac{1}{A}\{[\sum_{q=1}^{Q}\sum_{p=1}^{P} A_{pq}\sqrt{I_{Rq} I_{Tp}}\sin(\phi_{Rq} - \phi_{Tp})]^2 \tag{4.3}$$

$$+[\sum_{q=1}^{Q}\sum_{p=1}^{P} A_{pq}\sqrt{I_{Rq}I_{Tp}}cos(\phi_{Rq}-\phi_{Tp})]^2\}^{1/2}$$

$$tan\phi_{res} = tan(\varphi_R - \varphi_T) = \frac{\sum_{q=1}^{Q}\sum_{p=1}^{P} A_{pq}\sqrt{I_{Rq}I_{Tp}}sin(\phi_{Rq}-\phi_{Tp})}{\sum_{q=1}^{Q}\sum_{p=1}^{P} A_{pq}\sqrt{I_{Rq}I_{Tp}}cos(\phi_{Rq}-\phi_{Tp})} \tag{4.4}$$

where, I_{res} & ϕ_{res} are the time-varying resultant intensity and phase of the Doppler signal respectively, and the area A_{pq} overlaps the pth transmission wavelet and the qth reference wavelet. For the modulated Doppler signal, the measured velocity V_m becomes the combination of the actual vibration velocity v and the phasor variation (speckle noise).

$$V_m = \frac{\lambda}{2}(f_R - f_{beat}) = v - \frac{\lambda}{4\pi}\frac{d(\varphi_R - \varphi_T)}{dt} \tag{4.5}$$

According to equations (4.4) and (4.5), significant changes in ϕ_{res} can result in large velocity distortion, and the noise is basically produced by the intensity and phase distributions of speckle patterns. Considering these optical factors as stochastic variables, Rothberg [27] developed an approach for numerically simulating speckle noise that presented good agreement with experimental results.

Rothberg [27] assumed that speckles are rectangular and densely distributed, and divided the scanning surface into unaligned speckles, as shown in Fig. 4.1. These speckles are assigned different intensities and phases. The intensities satisfy a negative exponential probability distribution (equation (4.6)) and the phases are generated using a series of random numbers in the range of 0 to 2π [27, 26].

$$I_{Tp} = -\bar{I}ln[1 - \frac{x_p}{1+(10^{-10})}] \tag{4.6}$$

where $\bar{I}$ is the mean intensity and x_p is a random number satisfying $0 \le x_p \le 1$.

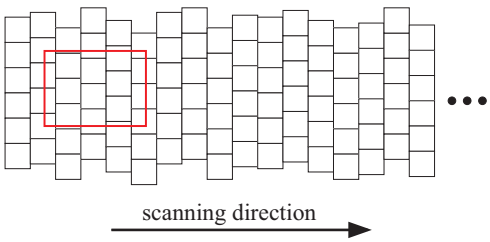

Figure 4.1: Speckle elements discretizing the object surface, as well as the photodetector along the scanning direction.

The photodetector (the red rectangle in Fig. 4.1) focuses on the scanning surface to acquire the transmission beam reflected from an area of $m_0 \times n_0$ speckle elements, and the focusing position moves along the scanning direction. The size of each speckle element is $40 \times 40\mu m^2$ in this paper. Since only fractions of some speckles are inside the photodetector, the overlapping area A_{pq} is calculated for each speckle. The contribution of the reference beam can be simulated as a stationary speckle pattern with a certain intensity and phase.

As the properties of both transmission and reference beams are defined, the speckle noise polluting the actual vibration can be determined by equations (4.3), (4.4) and (4.5). Fig. 4.2 illustrates simulated speckle noise with a sampling frequency of 102,400 Hz.

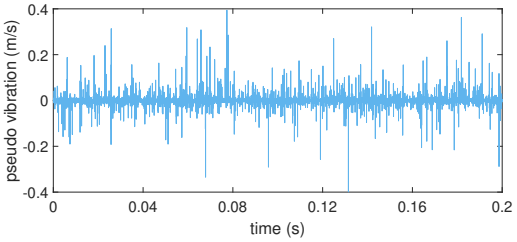

Figure 4.2: Simulated 0.2 s speckle noise with a sampling frequency of 102,400 Hz.

4.2.2 EEMD and the Hilbert-Huang spectrum

The EMD approach was originally proposed by Huang et al. [32] to self-adaptively decompose signals within natural bandwidths. Since numerous systems are nonlinear and nonstationary, the instantaneous frequency in the IMFs and Hilbert-Huang spectrum contains more physical meaning than the Fourier frequency spectrum. The LDV scanning signal represents the instantaneous vibration velocity, whose characteristics can be analyzed by the IMFs. Specific definitions were developed to acquire ideal IMFs: for an IMF, (1) the number difference between extrema and zero-cross points should be no more than 1 and (2) the envelopes determined by the extrema should on average be 0. The EMD algorithm is described as follows:

Algorithm 3 Pseudo codes of EMD

Input: original signal $v(t)$, maximum number of IMFs N_f, and the decomposition threshold SD;
$r_1 = v(t)$;
for $k = 1$; $k \le N_f$; $k = k + 1$ **do**:
  $h_{k,1} = r_k$;
  for $j = 1$; $j = j + 1$ **do**:
    Find the upper and lower envelopes (U_j, L_j) $m_j = (U_j + L_j)/2$
    Remove the envelope mean from the residual signal $h_{k,j+1} = h_{k,j} - m_j$
    Stop when $\sum_{k=1}^{j} \frac{m_k^2}{h_{i,j}^2} < SD$
  $C_k(t) = h_{k,j+1}$
  $r_{k+1}(t) = r_k(t) - C_k(t)$
Ouput: the kth IMF $C_k(t)$ $(k = 1, 2, ...)$ and the residual $r_{N_f+1}(t)$

However, the significant issue of mode mixing, as more than one oscillation appears in the local waveform of IMFs, has aroused research concerns. A white-noise-assisted decomposition approach, namely EEMD, was developed by Wu & Huang [38] to handle this issue. The EEMD algorithm is summarized as follows [38]:

Algorithm 4 Pseudo codes of EEMD

Input: original signal $v(t)$, maximum number of IMFs N_f, trials number n, and standard deviation of added noise σ_w;
for $k = 1$; $k \leq n$; $k = k + 1$ **do**:
Generate random Gaussian white noise $noise_k(t)$ with the standard deviation σ_w
$v'(t) = v(t) + noise_k(t)$
Decompose $v'(t)$ by EMD [32] to obtain the ith IMFs $C_{k,i}(t)$ and residual $r_k(t)$
$C_i(t) = \sum_{k=1}^{n} C_{k,i}(t)/n$
$r(t) = \sum_{k=1}^{n} r_k(t)/n$
Ouput: the final ith IMF $C_i(t)$ $(i = 1, 2, ...)$ and the ultimate residual $r(t)$

To effectively apply EEMD in signal analysis, it is significant to determine the standard deviation σ_w of added noise and the trials number n of EMD. As mentioned in [38] and [33], setting σ_w to 0.2 times the standard deviation of the original signal and n to several hundred is a good practice.

The Hilbert transform considers the signal as the projection of a spiral curve and calculates the complex conjugate pair of the signal. With the specific definitions, the Hilbert transform of any IMF has physical meanings that can be expressed as [32]

$$C_i'(t) = \frac{1}{\pi} P_c \int_{-\infty}^{\infty} \frac{C_i(\tau)}{t - \tau} d\tau \tag{4.7}$$

where, P_c is the Cauchy principal value and $C_i(\tau)$ represents any IMF. Therefore, the analytical signal of any IMF can be expressed as

$$Z_i(t) = C_i(t) + \mathbf{j} C_i'(t) = a_i(t) e^{\mathbf{j}\theta_i(t)} \tag{4.8}$$

where, $a_i(t) = \sqrt{C_i^2(t) + C_i'^2(t)}$ is the signal amplitude, $\theta_i(t) = arctan(\frac{C_i'(t)}{C_i(t)})$ is the signal phase, and $\mathbf{j}$ represents the imaginary unit. Through the application of the Hilbert transform to all IMFs, the analytical signal of the original data can be obtained [32].

$$Y(t) = \sum_{i=1}^{N_f} a_i(t) e^{\mathbf{j} \int \omega_i(t) dt} \tag{4.9}$$

where $\omega_i(t)$ represents the instantaneous frequency. Therefore, the analytical amplitudes are represented as functions of instantaneous frequency and time, and the Hilbert-Huang spectrum can be illustrated simply as amplitudes in the frequency-time domain. Indeed, the amplitude in an IMF corresponds to the operating deflection shape inside a specific frequency band, and thus the Hilbert-Huang spectrum has potential for vibration analysis using the LDVom signals.

4.2.3 Proposed despeckling algorithm

As the amplitudes of signal drop-outs are considerably larger than the actual vibration, they dramatically can distort local waveforms. The moving root-mean-square (MRMS) thresholds are used for cutting off the outliers to reduce this effect.

$$T_u(t) = M(t) + 2\sqrt{\frac{v^2(t) \bigotimes e_N}{N}} \tag{4.10}$$

$$T_l(t) = M(t) - 2\sqrt{\frac{v^2(t) \bigotimes e_N}{N}}$$

where, $T_u(t)$ & $T_l(t)$ are upper and lower thresholds respectively; $M(t)$ is the moving signal average; $v(t)$ is the original signal; $\bigotimes$ represents the convolution calculation; N is the window length of MRMS; and e_N is the all-one vector with length N. Hence, the signal amplitudes outside the thresholds are replaced by values on the thresholds. This procedure has two potential effects, reducing drop-out amplitudes and generating oscillation discontinuities that represent noise locations.

The following is the algorithm developed in this paper for eliminating speckle noise:

Algorithm 5 Removing speckle noise

Input: original signal $v(t)$
1. Apply MRMS thresholds to cut off signal drop-outs and obtain $y_0(t)$
2. Decompose $y_0(t)$ by EEMD and obtain all IMFs $C_i(t)$ and the residual $r(t)$
3. Discard the first few IMFs related to noise
4. Calculate the despeckled signal $V(t)$ by summing the remaining IMFs and the residual
Ouput: despeckled signal $V(t)$

4.3 Simulated signal analysis

4.3.1 Simulated signal construction

Three simulated signals polluted by speckle noise with different signal-to-noise ratios (SNRs) are constructed hereafter to evaluate the despeckling effects. All simulated signals are sampled at frequencies of f_s =102,400 Hz.

The first signal $v_1(t)$ consists of two harmonic vibrations and randomly simulated speckle noise. A multiplication parameter ρ is utilized to adjust the SNR. Fig. 4.3 illustrates the polluted signal with SNR = −10 dB (usually, SNR < 0 in practical cases). The actual vibration component is almost invisible in Fig. 4.3a, and the noise dramatically distorts the waveforms in the magnified signal (Fig. 4.3b).

$$v_1(t) = 0.005[cos(2\pi \times 2000t) + sin(2\pi \times 1200t)] + \rho \cdot noise \tag{4.11}$$

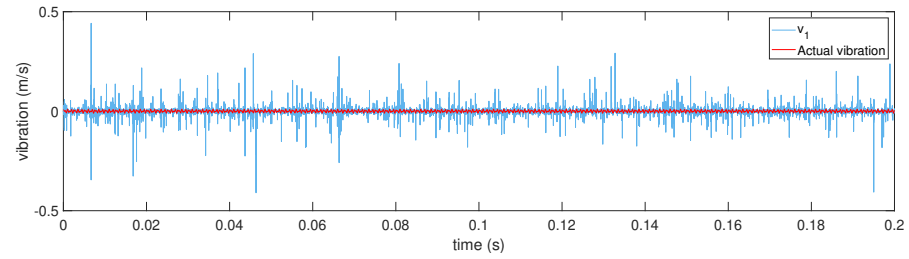

(a)

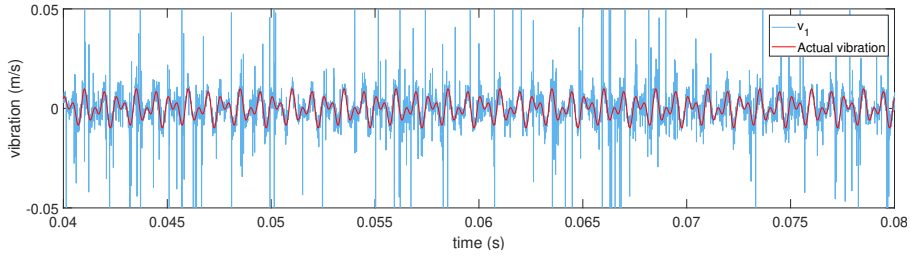

(b)

Figure 4.3: (**a**) $v_1(t)$ with SNR=−10 dB; (**b**) magnified signal of (**a**).

The signal $v_2(t)$ is produced by adding speckle noise to the data taken from [41]. Fig. 4.4 presents the polluted signals with SNR = −10 dB. Similar to the signal $v_1(t)$, the speckle noise dramatically distorts the actual waveforms.

$$v_2(t) = \frac{1}{200(1.2 + cos(100\pi t))} + \frac{cos(160\pi t + 0.2cos(320\pi t))}{200(1.5 + sin(100\pi t))} + \rho \cdot noise \tag{4.12}$$

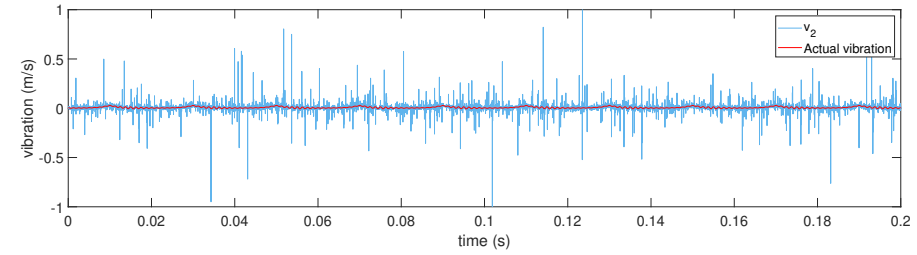

(a)

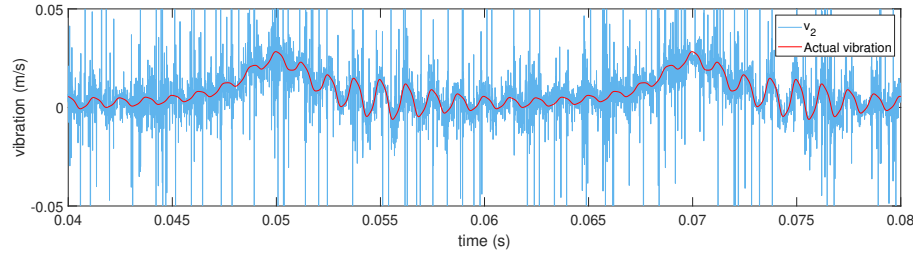

(b)

Figure 4.4: (**a**) $v_2(t)$ with SNR=-10 dB; (**b**) magnified signal of (**a**).

The signal $v_3(t)$ is produced by adding speckle noise to the data taken from [42]. This signal is an unusual one without physical meanings. We only evaluate the despeckle effect on this signal. Fig. 4.5a presents the polluted signals with SNR = −10 dB.

$$v_3(t) = v_{3a}(t) + \rho \cdot noise \tag{4.13}$$

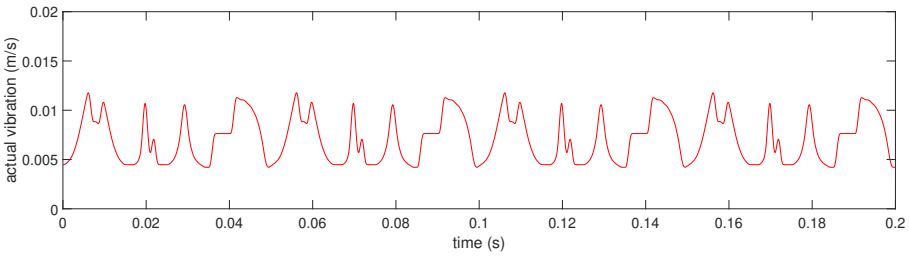

(a)

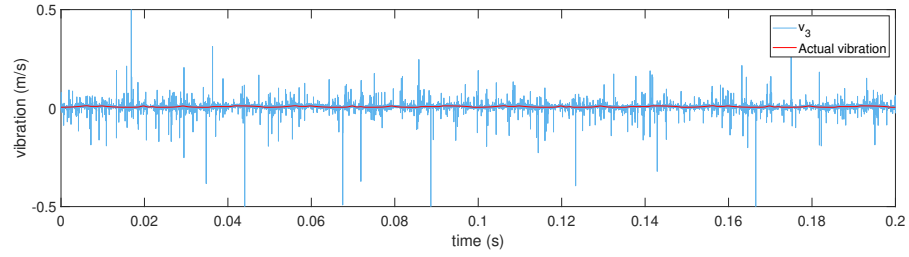

(b)

Figure 4.5: (**a**) The actual vibration $v_{3a}(t)$; (**b**) $v_3(t)$ with SNR=-10 dB.

4.3.2 Despeckling results

Two criteria, the SNR after despeckling processing and correlation coefficient δ (equation 4.14) between the actual vibrations and despeckled signals, are used to evaluate the developed approach. Three different noise conditions with initial SNR = -10 dB, -5 dB & -15 dB are considered by modifying the parameter ρ. Other signal processing approaches including the BPF [43] and the discrete wavelet transform (DWT) [44] are utilized for comparison.

$$\delta(v, v_a) = \frac{Cov(v, v_a)}{\sqrt{Var(v)Var(v_a)}} \tag{4.14}$$

where v & v_a represent the noisy and despeckled signals, respectively, $Cov()$ calculates the covariance, and $Var()$ calculates the variance.

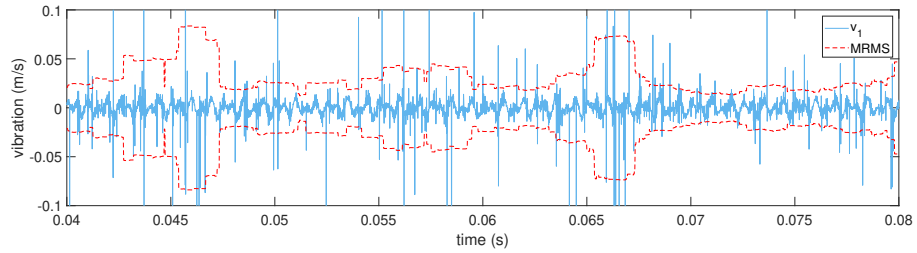

(a)

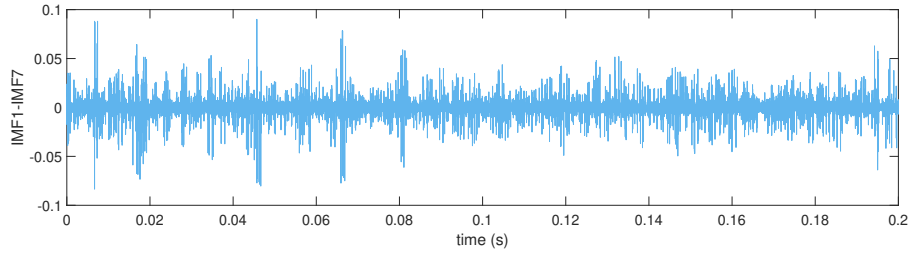

(b)

Figure 4.6: (**a**) The MRMS thresholds of $v_1(t)$ (magnified signal); (**b**) the summation of IMF1 to IMF7.

First, the simulated signal $v_1(t)$ with SNR = -10 dB is processed by the despeckling algorithm in section 4.2. Fig. 4.6a presents the MRMS thresholds, which cut off the signal drop-outs but preserve the dominant speckle-noise energy, and we get the cut-off signal $v_1'(t)$. Using $v_1'(t)$ minus the summation of IMF1 to IMF7 (Fig. 4.6b), the remaining component agrees well with the actual vibration, as shown in Fig. 4.7a. The post SNR increases to 12.48 dB, and the correlation coefficient is δ = 0.9728, which means that the processed signal is almost the same as the true vibration. However, the BPF and DWT methods fail to achieve comparable results, as numerous visible distortions remain in Fig. 4.7b & 4.7c. We use the cut-off frequency of 600 Hz for the BPF and 4 frequency bands for the DWT with 'db4' wavelets. These choices are best in our trials but not the optimized one. The post SNRs of the BPF and DWT results are 5.53 dB and 0.23 dB, respectively, while their correlation coefficients are only 0.8597 and 0.7478.

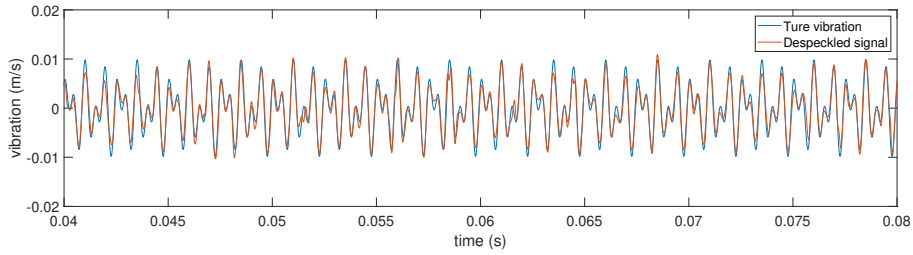

(a)

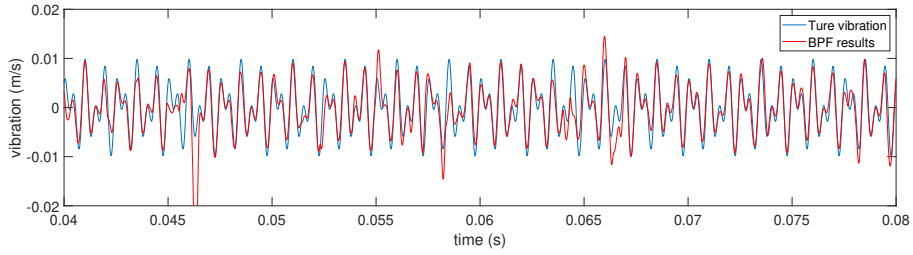

(b)

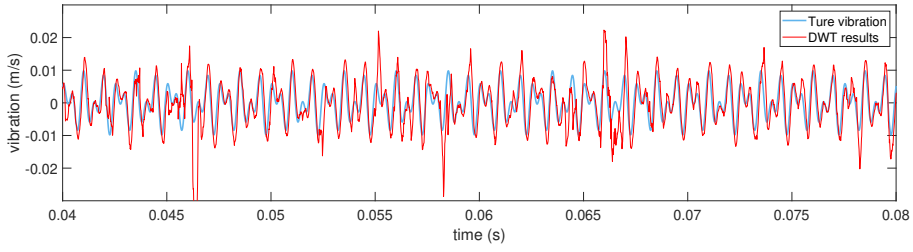

(c)

Figure 4.7: The despeckling results of (**a**) the proposed approach, (**b**) BPF, and (**c**) DWT. The signals are magnified between 0.04 s and 0.08 s.

Second, the simulated signals $v_2(t)$ & $v_3(t)$ are processed to remove speckle noise, with the results presented in Fig. 4.8. The EEMD-based approach effectively eliminates the speckle noise, as shown in Fig. 4.8a & Fig. 4.8b. The post SNRs increase to 18.71 dB for the signal $v_2(t)$ and 25.69 dB for the signal $v_3(t)$, and their correlation coefficients are 0.9872 and 0.9868, respectively. However, the BPF and DWT approaches preserve numerous distortions. Both their post SNRs and correlation coefficients are far lower than those of the EEMD-based results (seen in Table 4.2). Therefore, our proposed algorithm demonstrates advantages in removing speckle noise.

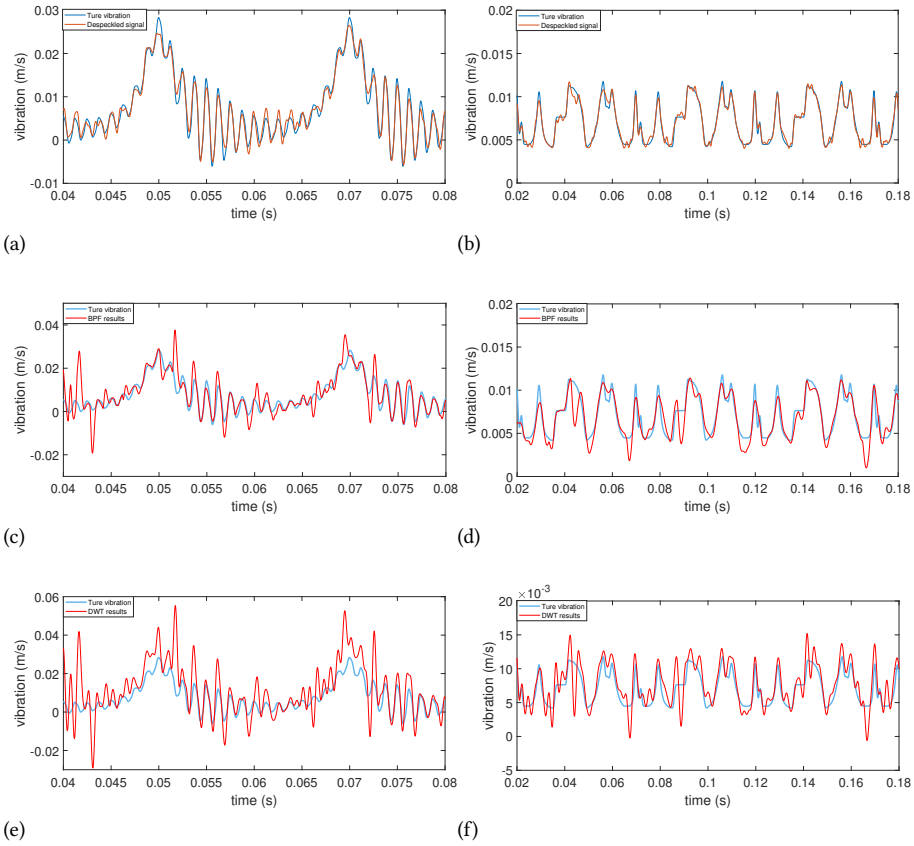

Figure 4.8: The despeckling results for (**a**) $v_2(t)$ by the proposed approach, (**b**) $v_3(t)$ by the proposed approach, (**c**) $v_2(t)$ by the BPF, (**d**) $v_3(t)$ by the BPF, (**e**) $v_2(t)$ by the DWT, and (**f**) $v_3(t)$ by the DWT. The signals have been magnified.

To evaluate the robustness of the EEMD-based approach, we modify the initial SNRs, with the results shown in Table 4.2. Generally, all three approaches perform better with increasing initial SNR. When the initial SNR is −5 dB, the proposed approach outperforms the others, although the BPF and DWT achieve acceptable despeckling results (with correlation coefficients over 0.89). When the initial SNR decreases to −15 dB, the BPF and DWT methods fail to eliminate speckle noise with correlation coefficients below 0.71. Nonetheless, the EEMD-based approach achieves correlation coefficients over 0.93, which means that the processed signals are almost the same as the true vibrations. These promising results regardless of the noise intensity indicate the advantages and robustness of our developed method.

Table 4.2: Post SNRs and correlation coefficients of the despeckling results

$v_1(t)$ initial SNR		-10 dB	-5 dB	-15 dB
Proposed approach	post SNR	12.48 dB	13.11 dB	8.87 dB
	correlation	0.9728	0.9754	0.9403
BPF	post SNR	5.53 dB	9.41 dB	0.96 dB
	correlation	0.8597	0.9413	0.6887
DWT	post SNR	0.23 dB	9.71 dB	-0.30 dB
	correlation	0.7478	0.9488	0.6709
$v_2(t)$ initial SNR		-10 dB	-5 dB	-15 dB
Proposed approach	post SNR	18.71 dB	22.61 dB	15.21 dB
	correlation	0.9872	0.9947	0.9708
BPF	post SNR	6.97 dB	12.55 dB	2.78 dB
	correlation	0.8481	0.9492	0.7069
DWT	post SNR	4.50 dB	9.66 dB	0.44 dB
	correlation	0.8169	0.9382	0.6613
$v_3(t)$ initial SNR		-10 dB	-5 dB	-15 dB
Proposed approach	post SNR	25.69 dB	30.33 dB	18.99 dB
	correlation	0.9868	0.9954	0.9350
BPF	post SNR	13.86 dB	17.98 dB	9.14 dB
	correlation	0.8100	0.9176	0.6023
DWT	post SNR	9.91 dB	16.28 dB	6.29 dB
	correlation	0.7418	0.8972	0.5131

4.4 Experimental investigation

4.4.1 First scenario

First, we use a small-scale setup to evaluate the despeckling approach for LDVom measurements. Although the setup is similar to some SLDV and CSLDV research (e.g., [20]), the conditions of using the LDVom are held: one-way scanning and unable to enhance the surface reflection. Fig. 4.9 illustrates its schematic, and the experimental setup with multiple instruments is presented in Fig. 4.11. An artificially excited steel strip with defected surface is monitored by the LDVom. This steel strip (length 540 mm) has three artificial defects (with a profile of 6×4 mm at different locations 40 mm, 220 mm, and 450 mm) through the strip width, as shown in Fig. 4.10. We firmly mount the steel strip as a cantilever beam over the base. The left end of the strip is excited by a shaker with a 500 Hz sinusoidal wave. During the scanning progress, the rotating mirror first deflects the transmission laser beam onto the left end and then scans the strip surface at a constant speed around 0.85 m/s. The sampling frequency is 102,400 Hz. A high sampling frequency is chosen to avoid mixing the vibration frequency with the signal drop-outs. If the sampling frequency is low, the signal drop-outs will appear in low-frequency bands and make the vibration confusing. The LDV used is 'RSV-150' made by 'Polytec' and the measurement resolution used is 100 mm/s/V. It should be noticed that adjusting the measurement range cannot

change speckle noise, since the noise is produced by the laser but not by the instrument units [10].

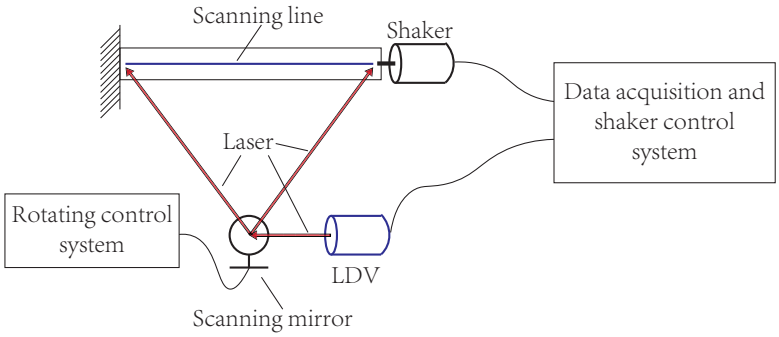

Figure 4.9: A schematic of an LDVom scanning a beam.

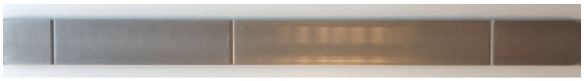

Figure 4.10: Steel strip with three artificial defects.

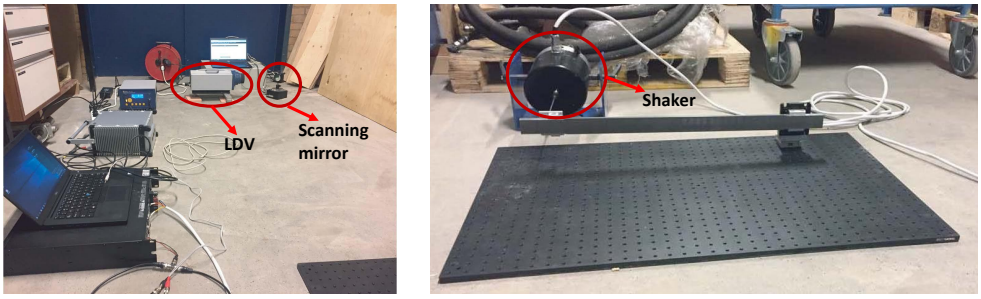

Figure 4.11: Experimental setup for scanning the steel strip.

Fig. 4.12 shows the original vibration signal acquired by the LDVom. The speckle noise is extremely intense as the actual vibration (marked inside the red rectangle) is nearly invisible. The amplitudes of the signal drop-outs reach approximately 3 m/s, over 60 times the true vibration at approximately 500 Hz. Fig. 4.12b presents the magnified signal between 1.5 s and 1.7 s. The speckle noise covers numerous local oscillations, increasing difficulties in local modal analysis. The fast Fourier transform (FFT) spectrum of the original signal is presented in Fig. 4.13, which also shows the vibration frequency is 500 Hz. Since the LDVom measurement is one-way, the spectrum has no sideband harmonics that appear in CSLDV signal spectrum.

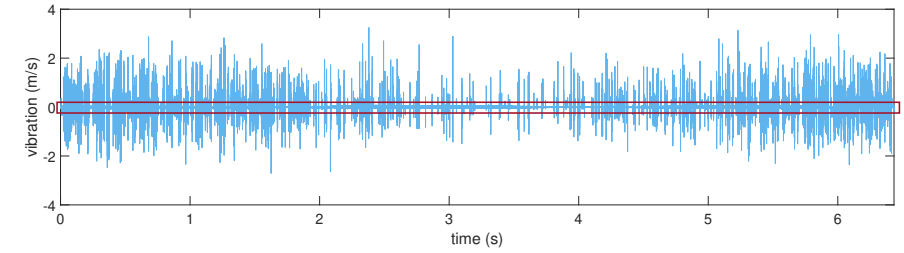

(a)

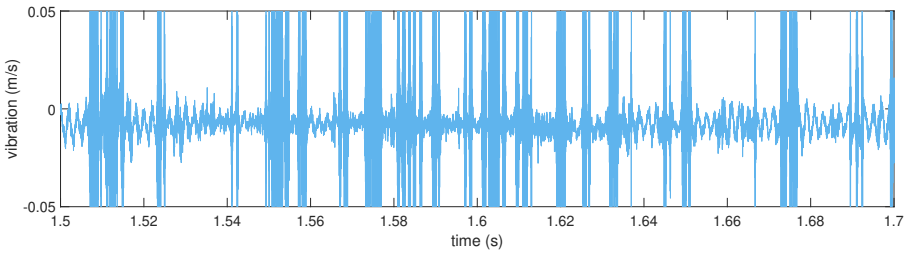

(b)

Figure 4.12: (**a**) The original signal; (**b**) magnified signal between 1.5 s and 1.7 s.

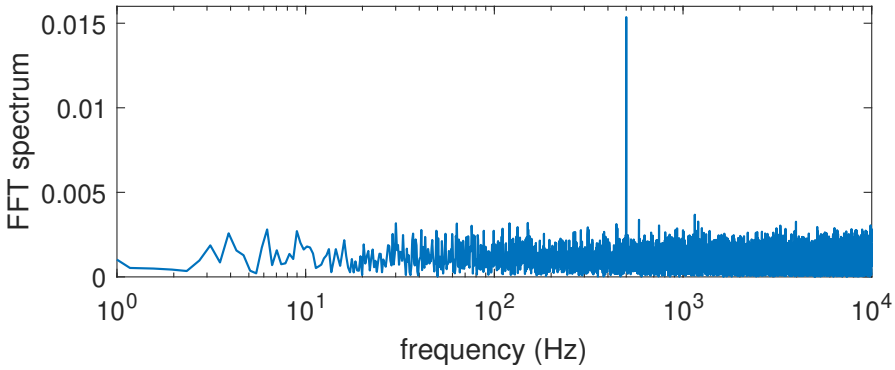

Figure 4.13: The FFT spectrum of the original signal.

Since the EEMD-based approach is time- and memory-consuming in processing complicated signals, we divide the data into multiple 0.1 s time series to remove the speckle noise and then merge the processed series. With IMF1 to IMF8 discarded, the despeckling results are presented in Fig. 4.14. The vibration amplitudes are recovered to normal levels, and the energy distribution becomes visible. The initial SNR is estimated to be -14.63 dB by regarding the despeckled signal as the actual vibrations. This also means the speckle noise is extremely intense, similar to the simulated cases in section 4.3.

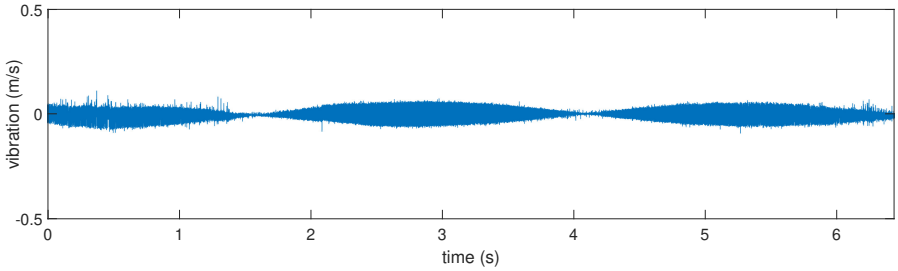

Figure 4.14: The despeckled signal obtained by the proposed EEMD-based approach.

Fig. 4.15 shows the magnified despeckled signal between 0.8 s and 0.9 s. The developed approach reveals the true vibration surrounding 500 Hz, especially from oscillations polluted by intense speckle noise (marked with black circles). At the locations covered by continuously intense speckle noise (marked with a black rectangle), the processed results approximately recover the true waveforms. However, speckle noise significantly distorts the BPF and DWT results, especially at approximately 0.86 s.

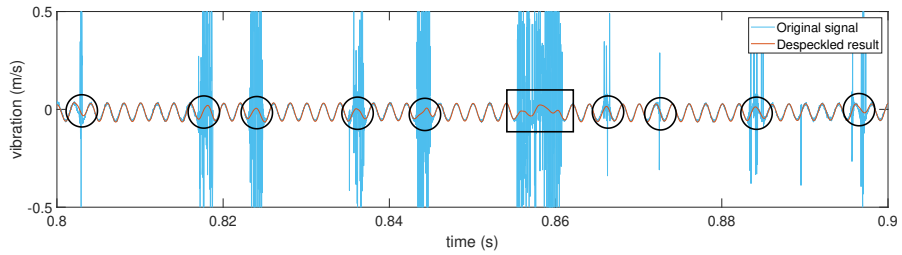

(a)

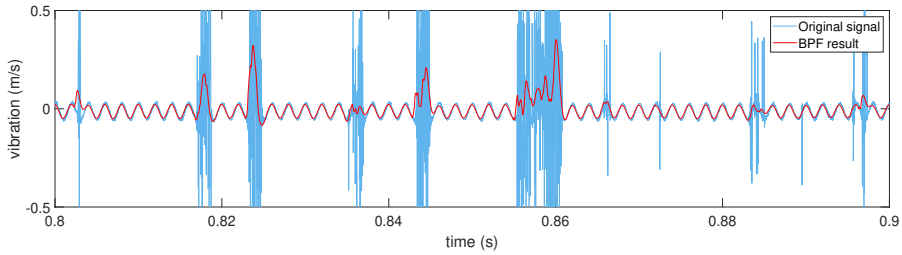

(b)

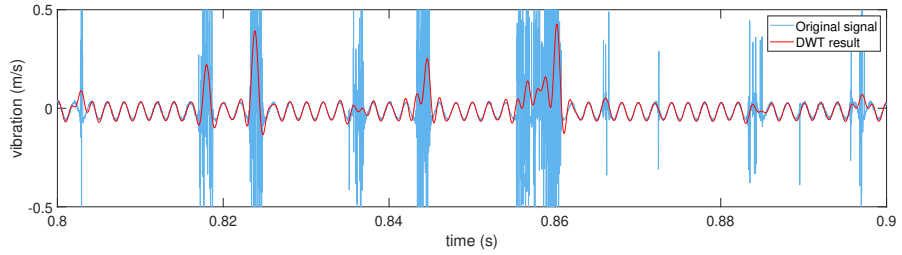

(c)

Figure 4.15: The despeckling results of (**a**) the proposed approach, (**b**) BPF, and (**c**) DWT. Signals are magnified between 0.8 s and 0.9 s.

Fig. 4.16 shows the magnified despeckled signal where the initial SNR is estimated to be -27.79 dB and the actual vibration amplitudes are 1/5 to 1/10 of those in Fig. 4.15. Although the vibration responses are extremely weak, signals covered by intense noise (marked with a black rectangle) are approximately revealed. However, the results of BPF and DWT are unpromising, containing significant distortions at intense speckle locations. Therefore, the developed EEMD-based approach demonstrates advantages in processing signals to eliminate speckle noise.

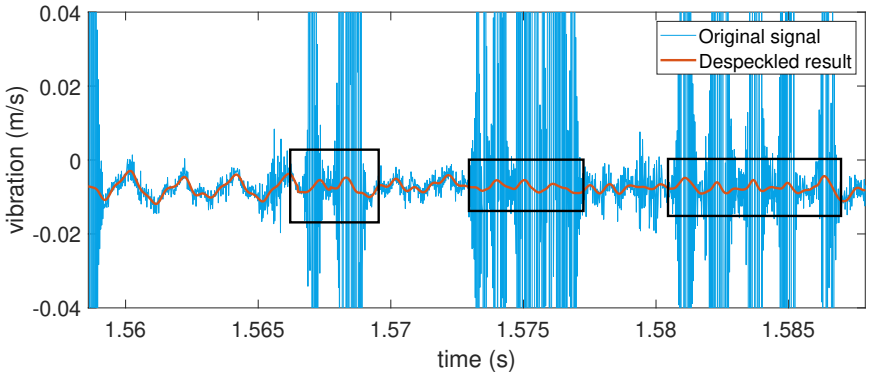

(a)

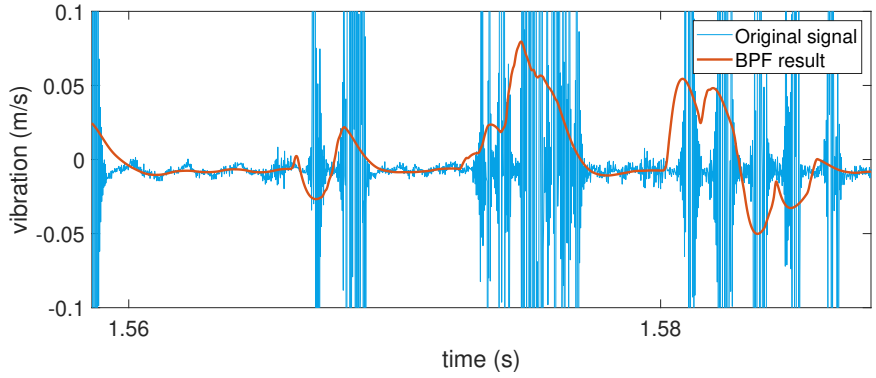

(b)

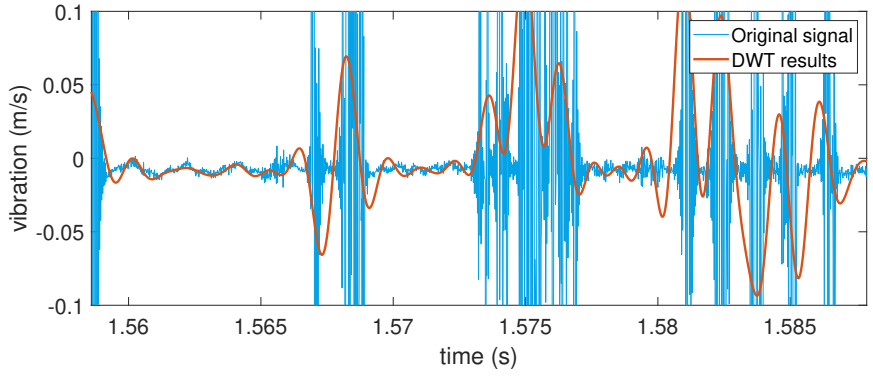

(c)

Figure 4.16: The despeckling results of (**a**) the proposed approach, (**b**) BPF, and (**c**) DWT. The signal segment with an estimated SNR of -27.79 dB is magnified.

For further vibration analysis and damage inspection, the Hilbert-Huang spectrum has potential for signal interpretation, as illustrated in Fig. 4.17. The despeckled signal in Fig. 4.14 contains three bulbous segments corresponding to three defects. In the Hilbert spectrum, the signal frequency varies around the central frequency of 500 Hz. The actual vibration is not an absolute sinusoidal wave, thus causing instantaneous variant frequencies. It is noticeable that the vibration energy at the defect locations is larger than that in other areas. Therefore, we identify the local maximum energy locations as defect locations. In this case, we estimate defect centers at 0.4931 s, 2.748 s and 5.477 s from the Hilbert-Huang spectrum, corresponding to 41.4 mm, 230.6 mm and 459.7 mm. Thus, the Hilbert-Huang spectrum can reveal the damage locations from the despeckled signal despite approximately 1 cm errors.

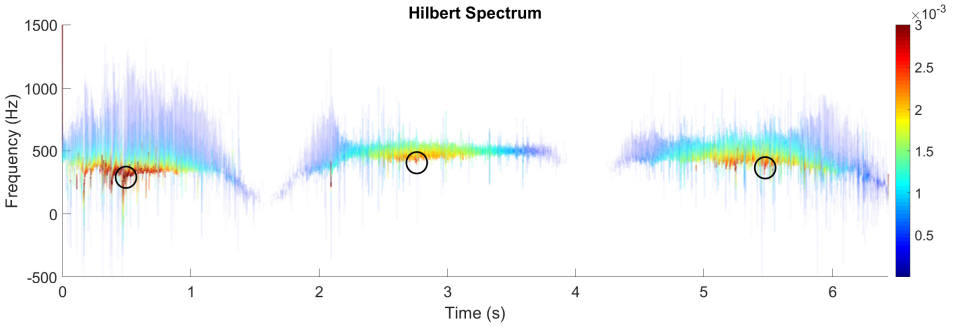

Figure 4.17: The Hilbert-Huang spectrum of the despeckled signal.

4.4.2 Second scenario

Second, we mount the LDVom on a downscaled running railway system [45] (as shown in Fig. 4.18) to acquire the vibrations excited by wheel-rail contact. The laser is deflected by a fixed mirror to focus on the rail surface. With the running system, the LDVom continuously scans the rail surface. The running speed is 10 km/h and the sampling frequency is 102,400 Hz.

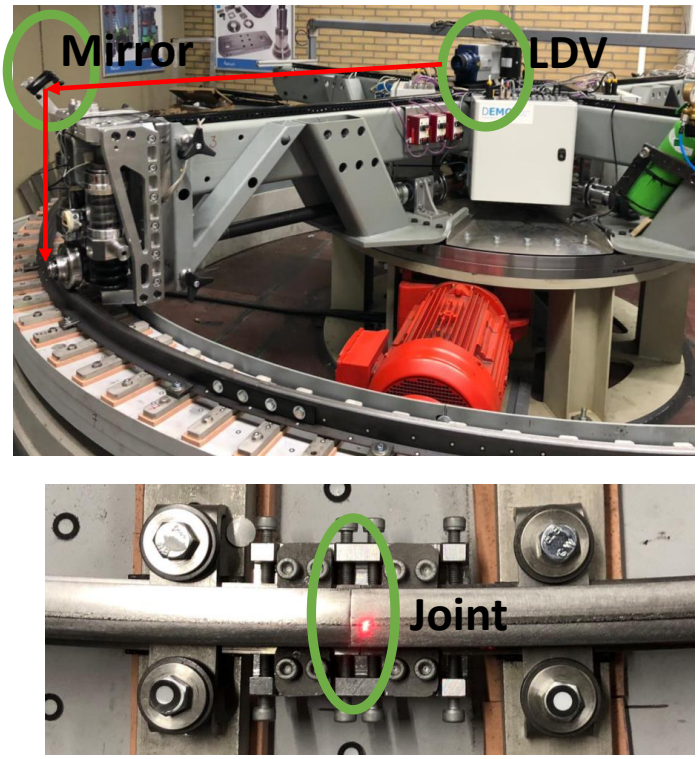

Figure 4.18: The experimental setup of the running railway system.

Here, we take the signal segment when the wheel passes the joint for analysis, with the signal illustrated in Fig. 4.19. The noise is intense with frequent signal drop-outs to cover the vibrations. Therefore, the waveform when wheel hits the joint (marked with the blue circle) becomes indistinguishable in the original signal. Using the EEMD-based approach and discarding the first 8 IMFs, the depseckled signal has revealed the trend of the original one, as shown in Fig. 4.19a. The despeckling process does not change or mitigate the vibration modes, as the vibration frequency peaks (marked in the black circles) in FFT spectra (Fig. 4.20) remains invariant between original and despeckling signals. These frequency peaks are not related to the speckle noise since the measurement is not cyclical. The dominant noise energy has attenuates sharply (marked in the red circle). However, the EEMD-based approach is different from a low-pass filter, as the low-frequency energy (which may related to speckle noise) also alters (e.g., marked in the red rectangle).

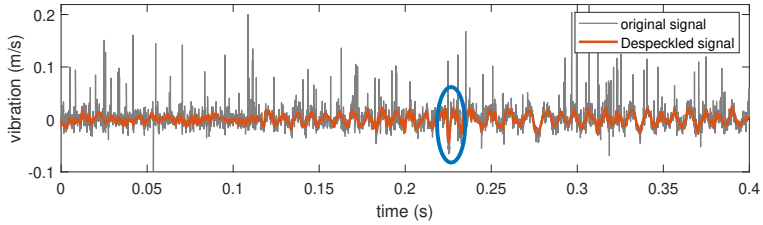

(a)

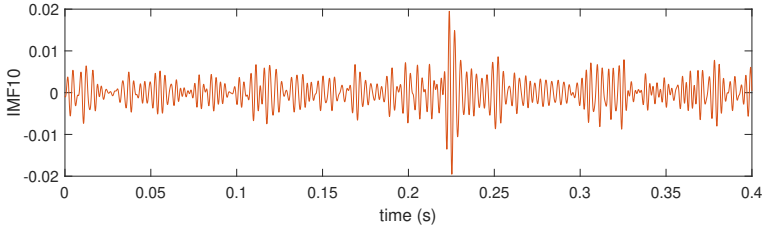

(b)

Figure 4.19: (**a**) The original and the despeckled signals when the wheel passing the joint; (**b**) The IMF10 achieved by EEMD.

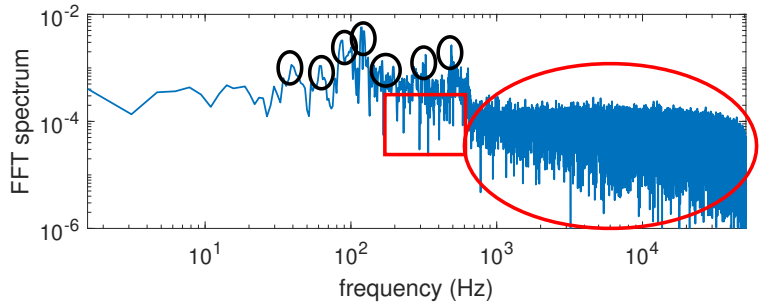

(a)

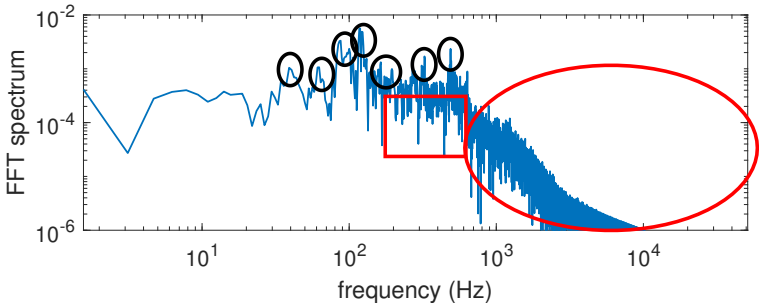

(b)

Figure 4.20: The FFT spectra of (**a**) the original signal and (**b**) the despeckled signal.

The waveform at the joint location becomes visible, and we can also use an IMF to locate the joint, e.g., IMF10. As illustrated in Fig. 4.19b, the IMF10 presents a sharp amplitude at around 0.225 s, corresponding to the wheel hitting the joint. The amplitude of an IMF is corresponding to the operating deflection shape, and thus can be used for vibration analysis. Hilbert-Huang spectrum also has potential for vibration analysis, with that of IMF10 shown in Fig. 4.21. Only one spike energy appears around 0.225 s, agreeing well with the joint location. Therefore, our proposed approach can eliminate the speckle noise and reveal the signals for vibration analysis.

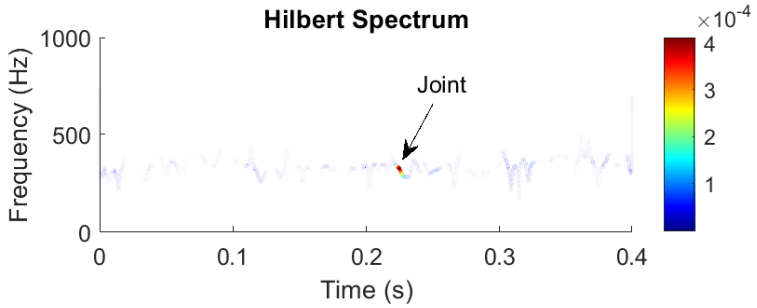

Figure 4.21: The Hilbert-Huang spectrum of the IMF10.

4.5 Conclusion and Discussions

In this paper, we propose an EEMD-based approach for eliminating speckle noise in LDVom signals. LDVom is a one-way continuously scanning technique especially used for large-scale structural monitoring, e.g., railway tracks, different from SLDV and CSLDV. Speckle noise, originating from phase variation of speckle patterns, is a significant issue when scanning from moving platforms. The noise amplitudes can exceed 30 times the true vibration, and the SNR can drop below -15 dB. The EEMD approach can acquire IMFs containing the instantaneous frequency, which relates to the instantaneous vibration velocity captured by the LDVom. The related Hilbert-Huang spectrum has the potential to highlight the damage locations. Since the instantaneous frequency in an IMF is continuous, the EEMD approach can restore the actual oscillations affected by intense speckle noise. MRMS thresholds are used for cutting off the outliers, which can reduce drop-out amplitudes and generate noise discontinuities that EEMD can identify properly. The proposed method is evaluated regarding processing numerically simulated and experimental acquired signals.

In the numerical simulation, randomly generated speckle noise is added to three different time series, including a stationary signal, a time-varying signal and an abnormal signal with oscillation discontinuities. When the initial SNR is -10 dB, our proposed approach can reveal the true vibrations, with post SNRs = 12.48 dB, 18.71 dB & 25.69 dB and correlation coefficients over 0.97. The BPF and DWT methods for comparison remove only part of the speckle noise and reserve numerous distortions. Generally, all three approaches perform better with increasing initial SNR. The EEMD-based approach can achieve promising results even with initial SNR = -15 dB, and the correlation coefficients remain over 0.93. However, the BPF and DWT results are unacceptable in such intensely noisy situations. Therefore, these results indicate the advantages and robustness of our proposed approach in eliminating speckle noise.

In the first physical experiment, a steel strip with three artificial defects is excited at 500 Hz. The speckle noise is intense as the noise amplitudes can reach 35 times the vibrations, and the estimated initial SNR is -14.63 dB. After IMF1 to IMF8 are discarded, the actual vibration is revealed with energy concentrating on the defect locations. Generally, the EEMD-based approach can restore the vibrations surrounding 500 Hz regardless of the speckle intensities, even at the locations where the actual vibrations are extremely weak and the initial SNR is estimated to be -27.79 dB. However, both the BPF and DWT methods

preserve amplitude distortions resulting from intense speckle noise. The Hilbert-Huang spectrum is illustrated to identify defect centers. The estimated damage locations are at 41.4 mm, 230.6 mm and 459.7 mm, corresponding well with the actual locations of 40 mm, 220 mm and 450 mm.

In the second physical experiment, a downscaled running railway system excited by wheel-rail contact is under detection. The speckle noise is intense to cover the vibration, especially the waveform at the joint location. The proposed approach successfully mitigates the speckle noise. The joint location is identified in both an IMF and the Hilbert-Huang spectrum. Therefore, our proposed approach is applicable to eliminating speckle noise and the despeckled signal can be used for damage inspection.

We want to mention that the simulated signals are much more challenging than the experimental signal of 500 Hz, and we want to evaluate the effect on these challenging signals. That is reason for the difference between the simulated ones and the experimental ones. Besides, the despeckling effect seems more visible in removing the signal drop-outs, which is a specific characteristic within the speckle noise resulting from large phase change. It is difficult to visibly evaluate the effect on other frequencies, and therefore we use 'signal-to-noise ratio' to evaluate the despeckling effect.

There are two issues when applying EEMD, which should be investigated in future research. First, EEMD has increased the computational burden since it repeats EMD several hundred times. This issue may be solved by paralleling computation for the hundred times of EMD. Second, the choice of IMFs for despeckled signals is dependent on the operating experience. Future research will develop automatic approaches to distinguish between the IMFs for noise and vibration.

Future research should also concern the despeckling effect in different scenarios. The experimental parameters like the vibration frequency, the sampling frequency and the scanning speed would change the signals, and the despeckling effect that changes with these parameters should be further investigated. Besides, the despeckling effect on the impulsive signal is unknown, which should also be investigated in the future research.

We also want to mention that using Hilbert-Huang transform is potential for vibration analysis. However, different strategies can present different analyzing effects. Since the issue of signal quality has been solved, the strategies to interpret LDVom signals can be developed in future research.

References

[1] A Mazzù, L Provezza, N Zani, C Petrogalli, A Ghidini, and M Faccoli. "Effect of shoe braking on wear and fatigue damage of various railway wheel steels for high speed applications". In: *Wear* 434 (2019), p. 203005.

[2] K Wang, Z Tan, K Gu, B Gao, G Gao, RDK Misra, and B Bai. "Effect of deep cryogenic treatment on structure-property relationship in an ultrahigh strength Mn-Si-Cr bainite/martensite multiphase rail steel". In: *Materials Science and Engineering: A* 684 (2017), pp. 559–566.

[3] E Magel and J Kalousek. "Designing and assessing wheel/rail profiles for improved rolling contact fatigue and wear performance". In: *Proceedings of the Institution of*

Mechanical Engineers, Part F: Journal of Rail and Rapid Transit 231.7 (2017), pp. 805–818.

[4] E Magel, P Mutton, A Ekberg, and A Kapoor. "Rolling contact fatigue, wear and broken rail derailments". In: *Wear* 366 (2016), pp. 249–257.

[5] OS Salawu. "Detection of structural damage through changes in frequency: a review". In: *Engineering structures* 19.9 (1997), pp. 718–723.

[6] R Hou, Y Xia, and X Zhou. "Structural damage detection based on l1 regularization using natural frequencies and mode shapes". In: *Structural Control and Health Monitoring* 25.3 (2018), e2107.

[7] C Zhou, M Hong, Z Su, Q Wang, and L Cheng. "Evaluation of fatigue cracks using nonlinearities of acousto-ultrasonic waves acquired by an active sensor network". In: *Smart Materials and Structures* 22.1 (2012), p. 015018.

[8] MTM Khairi, S Ibrahim, MAM Yunus, M Faramarzi, GP Sean, J Pusppanathan, and A Abid. "Ultrasound computed tomography for material inspection: Principles, design and applications". In: *Measurement* 146 (2019), pp. 490–523.

[9] AB Stanbridge and DJ Ewins. "Modal testing using a scanning laser Doppler vibrometer". In: *Mechanical systems and signal processing* 13.2 (1999), pp. 255–270.

[10] SJ Rothberg, MS Allen, P Castellini, D Di Maio, JJJ Dirckx, DJ Ewins, Ben J Halkon, P Muyshondt, N Paone, T Ryan, et al. "An international review of laser Doppler vibrometry: Making light work of vibration measurement". In: *Optics and Lasers in Engineering* 99 (2017), pp. 11–22.

[11] DM Siringoringo and Y Fujino. "Experimental study of laser Doppler vibrometer and ambient vibration for vibration-based damage detection". In: *Engineering Structures* 28.13 (2006), pp. 1803–1815.

[12] DM Chen, YF Xu, and WD Zhu. "Non-model-based multiple damage identification of beams by a continuously scanning laser Doppler vibrometer system". In: *Measurement* 115 (2018), pp. 185–196.

[13] M Martarelli and DJ Ewins. "Continuous scanning laser Doppler vibrometry and speckle noise occurrence". In: *Mechanical Systems and Signal Processing* 20.8 (2006), pp. 2277–2289.

[14] O Nishizawa, T Satoh, X Lei, and Y Kuwahara. "Laboratory studies of seismic wave propagation in inhomogeneous media using a laser Doppler vibrometer". In: *Bulletin of the Seismological Society of America* 87.4 (1997), pp. 809–823.

[15] P Sriram, JI Craig, and S Hanagud. "A scanning laser Doppler vibrometer for modal testing". In: *International Journal of Analytical and Experimental Modal Analysis* 5 (1990), pp. 155–167.

[16] AB Stanbridge and DJ Ewins. "Measurement of translational and angular vibration using a scanning laser Doppler vibrometer". In: *Shock and Vibration* 3.2 (1996), pp. 141–152.

[17] R Akamatsu, T Sugimoto, N Utagawa, and K Katakura. "Proposal of non contact inspection method for concrete structures using high-power directional sound source and scanning laser doppler vibrometer". In: *Japanese Journal of Applied Physics* 52.7S (2013), 07HC12.

[18] C Liu, C Zang, and B Zhou. "A novel algorithm for determining the pose of a scanning laser Doppler vibrometer". In: *Measurement Science and Technology* 31.2 (2019), p. 025202.

[19] MS Allen and MW Sracic. "A new method for processing impact excited continuous-scan laser Doppler vibrometer measurements". In: *Mechanical Systems and Signal Processing* 24.3 (2010), pp. 721–735.

[20] YF Xu, DM Chen, and WD Zhu. "Damage identification of beam structures using free response shapes obtained by use of a continuously scanning laser Doppler vibrometer system". In: *Mechanical Systems and Signal Processing* 92 (2017), pp. 226–247.

[21] DM Chen, YF Xu, and WD Zhu. "Identification of damage in plates using full-field measurement with a continuously scanning laser Doppler vibrometer system". In: *Journal of Sound and Vibration* 422 (2018), pp. 542–567.

[22] Z Huang and C Zang. "Fast modal rotation measurement using a dual sinusoidal-scan continuously scanning laser Doppler vibrometer". In: *Measurement Science and Technology* 31.8 (2020), p. 085201.

[23] D Di Maio, P Castellini, M Martarelli, S Rothberg, MS Allen, WD Zhu, and DJ Ewins. "Continuous Scanning Laser Vibrometry: A raison d'être and applications to vibration measurements". In: *Mechanical Systems and Signal Processing* 156 (2021), p. 107573.

[24] S Rahimi, Z Li, and R Dollevoet. "Measuring with laser Doppler vibrometer on moving frame (LDVMF)". In: *AIP Conference Proceedings*. Vol. 1600. American Institute of Physics. 2014, pp. 274–286.

[25] P Martin and S Rothberg. "Introducing speckle noise maps for laser vibrometry". In: *Optics and Lasers in Engineering* 47.3-4 (2009), pp. 431–442.

[26] JW Goodman. *Statistical properties of laser sparkle patterns*. Tech. rep. STANFORD UNIV CA STANFORD ELECTRONICS LABS, 1963.

[27] S Rothberg. "Numerical simulation of speckle noise in laser vibrometry". In: *Applied Optics* 45.19 (2006), pp. 4523–4533.

[28] P Chiariotti, M Martarelli, and GM Revel. "Delamination detection by multi-level wavelet processing of continuous scanning laser Doppler vibrometry data". In: *Optics and Lasers in Engineering* 99 (2017), pp. 66–79.

[29] J Zhu, Y Li, and R Baets. "Mitigation of speckle noise in laser Doppler vibrometry by using a scanning average method". In: *Optics letters* 44.7 (2019), pp. 1860–1863.

[30] YF Xu, DM Chen, and WD Zhu. "Modal parameter estimation using free response measured by a continuously scanning laser Doppler vibrometer system with application to structural damage identification". In: *Journal of Sound and Vibration* 485 (2020), p. 115536.

[31] Y Jin and Z Li. "Eliminating Speckle Noises for Laser Doppler Vibrometer Based on Empirical Wavelet Transform". In: *2021 13th International Conference on Measurement*. IEEE. 2021, pp. 72–75.

[32] NE Huang, Z Shen, SR Long, MC Wu, HH Shih, Q Zheng, N Yen, CC Tung, and HH Liu. "The empirical mode decomposition and the Hilbert spectrum for nonlinear and non-stationary time series analysis". In: *Proceedings of the Royal Society of London. Series A: Mathematical, Physical and Engineering Sciences* 454.1971 (1998), pp. 903–995.

[33] Z Feng, M Liang, Y Zhang, and S Hou. "Fault diagnosis for wind turbine planetary gearboxes via demodulation analysis based on ensemble empirical mode decomposition and energy separation". In: *Renewable Energy* 47 (2012), pp. 112–126.

[34] EJ OBrien, A Malekjafarian, and A González. "Application of empirical mode decomposition to drive-by bridge damage detection". In: *European Journal of Mechanics-A/Solids* 61 (2017), pp. 151–163.

[35] P Tian, X Cao, J Liang, L Zhang, N Yi, L Wang, and X Cheng. "Improved empirical mode decomposition based denoising method for lidar signals". In: *Optics Communications* 325 (2014), pp. 54–59.

[36] M Rakshit and S Das. "An efficient ECG denoising methodology using empirical mode decomposition and adaptive switching mean filter". In: *Biomedical signal processing and control* 40 (2018), pp. 140–148.

[37] JL Gómez and DR Velis. "A simple method inspired by empirical mode decomposition for denoising seismic data". In: *Geophysics* 81.6 (2016), pp. V403–V413.

[38] Z Wu and NE Huang. "Ensemble empirical mode decomposition: a noise-assisted data analysis method". In: *Advances in adaptive data analysis* 1.01 (2009), pp. 1–41.

[39] SJ Rothberg, JR Baker, and NA Halliwell. "Laser vibrometry: pseudo-vibrations". In: *Journal of Sound and Vibration* 135.3 (1989), pp. 516–522.

[40] NA Halliwell. "Laser vibrometry". In: *Optical Methods in Engineering Metrology*. Springer, 1993, pp. 179–211.

[41] TY Hou and Z Shi. "Adaptive data analysis via sparse time-frequency representation". In: *Advances in Adaptive Data Analysis* 3.01n02 (2011), pp. 1–28.

[42] A Mert and A Akan. "Detrended fluctuation thresholding for empirical mode decomposition based denoising". In: *Digital signal processing* 32 (2014), pp. 48–56.

[43] CM Rader and B Gold. "Digital filter design techniques in the frequency domain". In: *Proceedings of the IEEE* 55.2 (1967), pp. 149–171.

[44] T Edwards. "Discrete wavelet transforms: Theory and implementation". In: *Universidad de* (1991), pp. 28–35.

[45] M Naeimi, Z Li, RH Petrov, J Sietsma, and R Dollevoet. "Development of a new downscale setup for wheel-rail contact experiments under impact loading conditions". In: *Experimental Techniques* 42.1 (2018), pp. 1–17.

5

An adaptive despeckling and signal decomposition approach for vibration analysis using Laser Doppler Vibrometer

A laser Doppler Vibrometer (LDV) is a nondestructive vibration detector extensively applied in structural health monitoring. A significant signal issue, namely speckle noise, mainly from the LDV on moving platforms (LDVom) has prevailed as an analyzing obstacle. In this paper, a novel adaptive despeckling and signal decomposition (ADSD) approach is proposed for analyzing LDVom signals. The Fourier spectrum is naturally segmented with the identified vibration frequencies. The mode functions are basically derived from the wave equation and pointwisely calculated through optimization in a moving window. In the numerical simulation, the ADSD approach extracts the mode functions that agree well with the vibration components. The despeckling result reveals the true vibrations regardless of the initial signal-to-noise ratio (SNR). The proposed approach outperforms others from the literature. With experimentally acquired signals, the ADSD approach reveals the actual vibrations despite the intense speckle noise. Defect locations are identified from the despeckled signal or Hilbert spectrum. Therefore, the ADSD approach is effective and robust in eliminating the speckle noise and extracting the vibrations.

5.1 Introduction

Recently, vibration detection has become increasingly crucial to structural monitoring and mechanical damage inspection [1, 2, 3], promoting the evolution of relevant measurement

This chapter is based on the paper: Jin, Y., & Li, Z. An adaptive despeckling and signal decomposition approach for vibration analysis using Laser Doppler Vibrometer (to be submitted to a journal).

technologies. A laser Doppler Vibrometer (LDV) is a nondestructive detector for remotely measuring vibrations by laser beams [4]. It claims particular advantages over contact transducers, such as avoiding the difficulties of attaching to hot or rotating structures and avoiding mass loading that changes the structural dynamic of light objects [5]. This advanced instrument provides the benefits of high-precision and high-frequency measurement, as the spatial resolution of vibration velocity can reach 1 mm/s and the measuring frequency can reach 1 GHz. An LDV on moving platforms (LDVom) [6] can continuously scan the structural surface, thus solving the issue of intermittent measurement positions of the attached transducers. Different from the continuously scanning LDV (CSLDV) that requires multiple reciprocating scanning (e.g., [7, 8]), the LDVom one-way continuously scans the structures, especially those large or long like railway tracks. Besides, the LDVom does not require the constant excitation and structural conditions for the CSLDV measurement. However, a significant signal issue, speckle noise [5, 9, 10], becomes extremely troublesome for the LDVom without averaging the multiple measurements.

Speckle noise, or 'pseudo vibration', has prevailed as the obstacle of the LDV applications (e.g., [11, 12]). An optical phenomenon, namely speckle patterns, is the noise source produced by the coherent laser wavelets scattering over an optically rough surface. The dephased laser components interfere constructively and destructively; thus, the intensity and phase of speckle patterns are altered [13, 14]. Mainly when an LDVom scans, the phasor variation inside the photodetector results in signal fluctuations that constitute speckle noise. This noise occurs in two forms, including the signal drop-outs with amplitudes exceeding 30 times those of actual vibrations and the dominant noise with normal amplitudes. The signal-to-noise ratio (SNR) drops to -15 db in physical experiments [15]; thereby, the speckle noise significantly affects the signal quality and restricts the LDVom development. Some studies have quantified the pseudo-vibration sensitivities of commercial instruments in different scenarios [16] and provided evidence for experimentally reducing the noise [17], but without a proper solution to the speckle issue. Although several studies have reduced the adverse effect of signal drop-outs (e.g., [11, 18]), dominant noise remains uncontrolled. The frequency content of speckle noise comprises higher-order harmonics surrounding a fundamental frequency in periodic motions [19]. According to this pseudo-random property, [20] applied a scanning average method for mitigating the noise; but it requires a vibration period far larger than the scanning period. Others developed strategies to avoid noise [21] or to calculate signal energy [22, 23], but either inapplicable in large-scale measurements or overlooking the signal waveform. Therefore, a proper approach to eliminate speckle noise should be a subject of researches.

Time-frequency analysis is an effective strategy to represent nonstationary signals and extract mode functions [24]. It decomposes signals to several frequency bands and acquires the energy distribution in the time-frequency domain. Mechanical damages are usually visible at strong-signal positions with characteristic frequencies (e.g., [25, 26]). The short-time Fourier transform [27] and wavelet transform [28] are primary approaches for time-frequency analysis, but they fail to optimize the time-frequency resolution because of their certain bandwidths. Digital band-pass filters (BPF) can also acquire mode functions [29] but are limited by the certain bandwidth and the energy attenuation at fringe frequencies. Speckle noise produces spike energies varying in the frequency domain, different from the uniformly distributed white noise; thereby, certain-

bandwidth approaches usually become inapplicable. Adaptive analysis approaches can adjust relevant parameters to determine the bandwidths naturally [24]. The consequent time-frequency resolution is optimized according to signal characteristics, and thereby the decomposed mode functions can better present local mode features. A representative adaptive method, namely empirical wavelet transform (EWT) [30], has been extensively applied in extracting signal features and eliminating noise. The SNR dramatically increases in the recent despeckling application [15]. The shortcoming is that the local waveform, especially the weak vibration signal, at positions with consistent signal drop-outs remains distorted. Local waveform distortion affects the energy distribution in the time-frequency domain and further the defect identification. Therefore, an adaptive signal-processing approach that can restore local waveform against speckle noise should be developed.

In this paper, we propose a novel adaptive despeckling and signal decomposition (ADSD) approach for analyzing the LDVom signals. Fourier spectrum is utilized to identify possible vibration modes and adaptively segment frequency bands. The mode functions are basically derived from the wave equation and pointwisely calculated through optimization in a moving window. Numerically generated and experimentally acquired signals are analyzed to evaluate the despeckling and the signal decomposition effects. The remainder of this paper is organized as follows: section 5.2 describes the proposed adaptive approach; section 5.3 evaluates the despeckling effect in numerically simulated signals; section 5.4 investigates in physical experiments the applicability to despeckling and vibration analysis; and section 5.5 discusses and concludes this paper.

5.2 Methodology

5.2.1 Segment Fourier spectrum

Fourier spectrum presents the energy distribution of vibration and noise in the frequency domain. From the Fourier point of view, adaptive signal decomposition is equivalent to extracting mode functions through adaptively determined bandwidths. Therefore, the segmentation of the Fourier spectrum according to signal natures is significant for providing adaptability. The Fourier transform on a time-series can be expressed as:

$$Y(\omega) = \int_0^T y(t) \cdot e^{-i\omega t} dt \tag{5.1}$$

where, $\omega = 2\pi f/f_s$, f is the frequency, f_s is the sampling frequency, $y(t)$ represents the time-series, T is the signal duration, and i represents the imaginary unit. The distribution of the module $|Y(\omega)|$ constitutes the Fourier spectrum, and thereby the oscillations at approximately a certain frequency are represented as a spike in the spectrum.

The segmentation of the Fourier spectrum should avoid the dominant noise bands. Indeed, the speckle noise in higher-frequency bands is difficult to handle (e.g., the continuous signal drop-outs). Therefore, we preset the measuring frequency larger than 20 times the vibration frequency and only consider the Fourier spectrum within $\omega \in [0, \frac{\pi}{20}]$. Each ω segment should surround the frequency spikes that occupy the dominant oscillation energy. The spectrum segmentation algorithm in this paper is proposed as Algorithm 0.

Algorithm 6 Segment Fourier spectrum

Input: the original signal $y(t)$ and the segment number n
1. Calculate the Fourier spectrum $|Y(\omega)|$ of the signal $y(t)$
2. Find the local frequency maxima inside $\omega \in [0, \frac{\pi}{20}]$, and preserve the first n maxima ω_k with large amplitudes, $k = 1, 2, ..., n$
3. Calculate the medium frequency between neighbouring selected maxima
4. Determine the spectrum segments, $\Omega_1 = [0, \frac{\omega_1+\omega_2}{2}]$, $\Omega_n = [\frac{\omega_{n-1}+\omega_n}{2}, \frac{\pi}{20}]$, $\Omega_{n+1} = [\frac{\pi}{20}, \pi]$, $\Omega_k = [\frac{\omega_{k-1}+\omega_k}{2}, \frac{\omega_k+\omega_{k+1}}{2}]$, $k = 2, 3, ..., n-1$
Ouput: The spectrum segments Ω_k, $k = 1, 2, ..., n+1$

Figure 5.1 presents an example of spectrum segmentation.

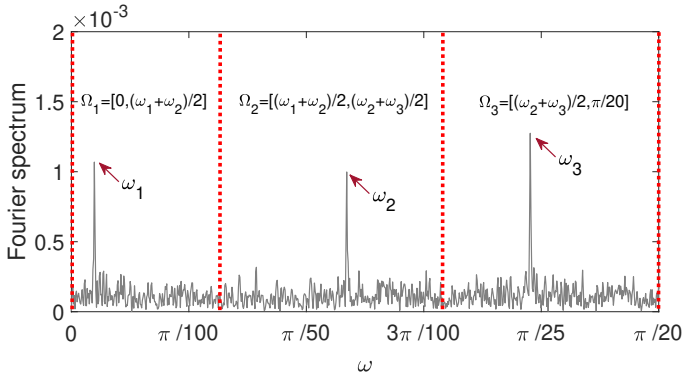

Figure 5.1: An example of spectrum segmentation by the proposed algorithm.

5.2.2 Signal decomposition

Signal decomposition is a crucial procedure after spectrum segmentation. Classic approaches, including the BPF and wavelet transform, calculate the convolution results with the original signal to acquire mode functions. These are general methods for signal processing, but the properties of structural waves are not considered. In our approach, we consider the waves propagating in structures for signal decomposition and despeckling.

On a short scanning line, the vibration velocity approximately obeys the one-dimensional wave equation [31]:

$$\frac{\partial^2 u(x,t)}{\partial t^2} = c^2 \frac{\partial^2 u(x,t)}{\partial x^2} \tag{5.2}$$

where, $u(x,t)$ represents the vibration velocity at the time t and transmission location x, and c is the propagation speed. Since the one-dimensional wave equation is linear, the vibration behaviour arising from numerous elastic waves obeys the superposition principle. The d'Alembert's formula [31] provides the general solution of equation (5.2).

$$u(x,t) = \frac{f(x-ct)+f(x+ct)}{2} + \frac{1}{2c}\int_{x-ct}^{x+ct} g(s)ds \tag{5.3}$$

where, $f(x) = u(x,0)$ and $g(x) = \frac{\partial u}{\partial t}(x,0)$ are initial conditions. The solutions considering specific harmonic components for stationary and nonstationary waves are derived to equations (5.4) and (5.5) respectively.

$$u_s(x,t) = A_0 cos(\omega t + \varphi_1) sin(\frac{2\pi}{\lambda}x + \varphi_2) \tag{5.4}$$

$$u_n(x,t) = A(x,t) sin(\omega t - \frac{2\pi}{\lambda}x + \varphi_0) \tag{5.5}$$

where, A_0 & $A(x,t)$ are wave amplitudes without and with modulation respectively, λ is the wavelength, and φ_0, φ_1 & φ_2 represent the initial phases. When an LDVom scans the vibrating surface, the scanning speed v_s is usually far lower than the propagation speed c of elastic waves, thereby producing the following approximation:

$$\frac{2\pi}{\lambda}x = \frac{\omega v_s}{c}t \approx 0 \tag{5.6}$$

Therefore, the stationary and nonstationary waves during LDVom scanning can be expressed as:

$$u_s(v_s t, t) = A_0 cos(\omega t + \varphi_1) sin(\varphi_2) \tag{5.7}$$

$$u_n(v_s t, t) = A(v_s t, t) sin(\omega t + \varphi_0) \tag{5.8}$$

The elastic waves propagating in structures usually consist of both stationary and nonstationary components. Since equations (5.7) & (5.8) have similar expression, the vibration can be derived according to the superposition principle.

$$y(t) = \sum y_\omega(t) = \sum a_\omega(t) sin(\omega t + \varphi) \tag{5.9}$$

where, $y_\omega(t)$ represents the specific harmonic of the vibration $y(t)$, $a_\omega(t)$ is the modulated amplitudes, and φ is the initial phase. According to equation (5.9), the vibration acquired by an LDVom can be decomposed to the mode functions represented by modulated sine waves. This is the basis for further extracting mode functions.

The modulated amplitude $a_\omega(t)$ is the deformation shape produced by the ω harmonic component, which determines the wave distribution in the corresponding mode function. Deriving the exact expression of $a_\omega(t)$ often requires specific structural mechanics analysis, which is complicated and time-consuming. From the signal point of view, a specific function can approximate $a_\omega(t)$ in a short-time window. The function coefficients vary when the window moves, so that $a_\omega(t)$ can be appropriately approximated in the time domain. Here we use the exponential function for energy attenuation, as expressed in equation (5.10).

$$a_\omega(t) = a_0(\tau) e^{b_0(\tau)t},\ t \in [\tau - \tau_0, \tau + \tau_0] \tag{5.10}$$

where, $a_0(\tau)$ & $b_0(\tau)$ are coefficients only varying with the moving window $[\tau-\tau_0, \tau+\tau_0]$, $2\tau_0$ is the window length, and $b_0(\tau) \in [-\infty, \infty]$ because of wave attenuation in all directions. Therefore, the oscillations with specific harmonic ω inside the short-time window are the optimized mode function $y_\omega(t)$ well-fitting the acquired signal.

$$\begin{aligned} &\min_{a_0,b_0,\omega,\varphi} \ (y_\omega(t) - y(t))^2 \\ &s.t. \quad y_\omega(t) = a_0 e^{b_0 t} sin(\omega t + \varphi) \\ &a_0,\ b_0 \in [-\infty, \infty],\ \varphi \in [0, 2\pi],\ t \in [\tau-\tau_0, \tau+\tau_0] \\ &\omega \in \Omega_k,\ k = 1, 2, ..., n \end{aligned} \tag{5.11}$$

5

where, $y(t)$ is the original signal, and Ω_k is the segment of Fourier spectrum in subsection 5.2.1. Here we utilize the least squares method for optimization. The initial direct-current signal in instruments or the long-wavelength structural shape can slightly migrate the output with low-frequency trends. A quartic polynomial function is optimized to extract this signal trend.

$$\begin{aligned} &\min_{\alpha_1,\alpha_2,\alpha_3,\alpha_4,\alpha_5} \ (y_0(t) - y(t))^2 \\ &s.t. \quad y_0(t) = \alpha_1 t^4 + \alpha_2 t^3 + \alpha_3 t^2 + \alpha_4 t + \alpha_5 \\ &\alpha_1,\ \alpha_2,\ \alpha_3,\ \alpha_4,\ \alpha_5 \in [-\infty, \infty] \end{aligned} \tag{5.12}$$

where $\alpha_1,\ \alpha_2,\ \alpha_3,\ \alpha_4,\ \alpha_5$ are quartic polynomial coefficients, and this optimization is conducted in the whole time domain instead of the short-time window. Equations (5.11) & (5.12) can extract the mode functions. In order to extract the instantaneous vibration to mode functions, the optimization in equation (5.11) is pointwisely conducted with a pointwise-moving window.

Since low-frequency components contain the most energy that affects the extraction of high-frequency components, we optimize the mode function in the low-frequency segment first. The algorithm to extract vibration mode functions is proposed as follows:

Algorithm 7 Pseudo codes of extracting vibration mode functions

Input: original signal $y(t)$, the signal length N, and the segment number n of Fourier spectrum;
Segment the Fourier spectrum to Ω_k adaptively according to Algorithm 0, $k = 1, 2, ..., n+1$;
Extract the low-frequency signal trend $y_0(t)$ according to equation (5.12);
$res_0(t) = y(t) - y_0(t)$;
for $k = 1$; $k \le n$; $k = k+1$ **do**:
  $\tau_0 = \eta \frac{2\pi}{\omega_k f_s}$, $\eta \in [2, 5]$;
  $\omega \in \Omega_k$;
  for $j = 1$; $j \le N$; $j = j+1$ **do**:
    τ_j is the time corresponding to the signal point j;
    Optimize the mode function $y_\omega(t)$ inside the short-time window $t \in [\tau_j - \tau_0, \tau_j + \tau_0]$, and obtain the point result $y_\omega(\tau_j)$;
  $y_{\Omega_k}(t) = \{y_\omega(\tau_j) \mid j = 1, 2, ..., N\}$;
  $res_k(t) = res_{k-1}(t) - y_{\Omega_k}(t)$;
Ouput: all mode functions $y_{\Omega_k}(t)$, $k = 0, 1, 2, ..., n$, and the ultimate residual $res_n(t)$

$$y(t) = \sum_{k=0}^{n} y_{\Omega_k}(t) + res_n(t); \tag{5.13}$$

This algorithm is also intended to eliminate the speckle noise, as the summation of mode functions represents the actual vibration and the residual component $res_n(t)$ consists of the unwanted speckle noise. Thus,Algorithm 0 is the proposed ADSD approach in this paper.

5.3 Simulation results

5.3.1 Simulated signals

Numerical simulation of LDVom scanning signals is based on the Doppler frequency shift, as expressed in equation (5.14). The summation of the true vibration v and speckle noise $-\frac{\lambda_l}{4\pi}\frac{d\phi}{dt}$ generates the LDVom signal V_m.

$$V_m = \frac{\lambda_l}{2}(f_R - f_{beat}) = v - \frac{\lambda_l}{4\pi}\frac{d\phi}{dt} \tag{5.14}$$

where, $f_R - f_{beat}$ represents the frequency shift, λ_l is the laser wavelength, and ϕ is the resultant laser phase.

The speckle noise is numerically simulated by the approach developed in [32], which achieves good agreement with the experimentally acquired noise. Fig. 5.2 illustrates simulated 0.2 s speckle noise. The signal drop-outs and dominant noise fluctuate intensely.

The true vibrations are simulated hereafter using three artificial signals. The first signal $y_{s_1}(t)$ is taken from [30], consisting of two harmonics and a linear trend.

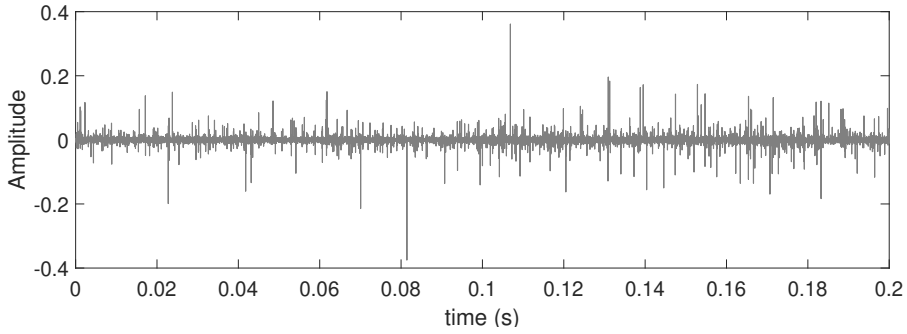

Figure 5.2: Simulated speckle noise with a sampling frequency of 102400 Hz.

$$\begin{aligned} y_{s_1}(t) &= y_{s_1,1}(t) + y_{s_1,2}(t) + y_{s_1,3}(t),\ 0 \le t \le 0.2 \\ y_{s_1,1}(t) &= 6t \\ y_{s_1,2}(t) &= cos(400\pi t) \\ y_{s_1,3}(t) &= 0.5cos(2000\pi t) \end{aligned} \tag{5.15}$$

The second signal $y_{s_2}(t)$ is taken from [33], consisting of a time-frequency variant series, two splicing harmonics and a low-frequency trend.

$$\begin{aligned} y_{s_2}(t) &= y_{s_2,1}(t) + y_{s_2,2}(t) + y_{s_2,3}(t),\ 0 \le t \le 0.2 \\ y_{s_2,1}(t) &= 6t^2 \\ y_{s_2,2}(t) &= cos(100\pi t + 500\pi t^2) \\ y_{s_2,3}(t) &= \begin{cases} cos(2000\pi t - 50\pi),\ 0 \le t \le 0.1 \\ cos(1500\pi t),\ 0.1 < t \le 0.2 \end{cases} \end{aligned} \tag{5.16}$$

The third signal $y_{s_3}(t)$ is also taken from [33], consisting of a time-frequency variant series and a low-frequency trend.

$$\begin{aligned} y_{s_3}(t) &= y_{s_3,1}(t) + y_{s_3,2}(t),\ 0 \le t \le 0.2 \\ y_{s_3,1}(t) &= \frac{1}{1.2 + cos(10\pi t)} \\ y_{s_3,2}(t) &= \frac{cos(160\pi t + cos(320\pi t))}{1.5 + sin(10\pi t)} \end{aligned} \tag{5.17}$$

To consider different initial SNRs, an adjustable parameter β is used to change the true vibration amplitudes, as expressed in equation (5.18).

$$y(t) = \beta y_{s_i}(t) + noise,\ i = 1, 2, 3 \tag{5.18}$$

Figure 5.3 presents the simulated signals $y_{s_i}(t),\ i = 1, 2, 3$, including the true vibrations and corresponding polluted signals, with initial SNR= −10 db. The true vibrations are nearly invisible in the polluted signals with such intense speckle noise.

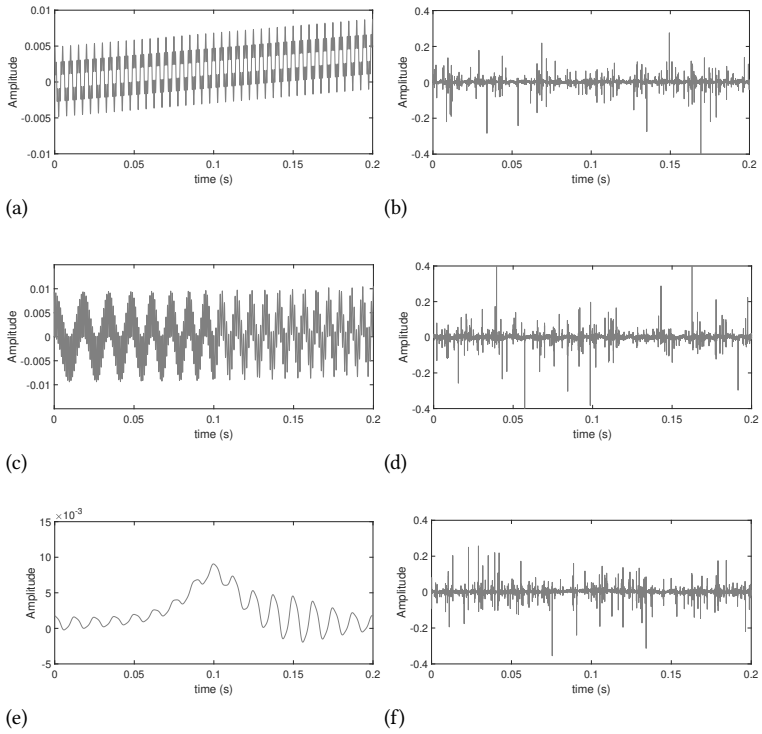

Figure 5.3: (**a**) The simulated signal $y_{s_1}(t)$, (**b**) the corresponding polluted signal of **a**, (**c**) the simulated signal $y_{s_2}(t)$, (**d**) the corresponding polluted signal of **c**, (**e**) the simulated signal $y_{s_3}(t)$, and (**f**) the corresponding polluted signal of **e**. SNR= −10 db.

5.3.2 Despeckle and vibration extraction

Firstly, the initial SNR is set −10 db to investigate the despeckling effects. To quantitatively evaluate the proposed approach, the post SNR and the correlation coefficient between $y_{s_i}(t)$, $i = 1, 2, 3$ and the despeckling results are calculated. The extracted vibration mode functions are compared with the simulated vibration components.

Figure 5.4 presents the despeckling and signal decomposition results of βy_{s_1}. Signals are magnified between 0.04 s and 0.08 s for oscillation details. The decomposed mode functions y_{Ω_1} & y_{Ω_2} agree well with the signal components $\beta y_{s_1,2}$ & $\beta y_{s_1,3}$, respectively, as shown in Figs. 5.4b & 5.4c. These results indicate that the proposed ADSD approach can extract the vibration components. The despeckling result is the summation of the mode functions and low-frequency oscillation, presenting a good agreement with the true vibration βy_{s_1} (Fig. 5.4a). The correlation coefficient is 0.9965 and the post SNR is 23.13 db, which indicates the effectiveness in eliminating the speckle noise and reconstructing the true vibrations. The EWT approach also achieves good despeckling results with correlation coefficient = 0.9567, but some distortions from the speckle noise remain (Fig. 5.4d). The BPF method fails to eliminate the speckle noise as sharp distortions from the noise remain.

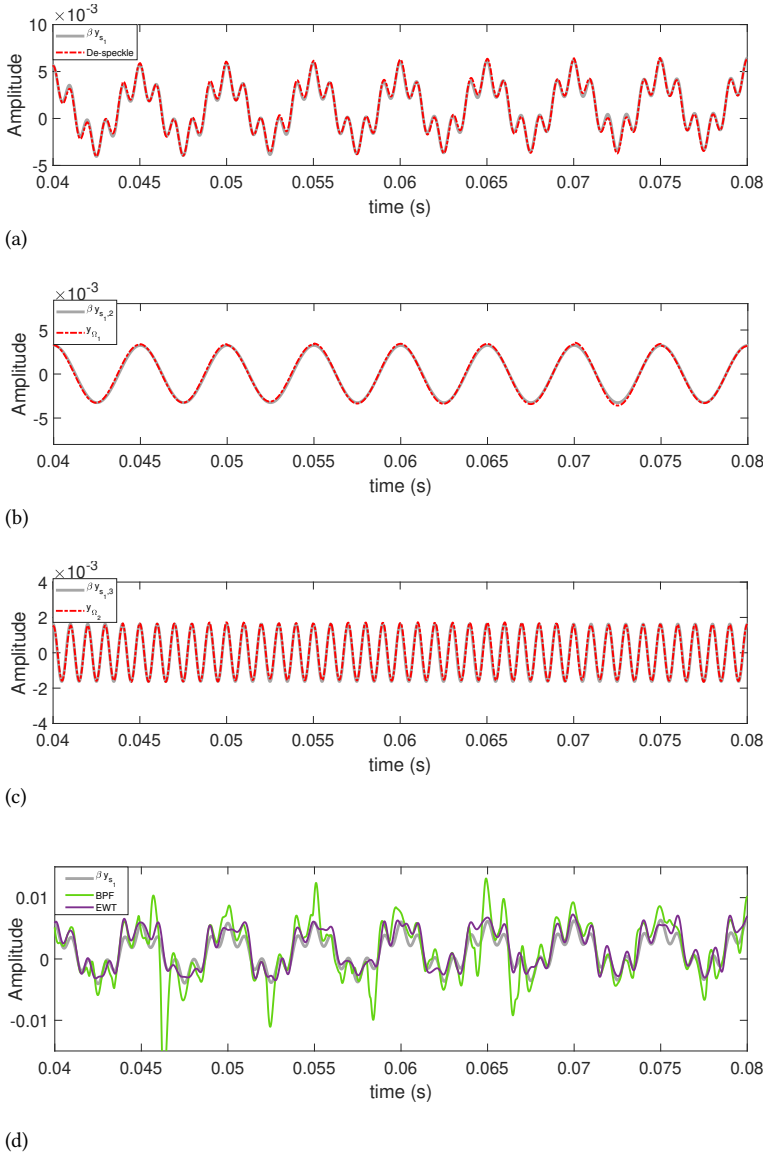

Figure 5.4: (**a**) The despeckling results of $\beta y_{s_1}(t)$ polluted by speckle noise, (**b**) the extracted mode function y_{Ω_1}, (**c**) the extracted mode function y_{Ω_2}, (**d**) and the despeckling results of BPF & EWT. Signals are magnified between 0.04 s and 0.08 s.

The ADSD results of the simulated signal βy_{s_2} are shown in Fig. 5.5. Good agreements between the extracted mode functions and signal components are visible in the illustrations. The mode function y_{Ω_1} reconstructs the time-frequency variant component $\beta y_{s_2,2}$, demonstrating the effectiveness in extracting wide-band vibrations. The segmented component $\beta y_{s_2,3}$ has been decomposed into y_{Ω_2} and y_{Ω_3}, each extending tiny oscillations

in the time domain. The despeckling result achieves a correlation coefficient of 0.9985 and a post SNR of 25.12 db. The EWT and BPF results both present large distortions although EWT achieves a correlation coefficient = 0.9629. The large local distortions would affect vibration analysis especially for locating the damages.

The ADSD results of the simulated signal βy_{s_3} are similarly promising, as shown in Fig. 5.6. The mode function y_{Ω_1} agrees well with the vibration component $\beta y_{s_3,2}$. The despeckling result achieves a correlation coefficient of 0.9979 and a post SNR of 25.29 db, demonstrating the effectiveness in eliminating the speckle noise. BPF fails to mitigate the distortions, while EWT also reveals the true vibration with post SNR = 16.94 db and correlation coefficient = 0.9782. Our proposed ADSD approach outperforms the BPF and EWT methods in eliminating the speckle noise and extracting the vibrations.

To evaluate the despeckling robustness, the initial SNR are altered to −15 db, −10 db and −5 db. Table 8.1 summaries the results of correlation coefficients and post SNRs. These evaluation parameters decrease when reducing the initial SNR. Nonetheless, the ADSD approach effectively eliminates the speckle noise regardless of the initial SNR, as the post SNRs reach over 16 db and the correlation coefficients are almost over 0.99. However, the BPF method fails to eliminate the noise especially when the initial SNR drops to −15 db. Although the EWT approach preforms well in mitigating the speckle noise, it preserves local distortions as in Fig. 5.5f. Therefore, our proposed approach outperforms others and demonstrates the robustness in eliminating the speckle noise.

Table 5.1: Post SNRs and correlation coefficients of despeckling results

	Initial SNR	Post SNR			Correlation		
		βy_{s_1}	βy_{s_2}	βy_{s_3}	βy_{s_1}	βy_{s_2}	βy_{s_3}
Proposed ADSD	-5 db	28.24 db	28.62 db	28.30 db	0.9993	0.9992	0.9992
	-10 db	23.13 db	25.12 db	25.29 db	0.9965	0.9985	0.9979
	-15 db	19.93 db	16.73 db	22.81 db	0.9949	0.9870	0.9953
BPF	-5 db	10.16 db	8.74 db	12.28 db	0.9350	0.9382	0.9548
	-10 db	7.43 db	4.93 db	6.97 db	0.8854	0.8697	0.8524
	-15 db	0.61 db	0.17 db	4.19 db	0.6617	0.7276	0.7852
EWT	-5 db	16.89 db	15.49 db	15.18 db	0.9848	0.9858	0.9884
	-10 db	12.16 db	11.26 db	14.94 db	0.9567	0.9629	0.9782
	-15 db	9.78 db	8.72 db	12.21 db	0.9267	0.9352	0.9473

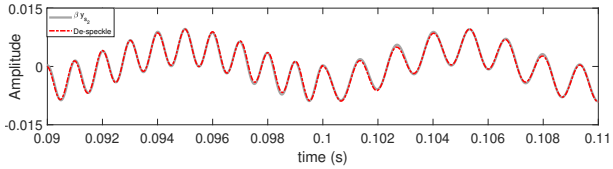

(a)

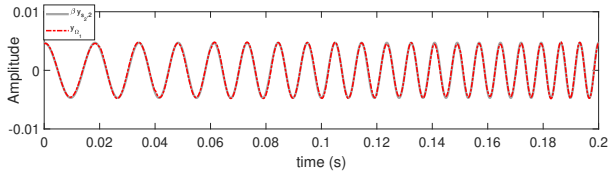

(b)

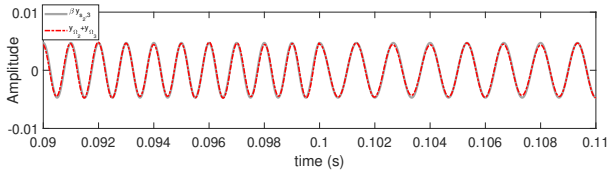

(c)

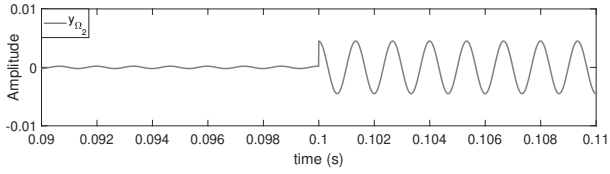

(d)

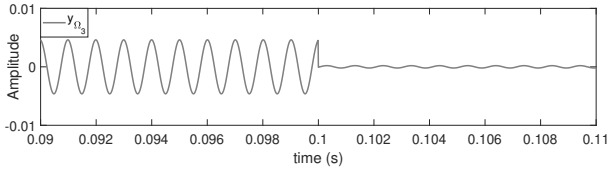

(e)

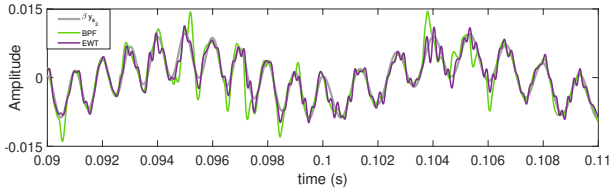

(f)

Figure 5.5: (**a**) The despeckling results of $\beta y_{s_2}(t)$ polluted by speckle noise, (**b**) the extracted mode function y_{Ω_1}, (**c**) the extracted mode function $y_{\Omega_2} + y_{\Omega_3}$, (**d**) the extracted mode function y_{Ω_2}, (**e**) the extracted mode function y_{Ω_3}, and (**f**) the despeckling results of BPF & EWT. Signals except **b** are magnified between 0.09 s and 0.11 s.

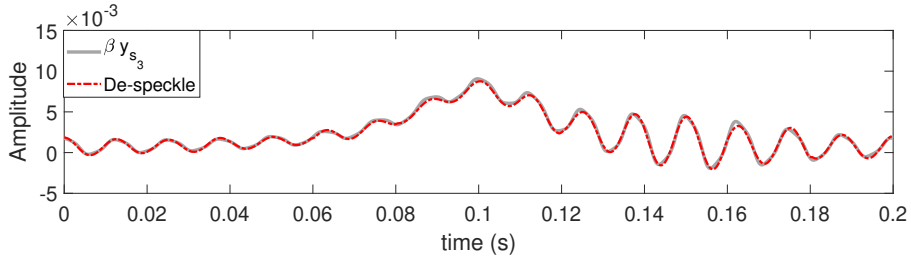

(a)

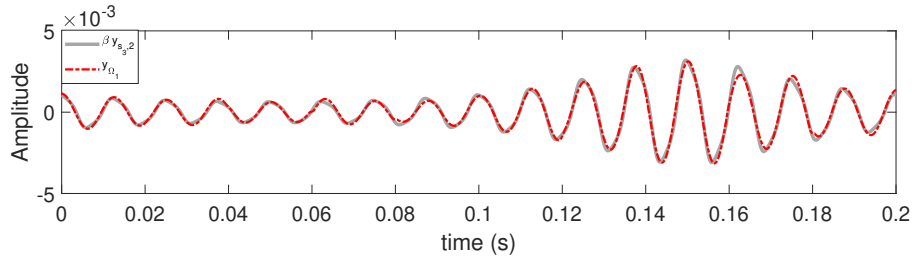

(b)

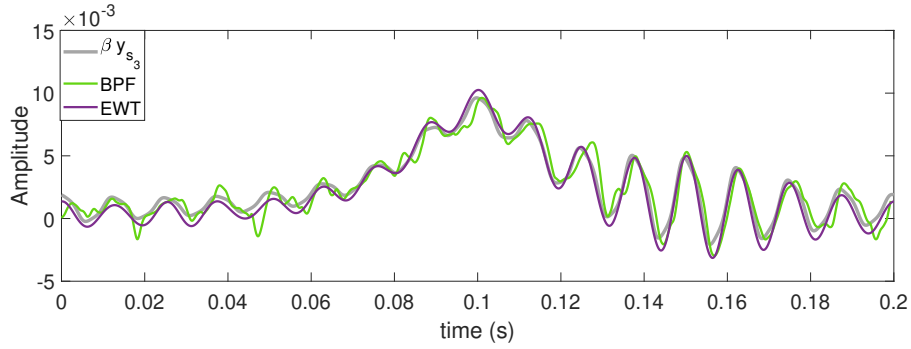

(c)

Figure 5.6: (**a**) The despeckling results of $\beta y_{s_3}(t)$ polluted by speckle noise, (**b**) the extracted mode function y_{Ω_1}.

5.4 Experimental results

5.4.1 First scenario

Three scenarios of physical experiments are considered to acquire LDVom signals and evaluate the ADSD approach. Firstly, a 540 mm steel strip, with three artificial defects (profile of 6×4 mm^2) at the positions of 40 mm, 220 mm, and 450 mm, is scanned by an LDVom, as shown in Fig. 5.7. The LDV transmits a laser beam deflected by the mirror to the vibrating surface. When the mirror rotates, the laser beam continuously scans the targets. The strip is mounted as a cantilever beam with the left side excited by a shaker. The input signal to the shaker is a stationary sinusoidal wave at 500 Hz. The scanning speed is approximately 0.085 m/s and the sampling frequency is 102400 Hz.

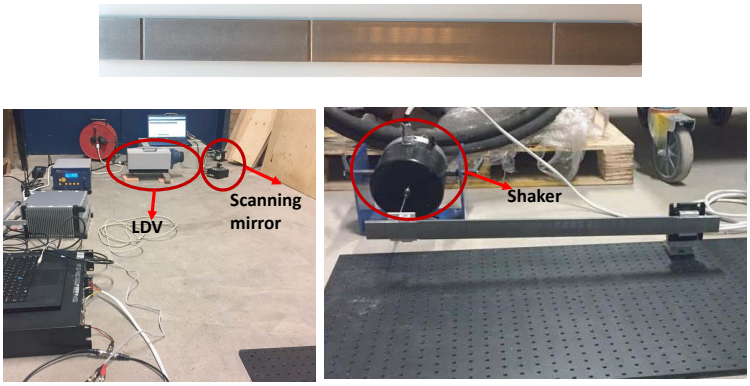

Figure 5.7: The experimental setup for scanning a steel strip.

The original signal contains intensely fluctuating speckle noise, as illustrated in Fig. 5.8. The amplitude of the actual vibration around 500 Hz varies below 0.05 (marked with a red rectangle), while the signal drop-outs exceed 40 times the vibration. The initial SNR is estimated approximately -14 db, indicating the poor signal quality. Continuously intense noise covers the 500 Hz oscillations especially at weak vibration positions (Fig. 5.8b), increasing the difficulty in extracting mode functions.

Figure 5.9 presents the despeckling results concerning strong vibrations (with amplitudes around 0.05). The BPF and EWT methods are adopted for comparison. The ADSD approach has revealed the 500 Hz vibration against the intense speckle noise (Fig. 5.9a). The EWT method reveals the vibration but distorts the amplitudes especially at intense-noise positions (marked with blue circles in Fig. 5.9c). BPF performs even worse as significant distortions (marked with blue circles) by speckle noise occupy many locations (Fig. 5.9b).

Figure 5.10 presents the despeckling result concerning weak vibrations (with amplitudes below 0.005), where the initial SNR is estimated -24 db. Although intense noise has covered the weak 500 Hz vibrations, our proposed approach properly revealed the actual vibration that fits the original signal well. However, the BPF results preserve significant distortions (Fig. 5.10b) and the EWT results lose weak oscillations (marked with blue circles in Fig. 5.10c). Therefore, the proposed approach outperforms others and demonstrates applicability

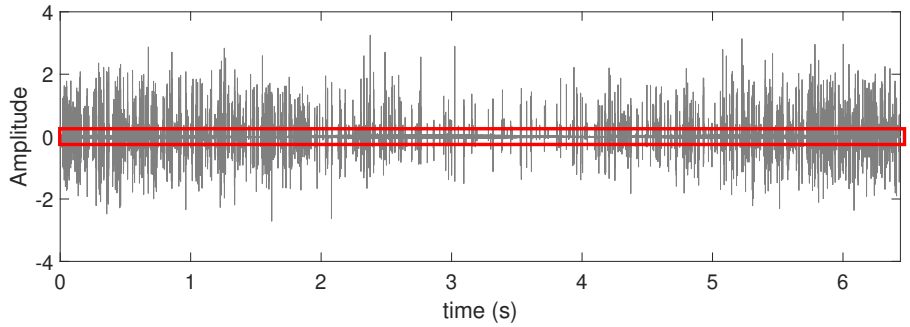

(a)

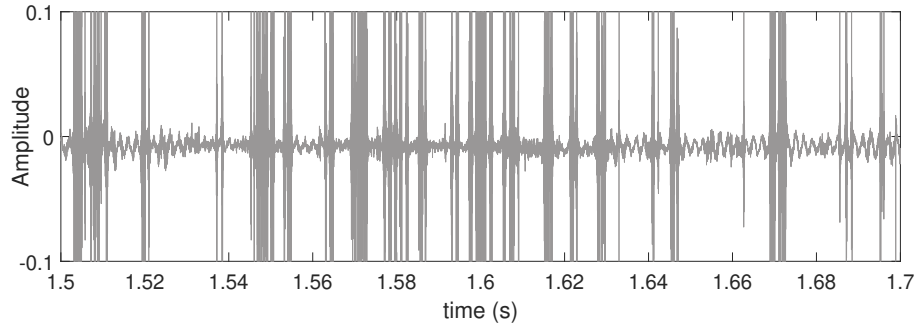

(b)

Figure 5.8: (**a**) The scanning signal from a steel strip, (**b**) and the magnified signal between 1.5 s and 1.7 s.

to eliminating the speckle noise and extracting the vibrations regardless of the noise and vibration intensity.

To further identify the defect locations, we conduct Hilbert transform on the extracted mode functions, with the spectrum illustrated in Fig. 5.11. The three artificial defects center at strong-energy locations that are identified at 39.16 mm, 226.23 mm and 455.73 mm. These identified defect locations agree well with the actual ones, which indicates the proper applications in damage inspection.

5.4.2 Second scenario

Secondly, a railway track sample is scanned by the LDVom, as shown in Fig. 5.12. To evaluate the applicability to extracting high-frequency vibrations, ultrasound generators are utilized to transmit a 0.5 MHz sinusoidal wave with 10 waveforms. The LDVom scans between the generators and acquires the resulted 0.5 MHz rail surface vibrations. The sampling frequency is 5 MHz.

Figure 5.13 presents the original scanning signal. The 0.5 MHz ultrasound wave appears at approximately 1.6×10^{-4} s, and other positions are severely polluted by speckle noise.

Figure 5.14 provides the extracted 0.5 MHz mode function. The continuous 10-waveform ultrasound wave has been revealed. Other positions also contain 0.5 MHz weak signals, which may arise from the residual ultrasound energy during transmission or the artefacts by the optimization calculation. Nonetheless, the proposed approach can eliminate the speckle noise and extract the wanted mode functions.

5.4.3 Third scenario

Thirdly, the LDVom scans the rail surface on a running railway system in the laboratory, as shown in Fig. 5.15. The laser beam is also deflected by a mirror onto the rail surface for scanning. The excitation is naturally produced by the wheel-rail contact and the running speed is 10km/h. The signal sampling frequency is 102400 Hz. The LDVom acquires the vibration signals during a wheel passing the rail joint.

Figure 5.16 illustrates the original signal and the despeckling result acquired by our ADSD approach. The original signal contains intense speckle noise as frequent signal drop-outs hide the actual vibration amplitudes. The dominant mode function acquired after despeckling fits the trend of the noisy signal. The mode excited by the wheel-rail contact is mainly at around 120 Hz. When the wheel approaches the joint, the vibration energy decreases; and when passing the joint, the wheel excites strong oscillations. The joint location is identified at approximately 0.175 s. Therefore, the proposed ADSD approach is applicable to eliminating the speckle noise and extracting the vibration for damage inspection.

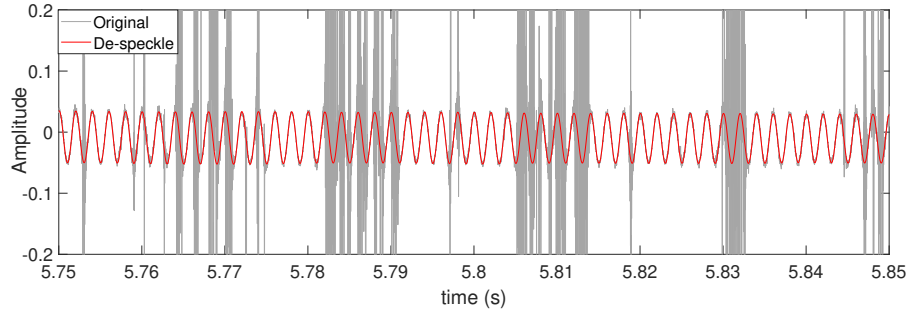

(a)

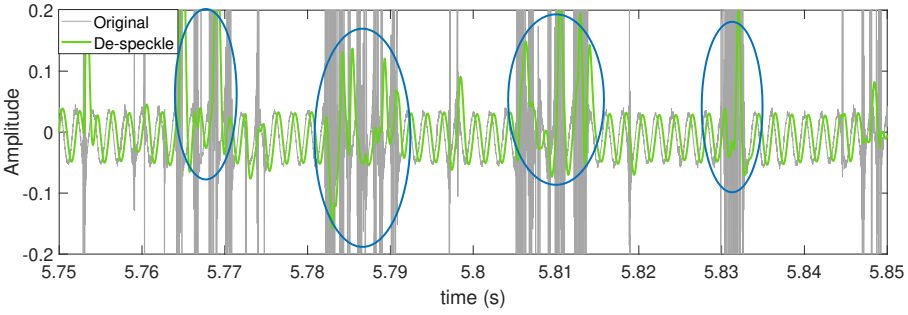

(b)

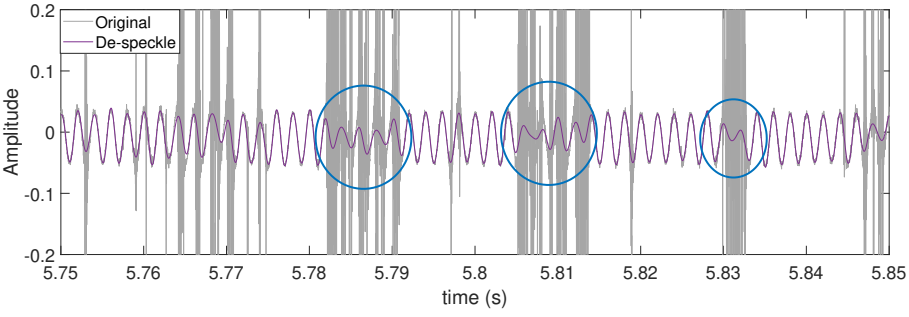

(c)

Figure 5.9: The despeckling results of (**a**) the ADSD approach, (**b**) BPF approach, and (**c**) EWT approach. Signals are magnified between 5.75 s and 5.85 s.

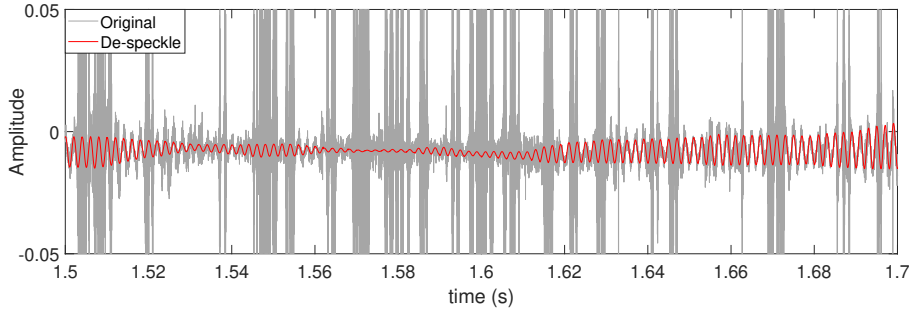

(a)

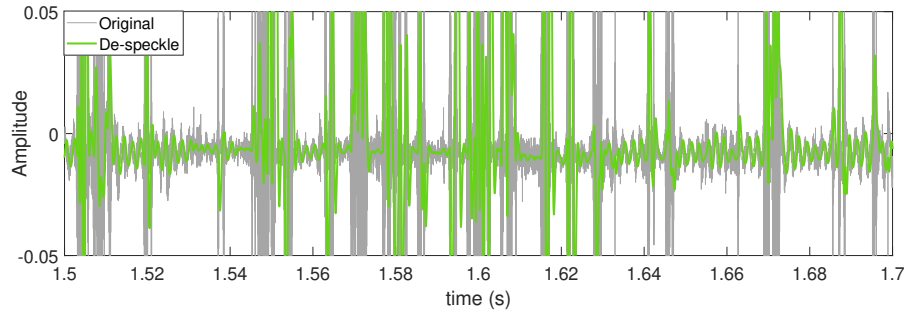

(b)

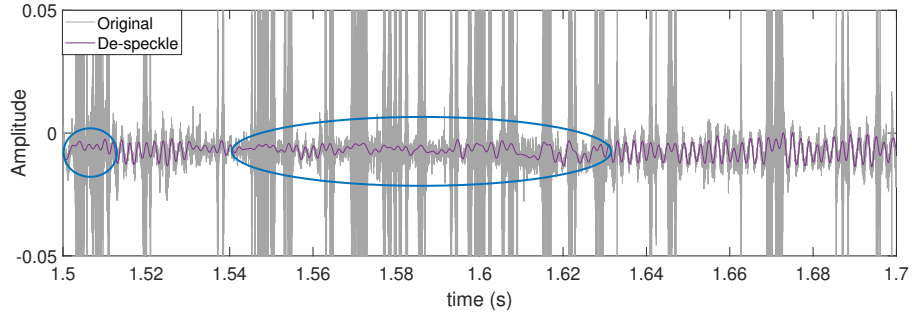

(c)

Figure 5.10: The de-speckle results of (**a**) the ADSD approach, (**b**) BPF approach, and (**c**) EWT approach. Signals are magnified between 1.5 s and 1.7 s.

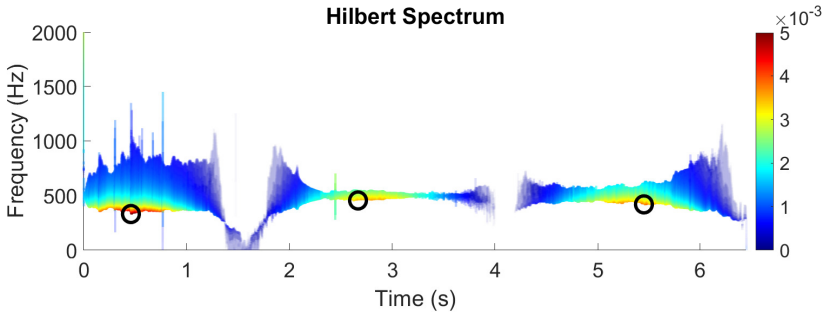

Figure 5.11: The Hilbert spectrum of the despeckled signal.

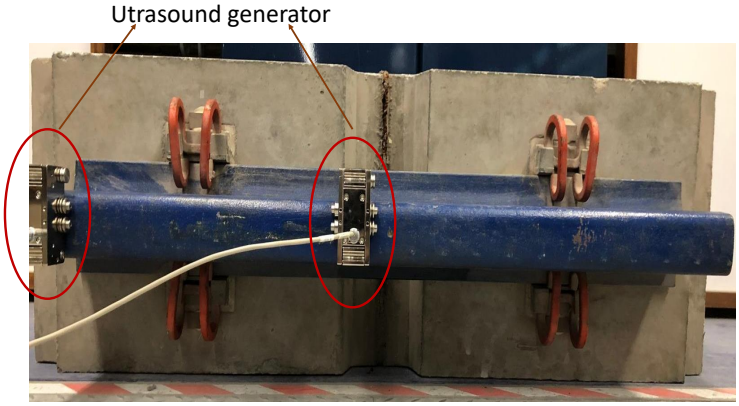

Figure 5.12: A railway track sample scanned by the LDVom.

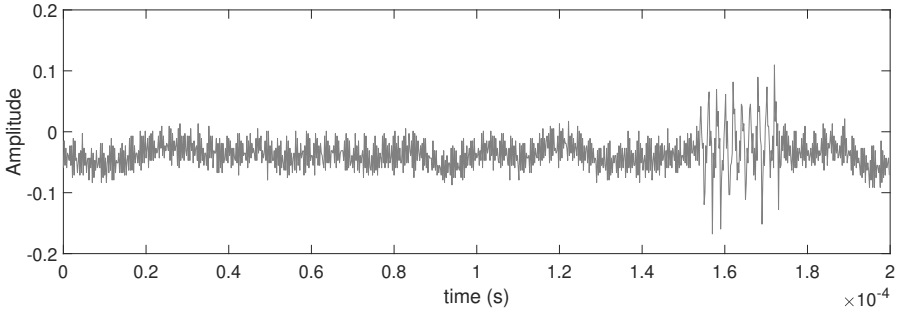

Figure 5.13: The scanning signal from a railway track sample.

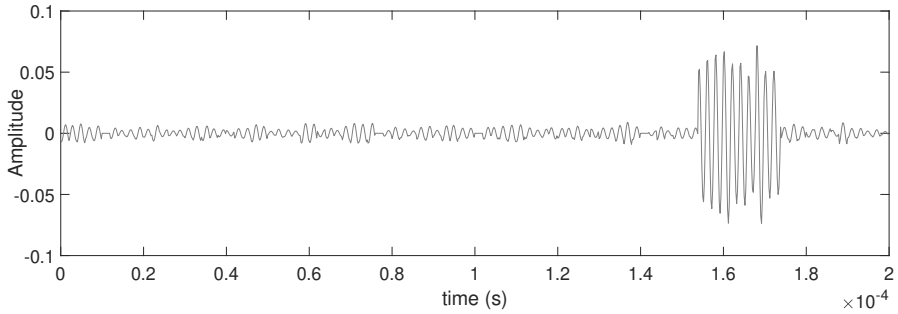

Figure 5.14: The extracted 0.5 MHz vibration.

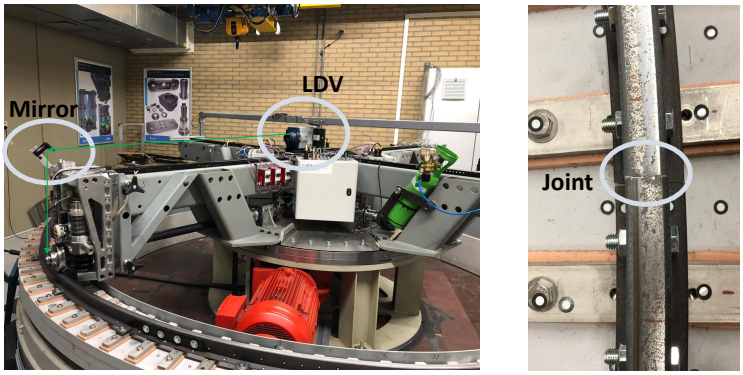

Figure 5.15: The LDVom scans from a running railway system in the laboratory.

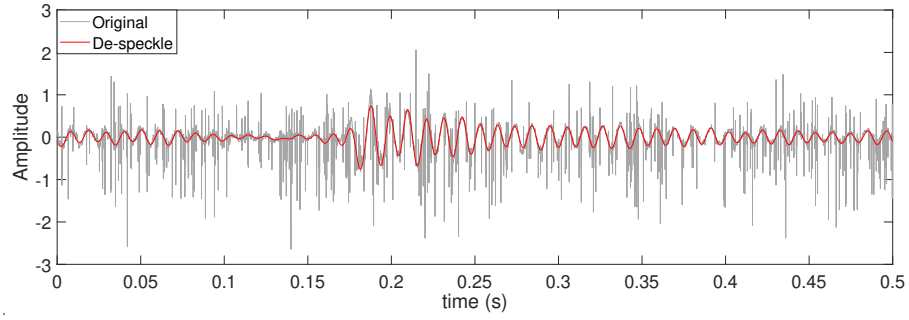

Figure 5.16: The original signal and the extracted vibration scanning from the running railway system.

5.5 Discussion and conclusion

In this paper, we propose a novel ADSD approach for analyzing LDVom signals. Speckle noise significantly distorts the vibration signal, as the signal drop-outs exceed 40 times the actual vibration and initial SNR drops to -14 db in physical experiments. This adaptive approach naturally determines the bandwidths of mode functions for time-frequency analysis. The Fourier spectrum is adaptively segmented with the identified vibration frequencies. The mode functions are basically derived from the wave equation and pointwisely calculated through optimization in a moving window. Since initial direct-current signals in instruments or the long-wavelength structural shape can migrate the outputs slightly with low-frequency trends, a quartic polynomial function is optimized to first extract these trends.

In the numerical simulation, three artificially produced signals (either stationary or nonstationary) are regarded as actual vibrations. The simulated speckle noise pollutes the signals with initial SNR controlled. When the initial SNR is -10 db, the ADSD approach extracts the mode functions that agree well with the signal components. A good agreement is also visible between the despeckled signal and true vibration. However, The BPF and EWT methods preserve numerous signal distortions by the speckle noise. When the initial SNR drops to -15 db, the ADSD results still achieve correlation coefficients almost over 0.99 and post SNRs over 16 db. The proposed approach outperforms the others and demonstrates the effectiveness and robustness in eliminating the speckle noise and extracting vibration mode functions.

Three physical experiments are conducted to acquire LDVom signals and evaluate the ADSD approach. In different scenarios with targets either artificially or naturally excited, the ADSD approach reveals the actual vibration against the intense speckle noise. The extracted mode function well fits the original signal regardless of the noise and signal intensity. The other methods preserve the distortions, especially when the waveform is covered by continuously intense noise. By analyzing the time series or Hilbert spectrum, the defect locations are properly identified. These promising results indicate the applicability to eliminating the speckle noise and extracting the vibrations. Future research will apply the ADSD results for modal analysis and damage inspection using an LDVom.

References

[1] W Fan and P Qiao. “Vibration-based damage identification methods: a review and comparative study”. In: *Structural health monitoring* 10.1 (2011), pp. 83–111.

[2] K Sugimoto, T Sugimoto, N Utagawa, and C Kuroda. “Detection of resonance frequency of both the internal defects of concrete and the laser head of a laser Doppler vibrometer by spatial spectral entropy for noncontact acoustic inspection”. In: *Japanese Journal of Applied Physics* 58.SG (2019), SGGB15.

[3] SH Abbas, JK Jang, DH Kim, and JR Lee. “Underwater vibration analysis method for rotating propeller blades using laser Doppler vibrometer”. In: *Optics and Lasers in Engineering* 132 (2020), p. 106133.

[4] AB Stanbridge and DJ Ewins. “Modal testing using a scanning laser Doppler vibrometer”. In: *Mechanical systems and signal processing* 13.2 (1999), pp. 255–270.

[5] SJ Rothberg, MS Allen, P Castellini, D Di Maio, JJJ Dirckx, DJ Ewins, Ben J Halkon, P Muyshondt, N Paone, T Ryan, et al. "An international review of laser Doppler vibrometry: Making light work of vibration measurement". In: *Optics and Lasers in Engineering* 99 (2017), pp. 11–22.

[6] S Rahimi, Z Li, and R Dollevoet. "Measuring with laser Doppler vibrometer on moving frame (LDVMF)". In: *AIP Conference Proceedings*. Vol. 1600. American Institute of Physics. 2014, pp. 274–286.

[7] YF Xu, DM Chen, and WD Zhu. "Damage identification of beam structures using free response shapes obtained by use of a continuously scanning laser Doppler vibrometer system". In: *Mechanical Systems and Signal Processing* 92 (2017), pp. 226–247.

[8] LF Lyu and WD Zhu. "Operational modal analysis of a rotating structure under ambient excitation using a tracking continuously scanning laser Doppler vibrometer system". In: *Mechanical Systems and Signal Processing* 152 (2021), p. 107367.

[9] P O'Malley, J Vignola, and J Judge. "Generalized laser Doppler vibrometer noise maps". In: *AIP Conference Proceedings*. Vol. 1457. 1. American Institute of Physics. 2012, pp. 24–34.

[10] P O'Malley, T Woods, J Vignola, J Judge, and A Kurdila. "Mapping LDV Noise As A Function Of Standoff Distance, Beam Focus, And Surface Roughness". In: *AIP Conference Proceedings*. Vol. 1253. 1. American Institute of Physics. 2010, pp. 291–297.

[11] P Hosek. "Algorithm for signal drop-out recognition in IC engine valve kinematics signal measured by laser Doppler vibrometer". In: *Optics & Laser Technology* 44.4 (2012), pp. 1101–1112.

[12] A Dräbenstedt. "Diversity combining in laser Doppler vibrometry for improved signal reliability". In: *AIP Conference Proceedings*. Vol. 1600. American Institute of Physics. 2014, pp. 263–273.

[13] SJ Rothberg, JR Baker, and NA Halliwell. "Laser vibrometry: pseudo-vibrations". In: *Journal of Sound and Vibration* 135.3 (1989), pp. 516–522.

[14] M Denman, NA Halliwell, and SJ Rothberg. "Speckle noise reduction in laser vibrometry: experimental and numerical optimisation". In: *Second International Conference on Vibration Measurements by Laser Techniques: Advances and Applications*. Vol. 2868. International Society for Optics and Photonics. 1996, pp. 12–21.

[15] Y Jin and Z Li. "Eliminating Speckle Noises for Laser Doppler Vibrometer Based on Empirical Wavelet Transform". In: *2021 13th International Conference on Measurement*. IEEE. 2021, pp. 72–75.

[16] P Martin and SJ Rothberg. "Pseudo-vibration sensitivities for commercial laser vibrometers". In: *Mechanical systems and signal processing* 25.7 (2011), pp. 2753–2765.

[17] P Martin and S Rothberg. "Introducing speckle noise maps for laser vibrometry". In: *Optics and Lasers in Engineering* 47.3-4 (2009), pp. 431–442.

[18] J Vass, R Šmıd, RB Randall, P Sovka, C Cristalli, and B Torcianti. "Avoidance of speckle noise in laser vibrometry by the use of kurtosis ratio: Application to mechanical fault diagnostics". In: *Mechanical Systems and Signal Processing* 22.3 (2008), pp. 647–671.

[19] M Martarelli and DJ Ewins. "Continuous scanning laser Doppler vibrometry and speckle noise occurrence". In: *Mechanical Systems and Signal Processing* 20.8 (2006), pp. 2277–2289.

[20] J Zhu, Y Li, and R Baets. "Mitigation of speckle noise in laser Doppler vibrometry by using a scanning average method". In: *Optics letters* 44.7 (2019), pp. 1860–1863.

[21] YF Xu, DM Chen, and WD Zhu. "Modal parameter estimation using free response measured by a continuously scanning laser Doppler vibrometer system with application to structural damage identification". In: *Journal of Sound and Vibration* 485 (2020), p. 115536.

[22] P Chiariotti, M Martarelli, and GM Revel. "Delamination detection by multi-level wavelet processing of continuous scanning laser Doppler vibrometry data". In: *Optics and Lasers in Engineering* 99 (2017), pp. 66–79.

[23] Ł Pieczonka, Ł Ambroziński, WJ Staszewski, D Barnoncel, and P Pérès. "Damage detection in composite panels based on mode-converted Lamb waves sensed using 3D laser scanning vibrometer". In: *Optics and lasers in engineering* 99 (2017), pp. 80–87.

[24] Y Yang, Z Peng, W Zhang, and G Meng. "Parameterised time-frequency analysis methods and their engineering applications: A review of recent advances". In: *Mechanical Systems and Signal Processing* 119 (2019), pp. 182–221.

[25] A Kumar and R Kumar. "Time-frequency analysis and support vector machine in automatic detection of defect from vibration signal of centrifugal pump". In: *Measurement* 108 (2017), pp. 119–133.

[26] T Liu, J Li, X Cai, and S Yan. "A time-frequency analysis algorithm for ultrasonic waves generating from a debonding defect by using empirical wavelet transform". In: *Applied Acoustics* 131 (2018), pp. 16–27.

[27] L Durak and O Arikan. "Short-time Fourier transform: two fundamental properties and an optimal implementation". In: *IEEE Transactions on Signal Processing* 51.5 (2003), pp. 1231–1242.

[28] RS Pathak. *The wavelet transform*. Vol. 4. Springer Science & Business Media, 2009.

[29] T Hinamoto and WS Lu. *Digital Filter Design and Realization*. River Publishers, 2017.

[30] J Gilles. "Empirical wavelet transform". In: *IEEE transactions on signal processing* 61.16 (2013), pp. 3999–4010.

[31] WA Strauss. *Nonlinear wave equations*. 73. American Mathematical Soc., 1990.

[32] S Rothberg. "Numerical simulation of speckle noise in laser vibrometry". In: *Applied Optics* 45.19 (2006), pp. 4523–4533.

[33] TY Hou and Z Shi. "Adaptive data analysis via sparse time-frequency representation". In: *Advances in Adaptive Data Analysis* 3.01n02 (2011), pp. 1–28.

6

Conclusions and recommendations

6.1 Conclusions

Speckle noise is a significant issue of LDV technology, especially the LDVom due to the one-way continuously scanning nature. The main research question of this thesis is: What are the characteristics and mitigation approaches of LDVom speckle noise? This thesis focuses on the following three aspects to better understand the formation and behaviours of LDV speckle noise and develop solutions for its mitigation. They are 1) numerical simulation of the speckle noise considering two variables, surface roughness and scanning speed. It provides insight into behaviour changes of speckle noise in response to the two variables and possible tools for minimizing noise strength (Chapter 2); 2) investigation of the theoretical Fourier spectrum of speckle noise series, as the frequency domain characteristics help design the de-noise signal filter accordingly (Chapter 3); 3) investigation of the effect of classic signal processing approaches for de-noising and develop an adaptive approach based on vibration mechanisms (Chapter 4 and 5). Experiments on the steel strip and the downscale V-Track test rig validate the proposed approaches. Four research sub-questions defined in Chapter 1 are addressed accordingly in Chapter 2-5.

Q1: The speckle noise should be characterized based on numerical simulation and physical experiments. How to perform a realistic simulation of the LDVom speckle noise and acquire a deep understanding of its characteristics?

Chapter 2 addresses the research question Q1. The only previous research on simulating the LDV speckle noise was conducted by Rothberg [1], where two important variables were not considered: surface roughness and the scanning speed. Surface roughness determines the reflection phases of laser and further affects the speckle pattern generated by the laser beam. The scanning speed influences the variation of the speckle pattern, and the phasor variation determines the speckle noise. In Chapter 2, a method is proposed to simulate the LDVom speckle noise numerically, considering surface roughness and the scanning speed. The simulated noise series are then characterized based on the changes of these two variables. The main conclusions are as follows:

- The amplitude distributions of the simulated speckle noise and the experimental one are similar, approximately a Gaussian distribution. The simulation approach is reliable according to the similarities between the simulated and experimental speckle noises.
- When the laser focuses on a single vibration point, the frequency spectra of speckle noise present constant intervals of frequency peaks. The frequency interval, as well as the noise period, is the same as the cyclical motion period of the focused vibration spot.
- The speckle noise energy increases with the surface roughness below a specific value and after that, fluctuates around a constant.
- For LDVom speckle noise, the energy increases with the scanning speed but the signal drop-outs reduces in intensity and density.

The characteristics discovered provide some evidences for future mitigation of the speckle noise:

- A bandpass filter would be effective to remove single-point speckle noise, but the speckle noise would increase or reduce the vibration energy at the vibration frequency.
- Using low scanning speed for LDVom can drop the speckle noise energy;
- Keeping the scanning surface smooth can reduce the speckle noise energy.

Q2: Based on the characteristics of the LDVom speckle noise shown in the Fourier spectrum, how to mitigate the speckle noise from the frequency domain?

Chapter 3 provides the answer to the research question Q2. Fourier transform is theoretically conducted on the speckle noise series to investigate the frequency domain features. Two de-noise approaches are proposed accordingly, with their advantages and limitations discussed. The effectiveness of the proposed approaches is evaluated by experiments of LDVom scanning a steel strip. The major conclusions are:

- A periodic oscillation has been discovered in the Fourier spectra of the LDVom speckle noise. The first frequency peak of this oscillation equals to $v_s/2L$, and the frequency peak intervals equal to v_s/L, where v_s is the scanning speed and L is the diameter of LDV focusing spot.
- When the maximum target vibration frequency is much smaller than the first frequency peak $v_s/2L$, the noise energy at the vibration frequency will be small. Therefore, a low-pass filter can mitigate most speckle noise and recover the vibration signal. This low-pass filter can be implemented as an equipment unit for the real-time de-speckling process. According to this finding, the LDVom scanning speed should be as large as possible to mitigate the speckle noise. However, fast scanning also means low measurement resolution and the scanning speed is limited by the optical equipment used.
- When the target vibration frequency is close to or larger than the first frequency peak $v_s/2L$, the vibration energy can be obtained by removing the oscillation trend of the frequency spectra. However, due to our assumption of infinite speckle noise series when conducting Fourier transform, this strategy is less effective with short signal series. In addition, effectiveness drops while handling many vibration frequencies.

Q3: How does the adaptive approach, ensemble empirical mode decomposition (EEMD), which processes signals from the time domain, perform on handling speckle noise?

Chapter 4 answers the research question Q3. Three signal processing approaches, including the discrete wavelet transform, the band-pass filter and the ensemble empirical mode decomposition (EEMD), are compared on their de-speckling effect. An algorithm is

proposed based on EEMD with two steps: 1) adaptively cut off the signal drop-outs with moving root-mean square envelopes; and 2) remove the first few intrinsic mode functions (IMFs) related to the speckle noise. In addition, the resulted Hilbert-Huang spectra can present the vibration features. The numerically simulated LDVom speckle noise is added to different non-linear signals with different signal-to-noise ratio, in order to investigate the effectiveness of the approaches. Signals from two experiments on the steel strip and the downscale V-Track test rig are also studied. The major conclusions are:

- The classic discrete wavelet transform and band-pass filter keeps large distortions produced by the speckle noise, especially when the original signal-to-noise ratio is low.
- The proposed EEMD-based approach is effective to eliminate the speckle noise. It achieves high correlation coefficient between noisy and processed signals, as well as high post signal-to-noise ratio.
- The damage locations present highest local vibration energy in the Hilbert-Huang spectrum.
- There are two issues of the EEMD-based approach. 1) It costs much computational resources. 2) The selection of IMFs is dependent on operating experience, which needs future investigation for automation.

Q4: How to develop a signal processing approach for mitigating speckle noise, as well as decomposing signals to frequency bands for vibration analysis?

Chapter 5 aims to answer the research question Q4. In this chapter, an adaptive denosing and signal decomposition (ADSD) approach is proposed to eliminate the speckle noise and decompose the signal to different vibration modes. This approach consists of three steps. In the first step, the signal series is divided to n segments, on each we assume that the vibration is continuous along the scanning direction. In the second step, the Fourier spectrum is adaptively segmented, with each spectrum segment containing one vibration mode. In the third step, a mathematical optimization is conducted to extract each vibration mode. The numerically simulated LDVom speckle noise is added to different non-linear signals with different signal-to-noise ratio, in order to investigate the effectiveness of the approaches. Signals from three experiments on a steel strip, a fixed rail and the downscale V-Track test rig are also studied. The major conclusions are:

- The proposed ADSD approach is effective to eliminate the speckle noise. It achieves high correlation coefficient between noisy and processed signals, as well as high post signal-to-noise ratio.
- The damage locations present highest local vibration energy in the Hilbert-Huang spectrum.
- The LDVom and ADSD approach are applicable to scanning the rail and acquiring high-frequency ultrasound vibrations.
- The ADSD approach still costs much computational resources.

6.2 Applications of the research findings

There are multiple approaches proposed in this dissertation to simulate and mitigate LDVom speckle noise. These approaches improve the signal quality of LDVom, so that LDVom becomes feasible in filed applications. The following potential applications are proposed accordingly:

- Based on the proposed approach to simulate speckle noise, it is convenient to characterize many aspects of speckle noise and evaluate any de-speckling approaches for LDVom. This numerical simulation is also flexible to change with different scanning strategy, and therefore evaluating the noise level of new LDV scanning technology is possible.
- Based on the Fourier analysis of speckle noise series, high scanning speed becomes an advantage in mitigating speckle noise. Therefore, LDVom mounted on the vehicle is suitable for railway scanning. With 30m/s running speed, the vibration with frequency under 20 kHz is possible to be revealed. However, other field issues may appear.
- With the EEMD-based and ADSD approaches, the signal quality has been improved. These two approaches can be applied to eliminate speckle noise in many LDV applications.
- Supported by our de-speckling strategies, LDVom technology can be applied in monitoring large field structures, especially those requires to monitor the continuous vibration responses.

6.3 Recommendations for future research

This dissertation provides an insight into the characteristics and the eliminating strategies of LDVom speckle noise. The following are recommended for future research to extend the current work.

- For the simulation of speckle noise, randomly distributed phasors from a Gaussian distribution were chosen to simulate the speckle elements on the rough surface. Measured distributions from rough surfaces should be adopted in the simulation. Besides, the effect of focusing spot size is worth investigating.
- The proposed signal processing approaches for mitigating speckle noises are computationally heavy. Future research can also concern fast but accurate algorithms.
- The investigation of LDVom field applications should be the next step to further develop this technology.

References

[1] S Rothberg. “Numerical simulation of speckle noise in laser vibrometry”. In: *Applied Optics* 45.19 (2006), pp. 4523–4533.

7

Appendix I: A Theoretical Framework for A Succinct Empirical Mode Decomposition

Empirical mode decomposition (EMD) lacks a strong theoretical support although extensively applied. We propose a theoretical framework for a succinct EMD in this work, with the assumption of invariant extrema locations for one IMF extraction. We define the envelope mean filter (EMF) and prove that the filter matrix satisfies five properties. The sifting matrix is convergent to an idempotent matrix. An IMF is the projection of the input signal on the generalized eigenspace of the EMF matrix. An IMF is orthogonal to the residual signal, but different IMFs have no orthogonality. With numerical experiments on different signals, our framework achieves similar results to the classic EMD.

7.1 Introduction

Empirical mode decomposition (EMD) [1] is an adaptive time-frequency analysis technique for processing nonstationary and nonlinear signals. It has evolved in algorithms [2, 3, 4, 5] and presented superior performances in extensive applications [6, 7, 8]. The intrinsic mode functions (IMFs) acquired within naturally determined bandwidths represent the oscillation modes and have physical meanings for Hilbert transform. An IMF should satisfy that: (1) the numbers of extrema and zero-crossings differ by 0 or 1, and (2) the local mean determined by envelopes is 0. For a discrete signal $y(t)$, Huang et al. [1] developed the following sifting process to extract an IMF:

1. Identify the local extrema of the input signal $h_i(t)$, where $h_0(t) = y(t)$;

This chapter is based on the paper: Jin, Y., & Li, Z. Theoretical Framework for A Succinct Empirical Mode Decomposition. IEEE signal processing letters (accepted).

2. Calculates the upper and lower envelopes using the extrema and then calculate the envelope mean $M(t)$;

3. Update $h_{i+1}(t) = h_i(t) - M(t)$;

4. Repeat the upper steps with $i = 0, 1, 2, ...$ until $h_{i+1}(t)$ becomes an IMF.

Although EMD is proposed on the basis of the Hilbert transform, its data-driven algorithm lacks strong theoretical support. This is a significant issue of EMD. The primary research decomposing the fractional Gaussian noise [9] revealed the filter characteristic of EMD experimentally, with similar findings in [10, 11, 12, 13]. Yang et al. [14] demonstrated that the cubic B-spline interpolation to formulate the local envelopes is a low-pass filter. Indeed, the cubic spline filter constitutes a time-varying signal processing system [15], and the bandwidth narrows with iteration [16]. An alternative approach, namely partial differential equation [17, 18, 19], for calculating the envelope-mean provides an analytical expression of EMD. However, these researches only concerned the expression of envelopes and altering the envelope approach [20, 21, 22] did not promote the theory further. To our best knowledge, a theoretical framework that interprets the sifting process and IMFs and proves multiple properties (e.g., convergence and orthogonality) of EMD remains to be developed.

In our work, we propose a theoretical framework for a succinct EMD. The difference with classic EMD is our assumption that the locations of the extrema in the time domain are invariant when extracting one IMF. The cubic spline interpolation is discussed and several properties of the envelope mean are proved. The convergence of the sifting process and the orthogonality of IMFs are investigated. In numerical experiments, we compare the decomposition results under our framework with those of classic EMD.

7.2 Theory

7.2.1 Envelope mean

A time-varying filter bank consists of the decimator, filters and expander with their parameters altering with time [23, 24, 25]. The envelope mean calculated from cubic spline interpolation is demonstrated as a time-varying filter [15]. Indeed, there are multiple approaches (e.g., [5, 20]) to construct envelopes that present similar time-varying filter properties, and thus we define the envelope-mean filter (EMF) for EMD.

Definition 1: For a time series (t_m, y_m), $m = 1, 2, ..., N$, the signal envelopes are calculated by interpolating with all maxima (t_{u_k}, y_{u_k}) $(k = 1, 2, ..., N_u)$ and minima (t_{v_l}, y_{v_l}) $(l = 1, 2, ..., N_v)$. The EMF is a time-varying filter by averaging the envelopes and the filter matrix Q should satisfy the following properties:

1.1 Only the columns u_k and v_l contain non-zero values;

1.2 The summation of each row equals 1;

1.3 All entries $q_{i,j}$, $i, j = 1, 2, ..., N$ are dependent on t_m, u_k and v_l, and independent on any y_m;

1.4 The geometric multiplicity of eigenvalue 0 is at least $N - N_u - N_v + 1$;

1.5 All eigenvalues $\lambda \in [0,1]$.

The cubic spline envelopes construct such an EMF, and the proof requires the expression of matrix Q. First, we consider the upper envelopes using the maxima. Extracting the maxima (t_{u_k}, y_{u_k}) from the signal (t_m, y_m) is a time-varying multirate decimator [14, 15]. The general expression of natural cubic spline interpolation [26, 27, 28] on (t_{u_k}, y_{u_k}) is

$$\begin{aligned} S_k(t) = &\frac{t-t_{u_k}}{\Delta t_{u_k}} y_{u_{k+1}} + \left(\frac{(t-t_{u_k})^3}{6\Delta t_{u_k}} - \frac{\Delta t_{u_k}(t-t_{u_k})}{6}\right) z_{u_{k+1}} \\ &+ \frac{t_{u_{k+1}}-t}{\Delta t_{u_k}} y_{u_k} + \left(\frac{(t_{u_{k+1}}-t)^3}{6\Delta t_{u_k}} - \frac{\Delta t_{u_k}(t_{u_{k+1}}-t)}{6}\right) z_{u_k} \end{aligned} \tag{7.1}$$

$$\begin{aligned} &\frac{\Delta t_{u_{k-1}}}{6} z_{u_{k-1}} + \frac{\Delta t_{u_{k-1}} + \Delta t_{u_k}}{3} z_{u_k} + \frac{\Delta t_{u_k}}{6} z_{u_{k+1}} \\ =&\frac{1}{\Delta t_{u_{k-1}}} y_{u_{k-1}} - \left(\frac{1}{\Delta t_{u_{k-1}}} + \frac{1}{\Delta t_{u_k}}\right) y_{u_k} + \frac{1}{\Delta t_{u_k}} y_{u_{k+1}} \end{aligned} \tag{7.2}$$

where, $S_k(t)$ is the interpolating function with $t_{u_k} \le t \le t_{u_{k+1}}$, z_{u_k} are the coefficients, $\Delta t_{u_k} = t_{u_{k+1}} - t_{u_k}$, and $z_{u_1} = z_{u_{N_u}} = 0$. Considering vectors $Y_u = \{y_{u_k} \mid k = 1,2,...,N_u\}$, $Z_u = \{z_{u_k} \mid k = 1,2,...,N_u\}$ and $S = \{S_k t_m \mid m = 1,2,...,N\}$, Equations (7.1) and (7.2) are rewritten in the matrix form.

$$\begin{aligned} S^\dagger &= \widehat{A_1} Y_u^\dagger + \widehat{B} Z_u^\dagger \\ C Z_u^\dagger &= D Y_u^\dagger \end{aligned} \tag{7.3}$$

where $\dagger$ represents the transpose of matrices or vectors. $\widehat{A_1}$ (Eq. (7.4)) is a $N \times N_u$ matrix with entries $\hat{a}_{m,k} = \frac{t_{u_{k+1}} - t_m}{\Delta t_{u_k}}$, $\hat{a}_{m,k+1} = \frac{t_m - t_{u_k}}{\Delta t_{u_k}}$ $(m \in [u_k, u_{k+1}]$, $k = 1,2,...,N_u - 1)$ and others equaling 0. $\widehat{B}$ is a $N \times N_u$ matrix with entries $\hat{b}_{m,k} = \frac{(t_{u_{k+1}} - t_m)^3}{6\Delta t_{u_k}} - \frac{\Delta t_{u_k}(t_{u_{k+1}} - t_m)}{6}$, $\hat{b}_{m,k+1} = \frac{(t_m - t_{u_k})^3}{6\Delta t_{u_k}} - \frac{\Delta t_{u_k}(t_m - t_{u_k})}{6}$ $(m \in [u_k, u_{k+1}]$, $k = 1,2,...,N_u - 1)$ and others equaling 0. C is a $N_u \times N_u$ matrix with entries $c_{1,1} = c_{N_u,N_u} = 1$, $c_{k,k-1} = \frac{\Delta t_{u_{k-1}}}{6}$, $c_{k,k} = \frac{\Delta t_{u_{k-1}} + \Delta t_{u_k}}{3}$, $c_{k,k+1} = \frac{\Delta t_{u_k}}{6}$ and others equaling 0. D is a $N_u \times N_u$ matrix with entries $d_{1,1} = d_{N_u,N_u} = 0$, $d_{k,k-1} = \frac{1}{\Delta t_{u_{k-1}}}$, $d_{k,k} = -\left(\frac{1}{\Delta t_{u_{k-1}}} + \frac{1}{\Delta t_{u_k}}\right)$, $d_{k,k+1} = \frac{1}{\Delta t_{u_k}}$ and others equaling 0.

$$\widehat{A_1} = \begin{bmatrix} \ddots & \vdots & \vdots & \iddots \\ \cdots & \frac{t_{u_{k+1}} - t_m}{\Delta t_{u_k}} & \frac{t_m - t_{u_k}}{\Delta t_{u_k}} & \cdots \\ \cdots & \frac{t_{u_{k+1}} - t_{m+1}}{\Delta t_{u_k}} & \frac{t_{m+1} - t_{u_k}}{\Delta t_{u_k}} & \cdots \\ \iddots & \vdots & \vdots & \ddots \end{bmatrix} \tag{7.4}$$

Matrix C is strictly diagonally dominant and is thereby invertible [29, 30, 31]. Let $\vec{e}_n$ represent an all ones vector with length n, and $\vec{\mathbf{0}}_n$ represent a zero vector with length n. Since the summation of each row from matrix D equals 0, $\vec{e}_{N_u}$ is the eigenvector of D

corresponding to the eigenvalue 0. Considering the $N \times N_u$ matrix $\widehat{A_2} = \widehat{B}C^{-1}D$, we can obtain that

$$\widehat{A_2}\vec{e}_{N_u}^{\dagger} = \widehat{B}C^{-1}D\vec{e}_{N_u}^{\dagger} = \vec{\mathbf{0}}_N^{\dagger} \tag{7.5}$$

$$S^{\dagger} = (\widehat{A_1} + \widehat{A_2})Y_u^{\dagger} \tag{7.6}$$

According to Eq. (7.5), the summation of each row from matrix $\widehat{A_2}$ equals 0. The next step is upsampling the maxima Y_u to the signal Y, where vector $Y = \{y_m \mid m = 1, 2, ..., N\}$. Correspondingly, the matrices $\widehat{A_1}$ and $\widehat{A_2}$ are zero-padded with $u_{k+1} - u_k - 1$ columns between the column k and $k+1$, $k = 1, 2, ..., N_u - 1$ to achieve the $N \times N$ matrices A_1 and A_2. Eq. 7.7 shows the zero-padding of $\widehat{A_1}$.

$$A_1 = \begin{bmatrix} \ddots & \vdots & 0 & \cdots & 0 & \vdots & \iddots \\ \cdots & \frac{t_{u_{k+1}} - t_m}{\Delta t_{u_k}} & 0 & \cdots & 0 & \frac{t_m - t_{u_k}}{\Delta t_{u_k}} & \cdots \\ \cdots & \frac{t_{u_{k+1}} - t_{m+1}}{\Delta t_{u_k}} & 0 & \cdots & 0 & \frac{t_{m+1} - t_{u_k}}{\Delta t_{u_k}} & \cdots \\ \iddots & \vdots & 0 & \cdots & 0 & \vdots & \ddots \end{bmatrix} \tag{7.7}$$

We obtain the upper envelope interpolation matrix $A_u = A_1 + A_2$ and the upper envelope S as

$$S^{\dagger} = A_u Y^{\dagger} \tag{7.8}$$

Therefore, (1) according to the zero-padding process, only the columns u_k of A_1 and A_2 contain non-zero value and so for the matrix A_u. (2) Since the summation of each row of A_1 equals 1 and that of A_2 equals 0, the summation of each row of A equals 1. (3) Since the entries of $\widehat{A_1}$ and $\widehat{A_2}$ are only dependent on t_m and t_{u_k} and the zero-padding process is only dependent on u_k, A_u is only dependent on t_m and u_k.

Similarly, we can achieve the lower envelope matrix A_v that satisfies: (1) only the columns v_l contain non-zero value; (2) the summation of each row equals 1; and (3) all entries are only dependent on t_m and v_l. Therefore, the EMF matrix $Q = (A_u + A_v)/2$ meets the first three properties of our definition.

Since $N - N_u - N_v$ columns of Q are all zero, the matrix rank of Q is at largest $N_u + N_v$. The eigenspace for eigenvalue 0 contains at least $N - N_u - N_v$ linear-independent eigenvectors, which are $\vec{X}_i = (x_{i,1}, x_{i,2}, ..., x_{i,j}, ..., x_{i,N})$ with $x_{i,i} = 1$ and $x_{i,j} = 0$ $(j \neq i)$, $i \neq u_k, v_l$. We consider the vectors $\vec{P}_1 = (p_{1,1}, ..., p_{1,j}, ..., p_{1,N})$ with $p_{1,j} = 1$ $(j = u_1, u_2, ..., u_{N_u})$ and others equaling 0, and $\vec{P}_2 = (p_{2,1}, ..., p_{2,j}, ..., p_{2,N})$ with $p_{2,j} = 1$ $(j = v_1, v_2, ..., v_{N_v})$ and others equaling 0. Since the summation of each row of A_u or A_v equals 1, we can obtain

$$A_u\vec{P}_2^{\dagger} = A_v\vec{P}_1^{\dagger} = A_u\vec{P}_1^{\dagger} = A_v\vec{P}_2^{\dagger} = \vec{e}_N^{\dagger} \tag{7.9}$$

Therefore, Q has another eigenvector $\vec{X} = \vec{P}_1 - \vec{P}_2$ corresponding to eigenvalue 0. The geometric multiplicity of eigenvalue 0 is at least $N - N_u - N_v + 1$.

The last property is to determine the range of all eigenvalues. We consider the $(N_u+N_v)^2$ matrix $\widehat{Q}$ that only contains the rows and columns $u_k \cup v_l$ of Q. According to property **1.1**, except eigenvectors $\vec{X}_i$ of eigenvalue 0, the eigenvalue λ of Q is also that of $\widehat{Q}$ and the corresponding eigenvetor of Q is decimated at $u_k \cup v_l$ to that of $\widehat{Q}$. First, $\widehat{Q}$ has eigenvector $\vec{e}_{N_u+N_v}$ corresponding to eigenvalue 1. For any other eigenvector $\vec{P} = \{p_i \mid i = 1, 2, ..., N_u + N_v\}$ of $\widehat{Q}$ ($\widehat{Q}\vec{P}^\dagger = \lambda\vec{P}^\dagger$), it should have the first local maximum p_{s_1} and minimum p_{s_2}. Since $\widehat{Q}$ calculates the mean of interpolations $\hat{f}(p)$ for $\{p_{2i-1} \mid i = 1, 2, ...\}$ and $\hat{g}(p)$ for $\{p_{2_i} \mid i = 1, 2, ...\}$, we have the following relationships

$$\begin{aligned} &p_{s_1} - \widehat{Q}\vec{P}^\dagger \mid_{s_1} = (1-\lambda)p_{s_1} > 0 \\ &p_{s_2} - \widehat{Q}\vec{P}^\dagger \mid_{s_2} = (1-\lambda)p_{s_2} < 0 \\ &p_{s_1} > p_{s_2} \end{aligned} \tag{7.10}$$

Therefore, we can obtain $\lambda < 1$. Considering the entry p of $\vec{P}$ with maximum absolute value and $p \in \{p_{2i-1} \mid i = 1, 2, ...\}$ without loss of generality, we can obtain

$$\mid \hat{g}(p) \mid \leq \mid p_{2i} \mid_{max} \leq \mid p \mid \tag{7.11}$$

Thus, we can derive that

$$\lambda p^2 = (\frac{\hat{g}(p) + p}{2})p \geq 0 \tag{7.12}$$

Therefore, we can obtain $\lambda \geq 0$. In addition, we can use mathematical induction to prove that λ of $\widehat{Q}$ are all real. Considering all the aforementioned, $0 \leq \lambda \leq 1$ for matrix $\widehat{Q}$ as well as for matrix Q.

7.2.2 Sifting process

Huang et al. [1] developed the sifting process to extract an IMF. We assume that the extrema locations u_k, v_l are invariant when extracting one IMF. This is an approximation because the extrema locations only moves a little surrounding the initial ones during sifting process. Since Q is dependent on t_m, u_k and v_l and independent on any y_m, Q becomes invariant when extracting one IMF. Therefore, the sifting process can be expressed as

$$\vec{\xi}^\dagger = \lim_{\beta \to +\infty} (I_N - Q)^\beta Y^\dagger = GY^\dagger \tag{7.13}$$

where, $\vec{\xi}$ is an IMF, Y is the input signal, and I_N is the N^2 identity matrix. $G = \lim_{\beta \to +\infty}(I_N - Q)^\beta$ is the sifting matrix and the convergence of G should be determined.

Considering the unit linear-independent generalized eigenvectors [32] $\vec{\varrho}_i$ of Q and their corresponding eigenvalues λ_i ($i = 1, 2, ..., N$), the eigenvalues of $R = I_N - Q$ are $\mu_i = 1 - \lambda_i$. Thus we have

$$(R - \mu_i I_N)^\tau \vec{\varrho}_i^\dagger = \vec{\mathbf{0}}_N^\dagger, \ \exists\, \tau \in \mathbb{N}^+ \ \&\ \tau < N \tag{7.14}$$

$$\begin{aligned} R^{\beta} - \mu_i^{\beta} I_N &= (R - \mu_i I_N)(\sum_{j=0}^{\beta-1} \mu_i^j R^{\beta-1-j}) \\ &= (\sum_{j=0}^{\beta-1} \mu_i^j R^{\beta-1-j})(R - \mu_i I_N) \end{aligned} \tag{7.15}$$

Therefore, we can obtain

$$\begin{aligned} &(R^{\beta} - \mu_i^{\beta} I_N)^{\tau} \vec{\varrho}_i^{\dagger} \\ &= (\sum_{j=0}^{\beta-1} \mu_i^j R^{\beta-1-j})^{\tau} (R - \mu_i I_N)^{\tau} \vec{\varrho}_i^{\dagger} = \vec{\mathbf{0}}_N^{\dagger} \end{aligned} \tag{7.16}$$

Therefore, $\vec{\varrho}_i$ are the linear-independent generalized eigenvectors for eigenvalues μ_i^{β} of R^{β}. Since $\mu_i \in [0,1]$, $G = \lim_{\beta \to +\infty} R^{\beta}$ only has eigenvalues 0 and 1. Matrix G is similar to a Jordan normal form [33] with all diagonal entries of 0 and 1, and thus G is convergent. We also have

$$G^2 = \lim_{\beta \to +\infty} R^{2\beta} = G \tag{7.17}$$

Therefore, G is an idempotent matrix [34] and all the generalized eigenvectors $\vec{\varrho}_i$ are indeed eigenvectors.

7.2.3 Intrinsic mode functions

Eq. (7.13) is used to calculate an IMF. Considering the input signal Y represented by the unit linear-independent eigenvectors $\vec{\varrho}_i$, we can obtain

$$\vec{\xi}^{\dagger} = GY^{\dagger} = G \sum_{i=0}^{N} \alpha_i \vec{\varrho}_i^{\dagger} = \sum_{\mu_i = 1} \alpha_i \vec{\varrho}_i^{\dagger} \tag{7.18}$$

where α_i are the projection scalar of Y on $\vec{\varrho}_i$. Thus an IMF is indeed the projection of input signal Y on the generalized eigenspace for eigenvalue 0 of EMF Q, which corresponds to a high-pass filtering process.

The $\mathbb{C}^N$ Euclidean space W is the direct sum of two invariant eigenspaces W_0 and W_1 corresponding to the eigenvalues 0 and 1 of G, and $W_0 \perp W_1$. Since $\xi \in W_1$ and $Y - \xi \in W_0$, we have $\xi \perp (Y - \xi)$. Therefore, the sifting process to extract one IMF is an orthogonal decomposition.

Considering two IMFs $\xi_1^{\dagger} = G_1 Y^{\dagger}$ and $\xi_2^{\dagger} = G_2 (Y - \xi_1)^{\dagger}$, for any Y, $\xi_1 \perp \xi_2$ is equivalent to $(I_N - G_1^{\dagger}) G_2^{\dagger} G_1$ is an anti-symmetric matrix with all 0 diagonals. However, different Q mostly do not satisfy this condition. The classic EMD using cubic spline interpolation does not provide orthogonality between IMFs.

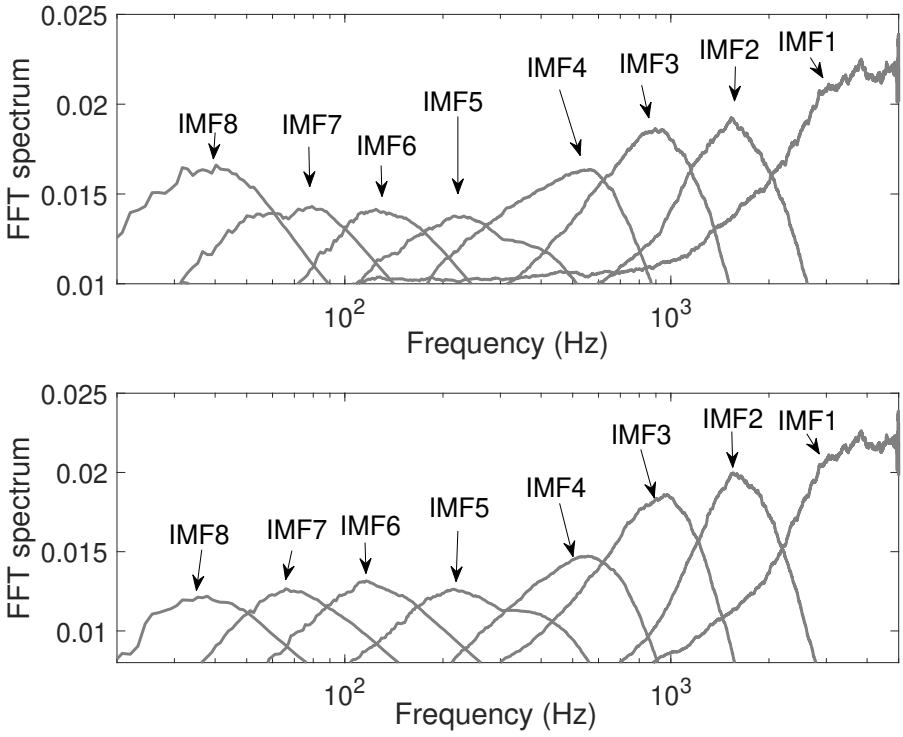

Figure 7.1: Top panel: FFT spectra of IMFs by projection on the generalized eigenspace for eigenvalue 0 of Q. Bottom panel: FFT spectra of IMFs by the classic EMD.

7

7.3 Numerical experiments

7.3.1 Filter bandwidth

First, we decompose Gaussian white noise by classic EMD procedures and by projection on the generalized eigenspace for eigenvalue 0 of Q. The sifting process iterates 100 times for the classic EMD procedures. The sampling frequency is 10 kHz and the length is 1 s for the Gaussian white noise. Fig. 7.1 illustrates the fast Fourier spectra of IMFs to demonstrate the filter bandwidths. Both FFT spectra present similar bandwidths for the corresponding IMFs. EMD works as overlapped bandpass filters on the time series [9]. The corresponding low-frequency IMFs with two decomposition procedures present different energy, which may arise from our assumption of invariant extrema locations and the finite iteration times of classic EMD.

7.3.2 Decomposition results

Second, a numerically generated signal Y consisting of a time-varying and a stationary components (Eq. (7.19)) is decomposed using the classic EMD and our framework. The sampling frequency is 10 kHz and the duration is 1 s.

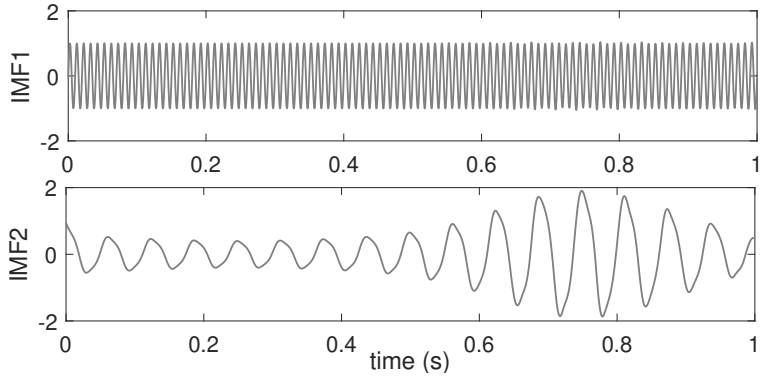

Figure 7.2: IMF1 and IMF2 achieved by projection on the generalized eigenspace for eigenvalue 0 of Q.

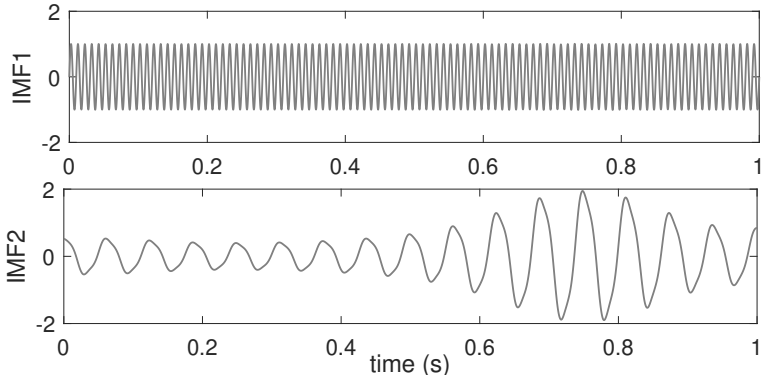

Figure 7.3: IMF1 and IMF2 achieved by the classic EMD.

$$\begin{aligned} Y_1 &= \frac{cos(32\pi t + cos(64\pi t))}{1.5 + sin(2\pi t)} \\ Y_2 &= sin(200\pi t) \\ Y &= Y_1 + Y_2 \end{aligned} \tag{7.19}$$

Fig. 7.2 illustrates the IMFs achieved by projection on the generalized eigenspace for eigenvalue 0 of Q. IMF1 and IMF2 agree well with Y_1 and Y_2, respectively. This indicates the decomposition accuracy of our EMD framework. The classic EMD also achieves similar results, as shown in Fig. 7.3.

Third, we decompose a seismic signal taken from [35], as shown in Fig. 7.4. Fig. 7.5 presents the Hilbert spectra by our EMD framework and the classic EMD. The spectra demonstrate similar distribution, e.g., large energy concentration at three close locations marked with the circles. The little decomposition difference may arise from our assumption of invariant extrema locations and the finite iteration times of classic EMD.

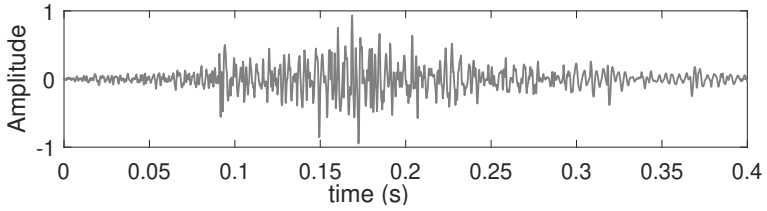

Figure 7.4: The seismic signal taken from [35].

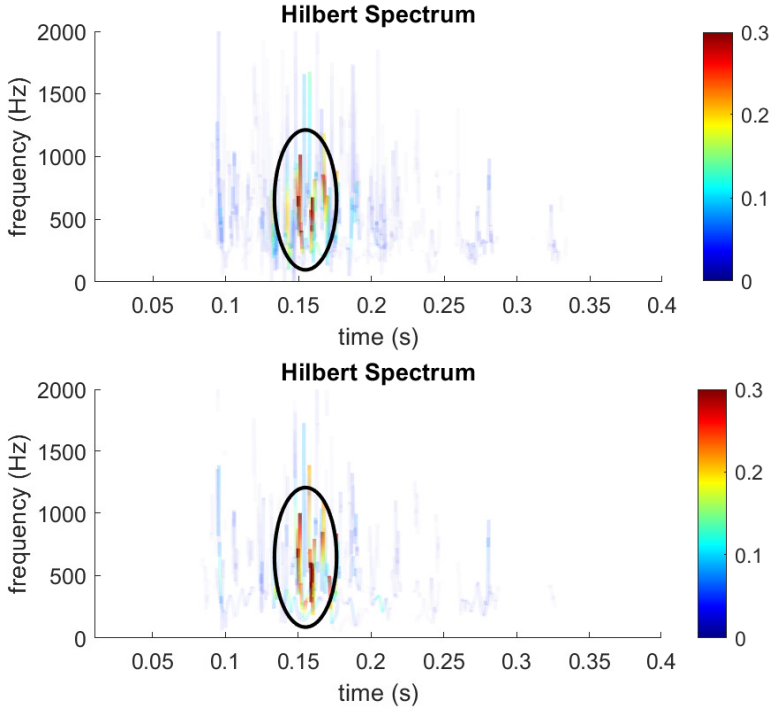

Figure 7.5: Top panel: Hilbert spectrum of IMFs by projection on the generalized eigenspace for eigenvalue 0 of Q. Bottom panel: Hilbert spectrum of IMFs by the classic EMD.

7.4 Conclusion

We propose a theoretical framework for EMD in this letter. The cubic spline interpolation works as an EMF with the filter matrix satisfying five properties. The sifting process matrix is convergent to an idempotent matrix only with eigenvalues 0 and 1. An IMF is the projection of the input signal on the generalized eigenspace of EMF matrix Q, which corresponds to a high-pass filtering process. Numerical experiments demonstrate that our framework achieves similar results to the classic EMD, although difference may result from the assumption of invariant extrema locations and the finite iteration times of classic EMD.

However, different IMFs are not orthogonal. Future work will concern the construction of the EMF matrix for IMF orthogonality. In addition, experiments should consider decomposing complicated signals and compare more EMD algorithms in the future work.

References

[1] NE Huang, Z Shen, SR Long, MC Wu, HH Shih, Q Zheng, N Yen, CC Tung, and HH Liu. "The empirical mode decomposition and the Hilbert spectrum for nonlinear and non-stationary time series analysis". In: *Proceedings of the Royal Society of London. Series A: Mathematical, Physical and Engineering Sciences* 454.1971 (1998), pp. 903–995.

[2] Z Wu and NE Huang. "Ensemble empirical mode decomposition: a noise-assisted data analysis method". In: *Advances in adaptive data analysis* 1.01 (2009), pp. 1–41.

[3] S Meignen and V Perrier. "A new formulation for empirical mode decomposition based on constrained optimization". In: *IEEE Signal Processing Letters* 14.12 (2007), pp. 932–935.

[4] ME Torres, MA Colominas, G Schlotthauer, and P Flandrin. "A complete ensemble empirical mode decomposition with adaptive noise". In: *2011 IEEE international conference on acoustics, speech and signal processing (ICASSP)*. IEEE. 2011, pp. 4144–4147.

[5] H Li, Y Hu, F Li, and G Meng. "Succinct and fast empirical mode decomposition". In: *Mechanical Systems and Signal Processing* 85 (2017), pp. 879–895.

[6] J Han and M Van der Baan. "Empirical mode decomposition for seismic time-frequency analysis". In: *Geophysics* 78.2 (2013), O9–O19.

[7] RJ Martis, UR Acharya, JH Tan, A Petznick, R Yanti, CK Chua, EYK Ng, and L Tong. "Application of empirical mode decomposition (EMD) for automated detection of epilepsy using EEG signals". In: *International journal of neural systems* 22.06 (2012), p. 1250027.

[8] L Wang and Y Shao. "Fault feature extraction of rotating machinery using a reweighted complete ensemble empirical mode decomposition with adaptive noise and demodulation analysis". In: *Mechanical systems and signal processing* 138 (2020), p. 106545.

[9] P Flandrin, G Rilling, and P Goncalves. "Empirical mode decomposition as a filter bank". In: *IEEE signal processing letters* 11.2 (2004), pp. 112–114.

[10] Z Wu and NE Huang. "A study of the characteristics of white noise using the empirical mode decomposition method". In: *Proceedings of the Royal Society of London. Series A: Mathematical, Physical and Engineering Sciences* 460.2046 (2004), pp. 1597–1611.

[11] G Rilling, P Flandrin, and P Gonçalves. "Empirical mode decomposition, fractional Gaussian noise and Hurst exponent estimation". In: *Proceedings.(ICASSP'05). IEEE International Conference on Acoustics, Speech, and Signal Processing, 2005.* Vol. 4. IEEE. 2005, pp. iv–489.

[12] P Flandrin and P Goncalves. "Empirical mode decompositions as data-driven wavelet-like expansions". In: *International journal of wavelets, multiresolution and information processing* 2.04 (2004), pp. 477–496.

[13] Z Wu and NE Huang. "On the filtering properties of the empirical mode decomposition". In: *Advances in Adaptive Data Analysis* 2.04 (2010), pp. 397–414.

[14] Y Yang, C Miao, and J Deng. "An analytical expression for empirical mode decomposition based on B-spline interpolation". In: *Circuits, systems, and signal processing* 32.6 (2013), pp. 2899–2914.

[15] Y Yang. "Empirical mode decomposition as a time-varying multirate signal processing system". In: *Mechanical Systems and Signal Processing* 76 (2016), pp. 759–770.

[16] H Li, Z Li, and W Mo. "A time varying filter approach for empirical mode decomposition". In: *Signal Processing* 138 (2017), pp. 146–158.

[17] E Deléchelle, J Lemoine, and O Niang. "Empirical mode decomposition: an analytical approach for sifting process". In: *IEEE Signal Processing Letters* 12.11 (2005), pp. 764–767.

[18] SD El Hadji, R Alexandre, and AO Boudraa. "Analysis of intrinsic mode functions: A PDE approach". In: *IEEE signal processing letters* 17.4 (2009), pp. 398–401.

[19] EHS Diop, R Alexandre, and V Perrier. "A PDE based and interpolation-free framework for modeling the sifting process in a continuous domain". In: *Advances in Computational Mathematics* 38.4 (2013), pp. 801–835.

[20] L Lin, Y Wang, and H Zhou. "Iterative filtering as an alternative algorithm for empirical mode decomposition". In: *Advances in Adaptive Data Analysis* 1.04 (2009), pp. 543–560.

[21] Y Kopsinis and S McLaughlin. "Investigation and performance enhancement of the empirical mode decomposition method based on a heuristic search optimization approach". In: *IEEE transactions on signal processing* 56.1 (2007), pp. 1–13.

[22] SD Hawley, LE Atlas, and HJ Chizeck. "Some properties of an empirical mode type signal decomposition algorithm". In: *IEEE Signal Processing Letters* 17.1 (2009), pp. 24–27.

[23] G Wang. "The most general time-varying filter bank and time-varying lapped transforms". In: *IEEE transactions on signal processing* 54.10 (2006), pp. 3775–3789.

[24] I Sodagar, K Nayebi, and TP Barnwell. "Time-varying filter banks and wavelets". In: *IEEE Transactions on Signal Processing* 42.11 (1994), pp. 2983–2996.

[25] M Vetterli and G Strang. "Time-varying filter banks and multiwavelets". In: *Proceedings of IEEE 6th Digital Signal Processing Workshop*. IEEE. 1994, pp. 223–226.

[26] CA Hall. "Natural cubic and bicubic spline interpolation". In: *SIAM Journal on Numerical Analysis* 10.6 (1973), pp. 1055–1060.

[27] SA Dyer and JS Dyer. "Cubic-spline interpolation. 1". In: *IEEE Instrumentation & Measurement Magazine* 4.1 (2001), pp. 44–46.

[28] T Lyche. "Discrete cubic spline interpolation". In: *BIT Numerical Mathematics* 16.3 (1976), pp. 281–290.

[29] O Taussky. "A recurring theorem on determinants". In: *The American Mathematical Monthly* 56.10P1 (1949), pp. 672–676.

[30] FO Farid. "Criteria for invertibility of diagonally dominant matrices". In: *Linear algebra and its Applications* 215 (1995), pp. 63–93.

[31] M Neumann. "A note on generalizations of strict diagonal dominance for real matrices". In: *Linear Algebra and its Applications* 26 (1979), pp. 3–14.

[32] H Anton. *Elementary Linear Algebra*. Wiley 2003 Support material, 1987.

[33] CG Cullen. *Matrices and linear transformations*. Courier Corporation, 2012.

[34] K Wainwright et al. *Fundamental methods of mathematical economics*. Boston, Mass. McGraw-Hill/Irwin, 2005.

[35] Wu. *seismic data*. Tech. rep. https://doi.org/10.6084/m9.figshare.8797502.v1, 2019.

8

Appendix II: A Fast Empirical Mode Decomposition

Although empirical mode decomposition (EMD) is extensively investigated and widely applied, its algorithm is time-consuming. We propose a fast EMD (FEMD) based on the newly developed theoretical framework. In our expression, the sifting process is a linear transform and only works on signal extrema. The theoretical time complexity dramatically decreases with FEMD, especially when requiring considerable iterations. Numerical experiments on white noise demonstrate the high time efficiency of FEMD. FEMD only costs 1/10 time of 'emd.m' in MATLAB when iterating 1,000 times. Other experiments on simulated and real signals indicate that FEMD can capture signal features with promising decomposition results.

8.1 Introduction

Empirical mode decomposition (EMD) is an adaptive signal processing approach for analyzing non-linear and non-stationary signals [**1**]. Although it works similar to filter banks [1] [2], its bandwidth changes over time to obtain instantaneous frequencies, different from Fourier transform and wavelet transform having certain bandwidths. The decomposition results represent the natural modes determined by the signal itself, not only the modes inside the preset frequency bands. Since proposed, this self-driven method [3] has been successfully applied for extracting signal features in wide-range areas, including medical and biological research [4] [5], analysing climate time-series [6] [7], identifying the mechanical faults [8] [9] and multi-dimension analysis [10] [11]. Many researches have also complemented EMD [12] [13] and handled the issues including mode mixing [14] and end effects [15]. In addition, a theoretical framework of EMD has been proposed recently to support the decomposition algorithm [16], which will be the foundation of this paper.

Low computational efficiency restricts the application extent, especially in real-time signal analysis and online mechanical system monitoring. Although showing better results, it took around 70 minutes to process complicated signals with 30 thousand points, 500 times

This chapter is based on the paper: Jin, Y., & Li, Z. A Fast Empirical Mode Decomposition. (to be submitted to a journal).

slower than the wavelet transform [17]. Wang et al. [18] demonstrated that the theoretical computational complexity of EMD is $41S \cdot nlog_2(n)$, comparable to that of the fast Fourier transform $O(nlog(n))$, where S is the maximum iteration times and n is the signal length; However, they overlooked sifting iterations that may repeat thousands of times when the signals are complicated [19]. Some researches focused on hardware acceleration to reduce the consumed time (e.g. [20, 21, 22]), but the accelerations would still be limited by the theoretical computational complexity. Developing a fast EMD (FEMD) algorithm is required for improving time efficiency.

Some novel approaches have complemented the fast algorithm of EMD. Most of them [23, 24, 25, 26] concentrated on the fast bidimensional and multivariate EMD algorithm, but they improved time efficiency in multi-dimension interaction instead of the basic EMD algorithm. An order-statistics filter was used in [27] [28], but the iteration times was reduced to decrease the decomposition time. Other approaches were not evaluated with signal-decomposition experiments [29] [30]. An effective FEMD algorithm remains to be developed.

In this work, we propose a novel FEMD approach based on the recently developed theoretical framework. Sifting process on the entire signal can be replaced by that on the extrema. The accuracy and time efficiency of FEMD are evaluated with numerical experiments.

8

8.2 Theory

8.2.1 Empirical mode decomposition

EMD decomposes the signals into intrinsic mode functions (IMFs) containing instantaneous frequency information, with local means equal to 0. IMFs are signal functions satisfying that (i) the number of extrema differs no more than 1 from that of zero-crossing points, and (ii) the averages of upper and lower envelopes determined by the extrema should be 0. The sifting process was designed to acquire IMFs using the following algorithm [**1**]:

Algorithm 8 Pseudo codes of EMD

Input: original signal $y(x)$, maximum iteration times S, number of IMFs a_f, original residual $res_0(x) = y(x)$, and stop criterion value c
for $j = 1; j <= a_f; j = j + 1$ **do**
  $h_{j,0}(x) = res_{j-1}(x)$
  for $i = 1; i <= S; i = i + 1$ **do**
    Search for extrema of $h_{j,i-1}(x)$ and **calculate** the upper and lower envelops $U_i(x)$ & $L_i(x)$
    $m_i(x) = (U_i(x) + L_i(x))/2$
    $h_{j,i}(x) = h_{j,i-1}(x) - m_i(x)$
    $SD = \sum_{x=0}^{N} \frac{|(h_{j,i-1}(x) - h_{j,i}(x))|^2}{h_{j,i-1}^2(x)}$
    if $SD < c$ **then**
      $C_j(x) = h_{j,i}(x)$
      $res_j(x) = res_{j-1}(x) - C_j(x)$
      break
    end if
  end for
end for
Output: all IMFs $C_j(x)$, and the ultimate residual $res_{a_f}(x)$.

The envelope mean calculation with cubic spline interpolation was demonstrated as a time-varying filter [31]. This envelope-mean filter (EMF) is a linear transform on the input signal $Y = (y_1, y_2, ..., y_n)$, and the corresponding matrix Q provides convergence for sifting process [16]. The sifting process is expressed as [16]:

$$\vec{\xi}^{\dagger} = \lim_{s \longrightarrow +\infty} (I_n - Q)^s Y^{\dagger} \tag{8.1}$$

where, $\dagger$ represents the transpose of a vector, ξ is an IMF, s is the iteration times, I_n is an identity matrix.

8.2.2 Fast algorithm design

Taking extrema (u_k, y_{u_k}) $(k = 1, 2, ..., N)$ and considering matrix $\widehat{P}$ that only contains the rows and columns u_k of Q, $\widehat{P}$ is an EMF on the extrema. According to [16], matrix Q only has non-zero entries at columns u_k. Considering matrix P with entries $p_{u_i,u_j} = q_{u_i,u_j}$ (entries of Q) and others equaling 0 and matrix $A = Q - P$, we can obtain

$$\begin{aligned} A^2 &= O_n \\ PA &= O_n \end{aligned} \tag{8.2}$$

where O_n is a n^2 zero matrix. Eq. (8.2) holds due to the entries $\alpha_{u_i,u_j} = 0$ of A. Indeed, P is obtained by zero-padding between u_i and u_{i+1} columns and rows of $\widehat{P}$. Therefore, P calculates the envelope mean at extrema and A calculates the envelope mean at other discrete signal points.

Considering the sifting matrix $G = (I_n - Q)^s$ and the matrix $R = I_n - P$ and using Eq. (8.2), we can obtain

$$G = (R + A)^s = R^s - A(R^{s-1} + R^{s-2} + \cdots + R + I_n) \tag{8.3}$$

R^s is the sifting process on extrema, and A only works once on sifting values $R^{s-1} + R^{s-2} + \cdots + R + I_n$ of extrema. Therefore, the input signal can be divided using two decimators for extrema and the other discrete signal points:

$$\begin{aligned} Y_1 &= Y\,|_{\downarrow e} \\ Y_2 &= Y\,|_{\downarrow o} \\ Y &= Y_1\,|_{\uparrow e} + Y_2\,|_{\uparrow o} \end{aligned} \tag{8.4}$$

where, $\downarrow e$ represents down-sampling to extrema, $\downarrow o$ represents down-sampling to the others, and $\uparrow e$ & $\uparrow o$ represent corresponding upsamling with zero-padding. Therefore, we have

$$\begin{aligned} RY_1^\dagger\,|_{\uparrow e} &= ((I_N - \widehat{P})Y_1^\dagger)\,|_{\uparrow e} \\ RY_2^\dagger\,|_{\uparrow o} &= Y_2^\dagger\,|_{\uparrow o} \\ RY^\dagger &= ((I_N - \widehat{P})Y_1^\dagger)\,|_{\uparrow e} + Y_2^\dagger\,|_{\uparrow o} \\ AY_2^\dagger\,|_{\uparrow o} &= \vec{0}_n^\dagger \end{aligned} \tag{8.5}$$

where, $\vec{0}_n^\dagger$ is nth all zero vector. According to Eqs. (8.3) and (8.5) and considering $\widehat{R} = I_N - \widehat{P}$, we can obtain

$$GY^\dagger = (\widehat{R}^s Y_1^\dagger)\,|_{\uparrow e} + Y_2^\dagger\,|_{\uparrow o} - A(\sum_{i=0}^{s-1}(\widehat{R}^i Y_1^\dagger)\,|_{\uparrow e}) \tag{8.6}$$

This expression dramatically reduces the calculation in Eq. (8.1). According to Eq. (8.6), our FEMD algorithm is developed as follows:

Algorithm 9 Pseudo codes of FEMD

Input: original signal $y(x)$, maximum iteration times S, number of IMFs a_f, and original residual $res_0(x) = y(x)$
for $j = 1; j <= a_f; j = j + 1$ **do**
  $Y = res_0(x)$, $Y_1 = Y\,|_{\downarrow e}$, $Y_2 = Y\,|_{\downarrow o}$
  Search for extrema of Y and construct matrices Q, A and $\widehat{R}$
  $h = Y_1$, $g = \vec{0}_N$
  for $i = 1; i <= S; i = i + 1$ **do**
    $g = g + h$
    $h^\dagger = \widehat{R} h^\dagger$
  end for
  $C_j(x)^\dagger = (h^\dagger)\,|_{\uparrow e} + Y_2^\dagger\,|_{\uparrow o} - A g^\dagger\,|_{\uparrow e}$
  $res_j(x) = res_{j-1}(x) - C_j(x)$
end for
Output: all IMFs $C_j(x)$, and the ultimate residual $res_{a_f}(x)$.

Since extrema far from the interpolation point would have little effect on the interpolation value, we approximate matrix Q and thus $\widehat{P}$ & A to reduce calculation. For any row $i \in [u_k, u_{k+1})$, we replace the entries $q_{i,j}$ with $j < u_{k-5}$ or $j > u_{k+5}$ in Q with 0, where $u_{k-5} = 0$ with $k \le 5$ and $u_{k+5} = n$ with $k \ge N - 4$.

Considering that all calculations, e.g, multiplication, division, addition and comparison have the same time complexity as in [18], the time complexity of the classic EMD is [18]:

$$f_c = 11n \sum_{j=1}^{a_f} S_j + 30 \sum_{j=1}^{a_f} S_j \cdot a_{k_j} \tag{8.7}$$

where, S_j is the iteration times to extract $C_j(x)$ and a_{k_j} is the extrema number. Similarly calculated, the time complexity of our FEMD is:

$$f_o = 14na_f + 12S \sum_{j=1}^{a_f} a_{k_j} + 10 \sum_{j=1}^{a_f} a_{k_j} \tag{8.8}$$

where, when extracting an IMF, extrema decimator costs $2n$, cubic spline interpolation and corresponding matrices cost $23a_{k_j}$ [18], calculating h and g costs $12Sa_{k_j} - a_{k_j}$, calculating $Y_2^\dagger\,|_{\uparrow o} - A g^\dagger\,|_{\uparrow e}$ costs $12(n - a_{k_j})$. All matrix calculations use sparse matrix forms. Considering $S_j = S$ and $\sum_{j=1}^{a_f} a_{k_j} = a \cdot a_f$, we can have

$$rf = \frac{f_o}{f_c} = \frac{14b + 10 + 12S}{11b \cdot S + 30S} \tag{8.9}$$

where $b = n/a > 1$. By comparison, f_o is less than f_c when each sifting process requires 2 or more iterations. With the increase of iteration times, their complexity ratio $rf \sim \frac{12}{11b+30}$. Therefore, the time complexity of our FEMD algorithm is far smaller, which theoretically demonstrates its time efficiency.

Table 8.1: The computational time with different algorithms.

f_s	iterations	FEMD	EMD in [16]	emd.m
0.1 MHz	100	1.929 s	6.383 s	4.297 s
	1000	5.238 s	32.208 s	45.342 s
1 MHz	100	20.561 s	62.348 s	58.125 s
	1000	66.926 s	441.048 s	634.366 s

8.3 Numerical experiments

8.3.1 Time efficiency

First, a white noise series with duration 1 s and sampling frequency f_s 0.1 MHz or 1 MHz to evaluate the time efficiency. The classic EMD with theoretical framework in [16] and that with 'emd.m' function in MATLAB are used for comparison. The iteration times are set 100 and 1000.

Table 8.1 summaries the computational time with different algorithms. The EMD with theoretical framework in [16] and the optimized MATLAB function 'emd.m' present similar computational complexity. Their computational time increases dramatically with increasing iterations. Our FEMD algorithm outperforms the others. With 1000 iterations, FEMD only costs around 1/10 time of 'emd.m'. Therefore, the proposed FEMD demonstrates high computational efficiency in decomposing signals.

8.3.2 Simulated signal analysis

Second, two simulated signals $y_{s_1}(t)$ and $y_{s_2}(t)$ (Eqs. (8.10) and (8.11)) taken from [32] are decomposed to evaluate the decomposition accuracy. The sampling frequency is 10 kHz and the duration is 1 s. The number of iterations is 1000.

$$y_{s_1} = 6t + cos(8\pi t) + \frac{1}{2}cos(40\pi t) \tag{8.10}$$

$$\begin{aligned} y_1(t) &= \frac{1}{1.2 + cos(2\pi t)} \\ y_2(t) &= \frac{1}{1.5 + sin(2\pi t)} cos(32\pi t + 0.2cos(64\pi t)) \\ y_{s_2} &= y_1(t) + y_2(t) \end{aligned} \tag{8.11}$$

Figs. 8.1 and 8.2 illustrate the decomposition results of y_{s_1}. FEMD achieves similar IMFs and residual signal to EMD. The IMFs reveal the signal components of y_{s_1}. End effects appear in the IMFs, which is a common issue of EMD [**1**]. The computational time of EMD is 1.075 s while that of our FEMD is 0.269 s.

The decomposition results of y_{s_2} are presented in Figs. 8.3 and 8.4. The two algorithms also achieve identical results. The IMFs and residual signals reveal the original signal components. The computational time of EMD is 0.199 s while that of our FEMD is 0.034 s.

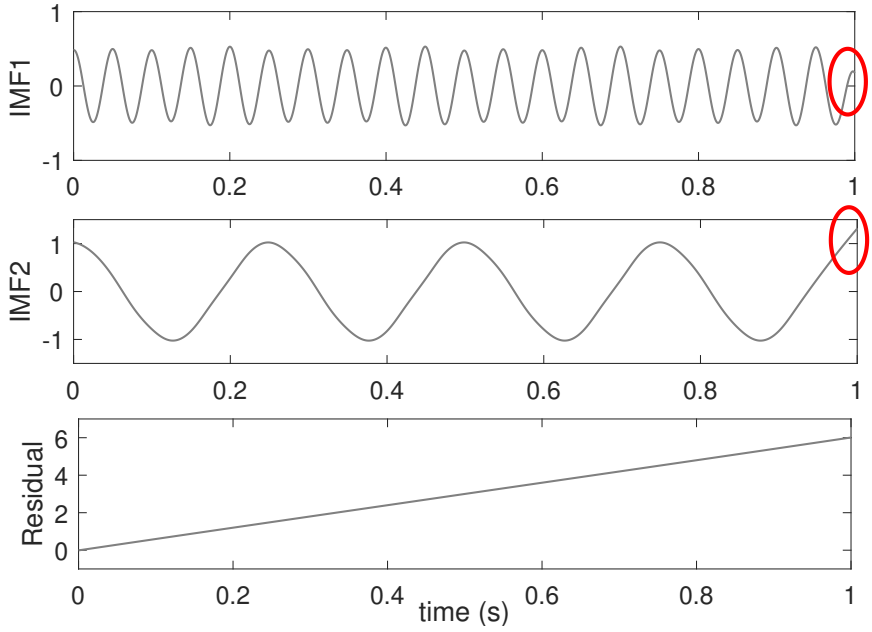

Figure 8.1: IMFs and residual signal of y_{s_1} achieved by FEMD.

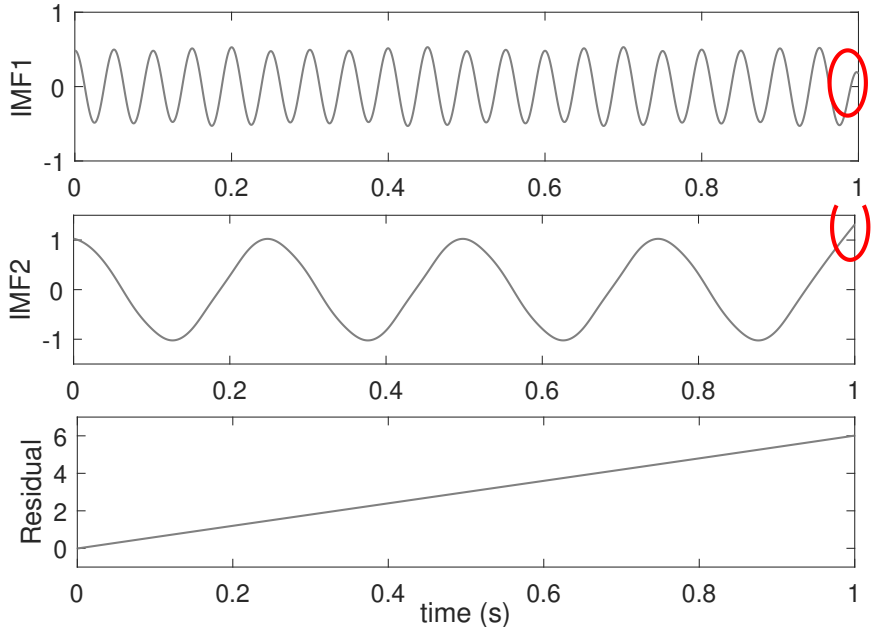

Figure 8.2: IMFs and residual signal of y_{s_1} achieved by the EMD in [16].

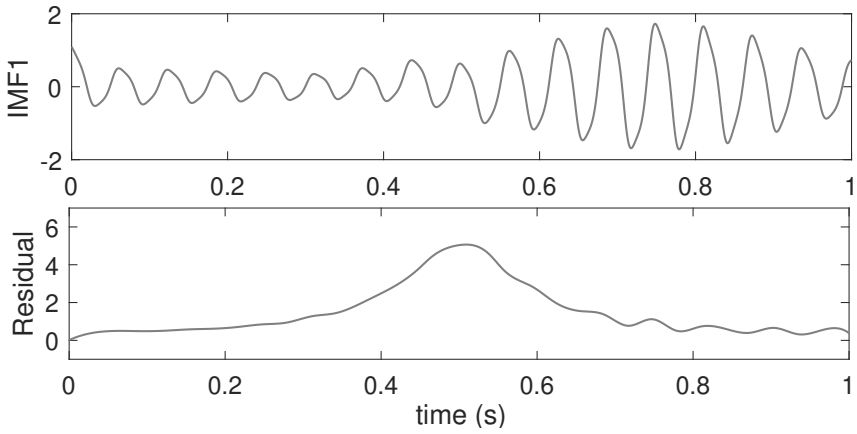

Figure 8.3: IMF and residual signal of y_{s_2} achieved by FEMD.

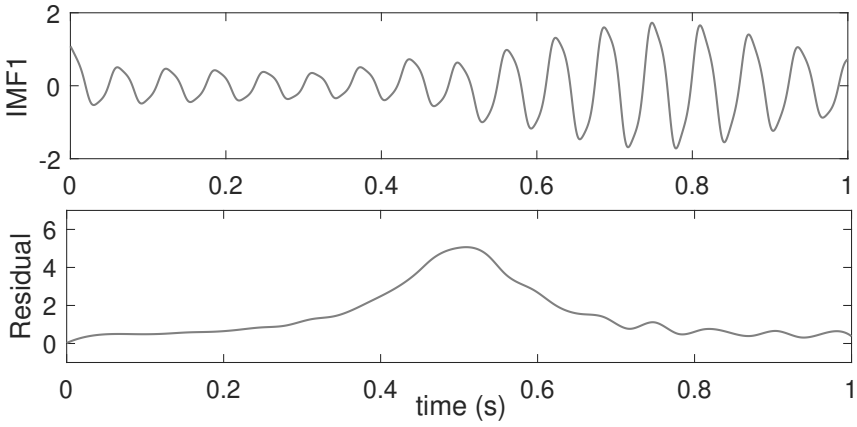

Figure 8.4: IMF and residual signal of y_{s_2} achieved by the EMD in [16].

8.3.3 Real signal analysis

Third, an electrocardiogram (ECG) signal taken from [33] and a seismic signal taken from [34] (Fig. 8.5) are decomposed by FEMD. Figs. 8.6 and 8.7 illustrates the IMFs of the ECG signal. The decomposition results of the two algorithms are identical, and the IMFs have revealed the regular heartbeat energy. The computational time of EMD is 0.564 s while that of our FEMD is 0.089 s. The decomposition results of the seismic signal are also promising, and the IMFs reveal the first arrival and large energy locations. The computational time of EMD is 0.436 s while that of our FEMD is 0.061 s. Our FEMD approach demonstrates accuracy and time efficiency in decomposing signals.

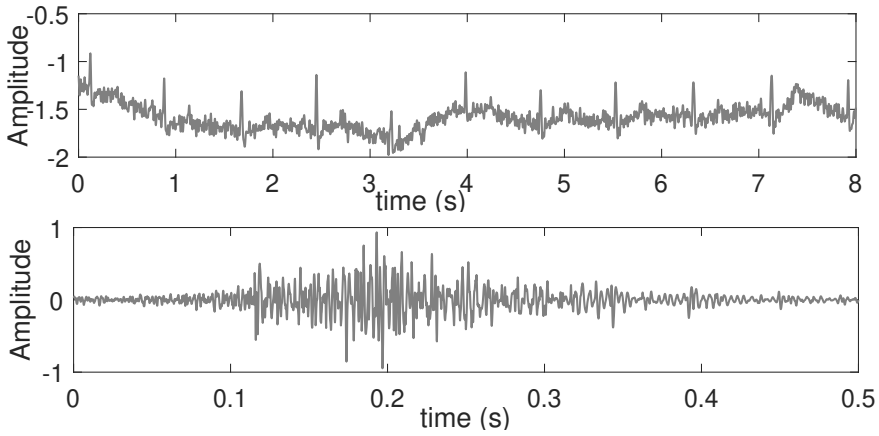

Figure 8.5: Top panel: an ECG signal. Bottom panel: a seismic signal.

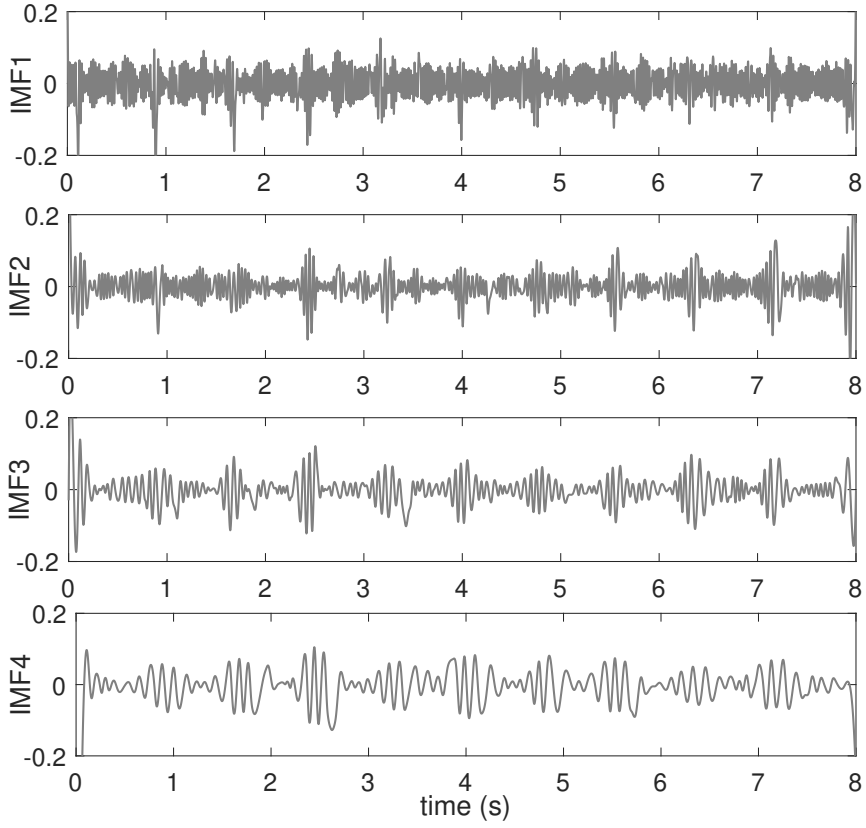

Figure 8.6: IMFs of the ECG signal achieved by FEMD.

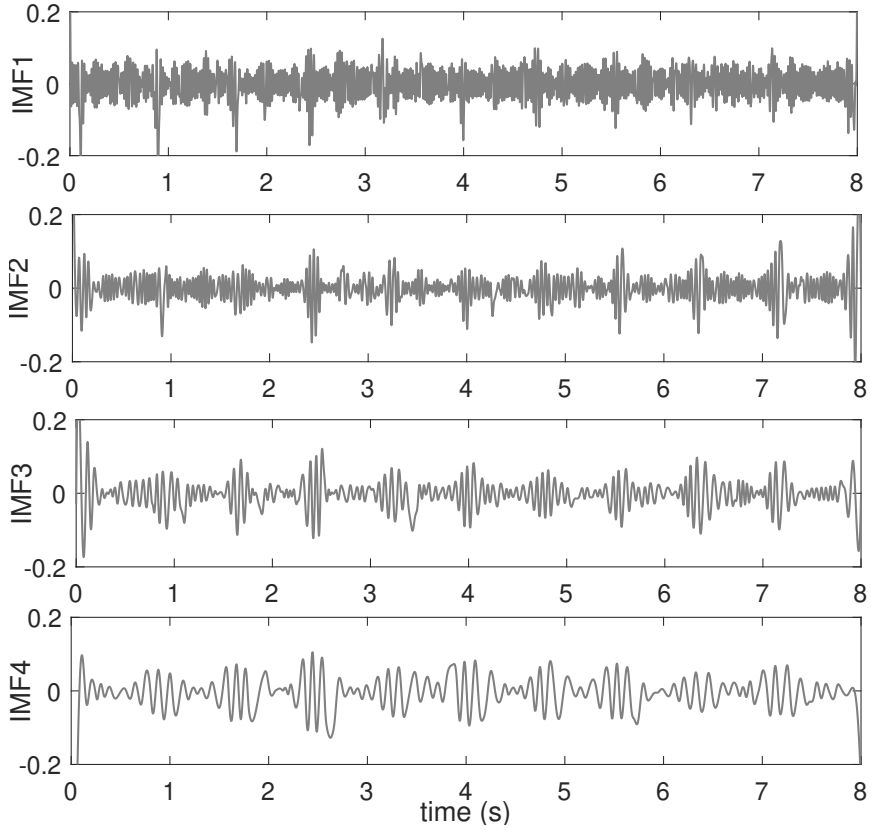

Figure 8.7: IMFs of the ECG signal achieved by the EMD in [16].

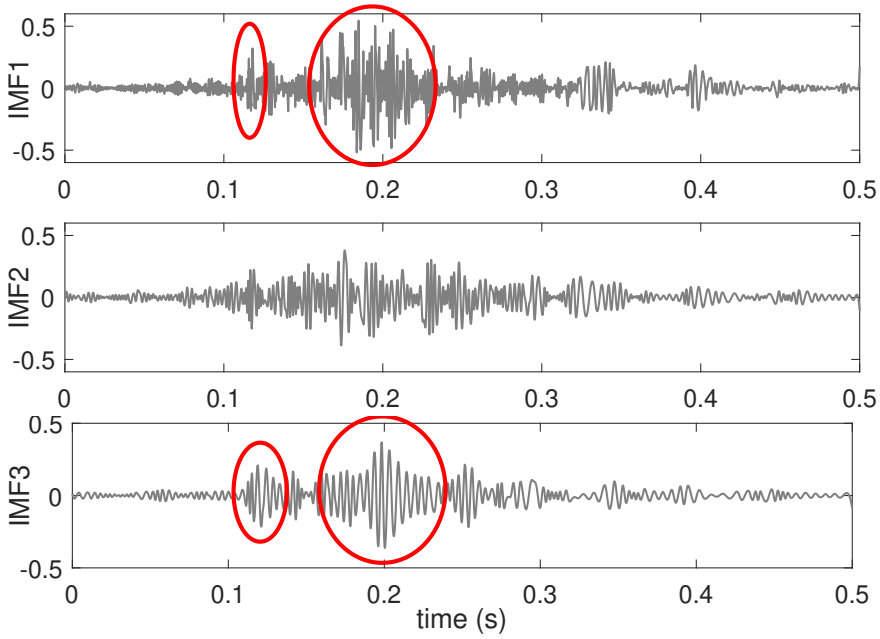

Figure 8.8: IMFs of the seismic signal achieved by FEMD.

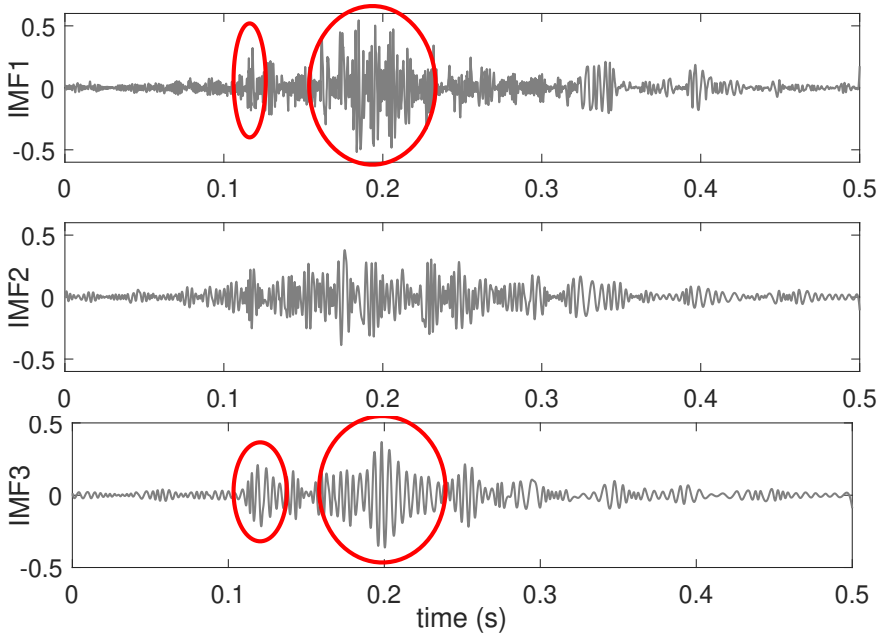

Figure 8.9: IMFs of the seismic signal achieved by the EMD in [16].

8.4 Conclusion

In this work, we propose a novel FEMD algorithm based on a recently developed theoretical framework [16]. By derivation, the sifting process only works on signal extrema. Using two decimators for extrema and the other discrete signal points, our FEMD dramatically reduces the time complexity, especially when requiring considerable iterations.

With numerical experiments on the white noise, our FEMD outperforms the others. The computational time reduces to 1/10 that of 'emd.m' in MATLAB. Other experiments demonstrate that FEMD can capture signal features with promising decomposition results.

References

[1] P Flandrin, G Rilling, and P Goncalves. "Empirical mode decomposition as a filter bank". In: *IEEE signal processing letters* 11.2 (2004), pp. 112–114.

[2] N Ur Rehman and DP Mandic. "Filter bank property of multivariate empirical mode decomposition". In: *IEEE transactions on signal processing* 59.5 (2011), pp. 2421–2426.

[3] AO Boudraa and JC Cexus. "EMD-based signal filtering". In: *IEEE transactions on instrumentation and measurement* 56.6 (2007), pp. 2196–2202.

[4] D Labate, F La Foresta, G Occhiuto, FC Morabito, A Lay-Ekuakille, and P Vergallo. "Empirical mode decomposition vs. wavelet decomposition for the extraction of respiratory signal from single-channel ECG: A comparison". In: *IEEE Sensors Journal* 13.7 (2013), pp. 2666–2674.

[5] M Lozano, JA Fiz, and R Jané. "Performance evaluation of the Hilbert–Huang transform for respiratory sound analysis and its application to continuous adventitious sound characterization". In: *Signal Processing* 120 (2016), pp. 99–116.

[6] GGS Pegram, MC Peel, and TA McMahon. "Empirical mode decomposition using rational splines: an application to rainfall time series". In: *Proceedings of the Royal Society A: Mathematical, Physical and Engineering Sciences* 464.2094 (2008), pp. 1483–1501.

[7] A Sankaran and MJ Reddy. "Analyzing the hydroclimatic teleconnections of summer monsoon rainfall in Kerala, India, using multivariate empirical mode decomposition and time-dependent intrinsic correlation". In: *IEEE Geoscience and Remote Sensing Letters* 13.9 (2016), pp. 1221–1225.

[8] Y Lei, J Lin, Z He, and M Zuo. "A review on empirical mode decomposition in fault diagnosis of rotating machinery". In: *Mechanical systems and signal processing* 35.1-2 (2013), pp. 108–126.

[9] L Wang and Y Shao. "Fault feature extraction of rotating machinery using a reweighted complete ensemble empirical mode decomposition with adaptive noise and demodulation analysis". In: *Mechanical systems and signal processing* 138 (2020), p. 106545.

[10] G Rilling, P Flandrin, P Gonçalves, and JM Lilly. "Bivariate empirical mode decomposition". In: *IEEE signal processing letters* 14.12 (2007), pp. 936–939.

[11] N ur Rehman and DP Mandic. "Empirical mode decomposition for trivariate signals". In: *IEEE Transactions on signal processing* 58.3 (2009), pp. 1059–1068.

[12] T Oberlin, S Meignen, and V Perrier. "An alternative formulation for the empirical mode decomposition". In: *IEEE Transactions on Signal Processing* 60.5 (2012), pp. 2236–2246.

[13] X Lang, N ur Rehman, Y Zhang, L Xie, and H Su. "Median ensemble empirical mode decomposition". In: *Signal Processing* 176 (2020), p. 107686.

[14] Z Wu and NE Huang. "Ensemble empirical mode decomposition: a noise-assisted data analysis method". In: *Advances in adaptive data analysis* 1.01 (2009), pp. 1–41.

[15] Q Wu and SD Riemenschneider. "Boundary extension and stop criteria for empirical mode decomposition". In: *Advances in Adaptive Data Analysis* 2.02 (2010), pp. 157–169.

[16] Y Jin and Z Li. "A Theoretical Framework for A Succinct Empirical Mode Decomposition". In: *IEEE signal processing letters (submitted)* ().

[17] LC Wu, HH Chen, JT Horng, C Lin, NE Huang, YC Cheng, and KF Cheng. "A novel preprocessing method using Hilbert Huang transform for MALDI-TOF and SELDI-TOF mass spectrometry data". In: *PLoS One* 5.8 (2010), e12493.

[18] YH Wang, CH Yeh, HV Young, K Hu, and MT Lo. "On the computational complexity of the empirical mode decomposition algorithm". In: *Physica A: Statistical Mechanics and its Applications* 400 (2014), pp. 159–167.

[19] Y Kopsinis and S McLaughlin. "Enhanced empirical mode decomposition using a novel sifting-based interpolation points detection". In: *2007 IEEE/SP 14th Workshop on Statistical Signal Processing*. IEEE. 2007, pp. 725–729.

[20] L Wang, MI Vai, PU Mak, and CI Ieong. "Hardware-accelerated implementation of EMD". In: *2010 3rd International Conference on Biomedical Engineering and Informatics*. Vol. 2. IEEE. 2010, pp. 912–915.

[21] M Lee, K Shyu, P Lee, C Huang, and Y Chiu. "Hardware implementation of EMD using DSP and FPGA for online signal processing". In: *IEEE Transactions on industrial electronics* 58.6 (2010), pp. 2473–2481.

[22] D Chen, L Wang, G Ouyang, and X Li. "Massively parallel neural signal processing on a many-core platform". In: *Computing in Science & Engineering* 13.6 (2011), pp. 42–51.

[23] C Damerval, S Meignen, and V Perrier. "A fast algorithm for bidimensional EMD". In: *IEEE signal processing letters* 12.10 (2005), pp. 701–704.

[24] C Chen, S Guo, W Chang, JSH Tsai, and K Cheng. "An improved bidimensional empirical mode decomposition: A mean approach for fast decomposition". In: *Signal Processing* 98 (2014), pp. 344–358.

[25] MR Thirumalaisamy and PJ Ansell. "Fast and adaptive empirical mode decomposition for multidimensional, multivariate signals". In: *IEEE Signal Processing Letters* 25.10 (2018), pp. 1550–1554.

[26] X Lang, Q Zheng, Z Zhang, S Lu, L Xie, A Horch, and H Su. "Fast multivariate empirical mode decomposition". In: *IEEE Access* 6 (2018), pp. 65521–65538.

[27] SMA Bhuiyan, RR Adhami, and JF Khan. "Fast and adaptive bidimensional empirical mode decomposition using order-statistics filter based envelope estimation". In: *EURASIP Journal on Advances in Signal Processing* 2008 (2008), pp. 1–18.

[28] H Li, Y Hu, F Li, and G Meng. "Succinct and fast empirical mode decomposition". In: *Mechanical Systems and Signal Processing* 85 (2017), pp. 879–895.

[29] R Wang, J Zhou, J Chen, and Y Wang. "Fast empirical mode decomposition based on Gaussian noises". In: *2016 Third International Conference on Mathematics and Computers in Sciences and in Industry (MCSI)*. IEEE. 2016, pp. 282–288.

[30] CD Blakely. "A fast empirical mode decomposition technique for nonstationary nonlinear time series". In: *Preprint submitted to Elsevier Science* 3 (2005).

[31] Y Yang. "Empirical mode decomposition as a time-varying multirate signal processing system". In: *Mechanical Systems and Signal Processing* 76 (2016), pp. 759–770.

[32] J Gilles. "Empirical wavelet transform". In: *IEEE transactions on signal processing* 61.16 (2013), pp. 3999–4010.

[33] H Khamis, R Weiss, Y Xie, CW Chang, NH Lovell, and SJ Redmond. "QRS detection algorithm for telehealth electrocardiogram recordings". In: *IEEE Transactions on Biomedical Engineering* 63.7 (2016), pp. 1377–1388.

[34] Wu. *seismic data*. Tech. rep. https://doi.org/10.6084/m9.figshare.8797502.v1, 2019.

List of Publications

1. : Yang Jin, Rolf Dollevoet, and Zili Li. "Removing speckle noise from the signals of a laser Doppler vibrometer on moving platforms (LDVom) by ensemble empirical mode decomposition." Measurement Science and Technology 33.12 (2022): 125205.

2. : Yang Jin, and Zili Li. "Mitigating speckle noise in a laser Doppler vibrometer using Fourier analysis." Optics Letters 47.18 (2022): 4742-4745.

3. : Yang Jin, Rolf Dollevoet, and Zili Li. "Numerical simulation and characterization of speckle noise for laser Doppler vibrometer on moving platforms (LDVom)." Optics and Lasers in Engineering 158 (2022): 107135.

4. : Yang Jin, and Zili Li. "Theoretical Framework for A Succinct Empirical Mode Decomposition." IEEE Signal Processing Letters (2023).

5. : Yang Jin, and Zili Li. A Fast Empirical Mode Decomposition. (submitted to IEEE Signal Processing Letters).

6. : Yang Jin, and Zili Li. An adaptive despeckling and signal decomposition approach for vibration analysis using Laser Doppler Vibrometer (submitted to Mechanical Systems and Signal Processing).

Conference

1. : Yang Jin, and Zili Li. "A new method for eliminating speckle noise from Laser Doppler Vibrometer signals." Journal of Physics: Conference Series. Vol. 2041. No. 1. IOP Publishing, 2021.

2. : Yang Jin, and Zili Li. "Eliminating speckle noises for laser doppler vibrometer based on empirical wavelet transform." 2021 13th International Conference on Measurement. IEEE, 2021.

Others

1. : Yang Jin, and Yunling Duan. "A new method for abnormal underground rocks identification using ground penetrating radar." Measurement 149 (2020): 106988.

2. : Yang Jin, and Yunling Duan. "Wavelet scattering network-based machine learning for ground penetrating radar imaging: Application in pipeline identification." Remote Sensing 12.21 (2020): 3655.

3. : Yang Jin, and Yunling Duan. "Identification of unstable subsurface rock structure using ground penetrating radar: An eemd-based processing method." Applied Sciences 10.23 (2020): 8499.

4. : Yang Jin, and Yunling Duan. "2d wavelet decomposition and fk migration for identifying fractured rock areas using ground penetrating radar." Remote Sensing 13.12 (2021): 2280.

Included in this thesis.